"Design and Synthesis of Metal Organic Framework (MOF)-Polymer Composite Membranes for Gas Separation"

Thesis submitted to the ACSIR

For the Award of the Degree of

DOCTOR OF PHILOSOPHY

In

CHEMICAL SCIENCE

By

ANAND BHASKAR

(Registration No. 10CC11J26062)

Under the guidance of

Dr. ULHAS K. KHARUL

POLYMER SCIENCE AND ENGINEERING DIVISION

NATIONAL CHEMICAL LABORATORY

PUNE-411008, INDIA

December 2015

Dedicated to my parents and my wife for their love and support

Acknowledgements

I would take this opportunity to express my sincere gratitude to my supervisor, Dr. Ulhas K. Kharul for his guidance and encouragement. He taught me useful skills for research work as well as technical writing during the course of work. His enthusiasm for transforming the knowledge into the technology for the improvement of quality of life was a great inspiration for me to pursing research as carrier. The other great person who has bestowed me with his guidance and encouragement is my co-supervisor Dr. Rahul Banerjee. I am very much thankful to him for his pursuance for improving me as a person as well as my scientific skills. I had a great experience in the lab where people work to make a difference. My Lab mates in all these years were very supportive. I would like thank Rahul, Sachin, Bhavana, Deepti, Anuja K., Anuja S., Neeraj, Vinaya, Majid, Sameer, Divya, Sagar, Nilesh, Nikita, Smita, Sneha T., Ashwini, Shilpa, Taran, Vasanti, Manisha, Amay, Rishit, Kiran, Rohit, Bharat, Varsha, Sudhir, Ganesh, Prakash, Praveen, Deekshith, Ramendra, Harsha, Vrushali, Shabeeb, Godavari, Supriya, Chetana, Vijay, Kanhu who have helped me in all possible ways & have been my extended family during the tenure of my work at NCL. I owe special thanks to my lab mates Anita, Sayali, Harshal and Bishnu for their constant encouragement & always being with me in all sorts of situations during my stay in NCL. I truly enjoyed the valuable discussions with them. I would also like to thank Mr. Swaraj Singh, Sneha D., and Hemchandra for their support in purchasing and indenting of the laboratory materials and other related issues. I would like to specially thank my senior Dr. Rupesh Bhavsar for his support and help in learning the basic laboratory practice. He has placed a great influence on me during the period of my stay here in NCL.

I am grateful to Dr. Vijayamohanan K Pillai, Director, NCL, Dr. Saurav Pal, former Director, NCL, Dr. Vivek Ranade, Deputy Director, NCL and Dr. A. K. Lele, Head, Polymer Science and Engineering Division for giving me opportunity to work in NCL and providing the wonderful characterization facilities of the institute. I would also like to thank Dr. Chetan Gadgil and AcSIR coordination committee for their efforts to fast track the process for the thesis submission. I duly acknowledged CSIR, New Delhi for monetary support in the form of JRF/SRF fellowship during my research period. It

gives me great pleasure to thanks my DAC committee members, Dr. P. P. Wadgaonkar, Dr. C. Ramesh, Dr. Satyanarayana Chilukuri for timely evaluation of my work and important suggestions. I would like to thank Mr. K. V. Pandare, Dr. Nandini Devi, Dr. R. S. Gholap, Dr. Rajmohan, Dr. Neelima Bulakh, Dr. Anuya Nisal, Mrs. Dhoble, Mrs. Sangita, Mrs. Purvi, and Mr. Saroj for their valuable suggestions and allowing me to use facilities. I would also like to acknowledge valuable support of Mr. Vivek Borkar and Swapnil in trouble shooting the problems related to the lab instruments.

I find no words to express my feelings for my parents whose dedication, moral support, love and constant encouragement have helped me to complete this journey. Especially my father is great inspiration for me to come out of every difficult time and think big irrespective of the situation. Here I also want to acknowledge my loving wife Anuradha, who deserve the credit for sacrifice she made for my work and recognition as a friend to improve me as a person. I take this chance to thank my brother-in-law (Bharat Swami) remembering our brainstorming for his great support as a family member. I would like to thank my Grandmother, father-in-law and mother-in-law for their love and affection making my life rich of happiness.

Finally, I am grateful to the mighty nature for my continuous source of inspiration and giving me a beautiful and healthy life.

Anand Bhaskar

Content

Part B: Composite membranes: Brief literature Survey

Chapter 2: Material synthesis and characterizations

Chapter 5: Olefin paraffin separation by ZIF-8@PBI composite membranes

Chapter 6: Conclusions and Future perspective

List of Schemes

List of Figures

List of Tables

Chapter 1

Introduction and literary survey

Part A: Introduction

1.1 History of membrane based separation

Membrane is a selective barrier that allows one or more compounds to permeate faster through it over the others from a mixture, resulting in the separation of mixture components. The first observation regarding selective transport of gases through dense films was reported in 1831. J. K. Mitchell observed that H_2 filled balloons prepared from natural rubber are descending from ceiling over the time due to passing of gas through the balloon wall [Mitchell (1831)]. Further experiments showed that various gases pass at different rate through the wall of a rubber balloon. He thought that due to stretching of rubber by balloon filling, pores are creates in the balloon wall, through which the gas is permeating. Later on in 1851, A. Fick conducted gas permeation through nitrocellulose films and formulated the Fick's first law of diffusion [Paul (1994)]. Thomas Graham (1866) repeated the permeation of gases through rubber films and determined the relative rates of permeation for various gases [Graham (1866)]. He noted that there is no correlation between these values and known diffusion coefficients of gases. He also studied the effect of temperature, pressure and membrane thickness on the gas flux through the membrane. All these early studies were in steady state conditions. H. A. Daynes devised a permeation set up using thermal conductivity detector and first measured transient permeation of gases through rubber films [Daynes (1920)]. He showed that extrapolation of the line after steady state permeation to the time axis gives the time lag, θ, which is directly related to the diffusion coefficient of the gas ($\theta = l^2/6D$). He concluded that the gas permeation through membrane is governed by two independent processes. This critical understanding directed further research in the field. Around 1950, Barrer, Von Amerongen and Stannett conducted the systematic gas permeation and sorption on the synthetic polymers (mainly semicrystalline polymers as they were promising barrier materials) in order to establish the structure property relationship

[Stannett (1978)]. Later on, with the development in synthetic polymer chemistry, the focus shifted to the glassy polymers due to their better separation properties. The discovery of phase inversion process by Loeb and Surirajan [Loeb (1962)] enabled the precise control over the porosity as well as thickness of selective skin, which guided the first application of polymer as the practical membrane for filtration (reverse osmosis, ultrafiltration, and microfiltration). The asymmetric integrally skinned membranes were developed with a thin skin layer. These membranes found applications in gas separation when Henis and Tripodi discovered effective defect healing process in 1980 [Henis (1980)]. This discovery led to the launch of PRISM membrane (integrally skinned asymmetric polysulfone membrane) by Permea for the hydrogen recovery from the NH_3 purge gas. The chronology of the membrane development is shown in Figure 1.1.

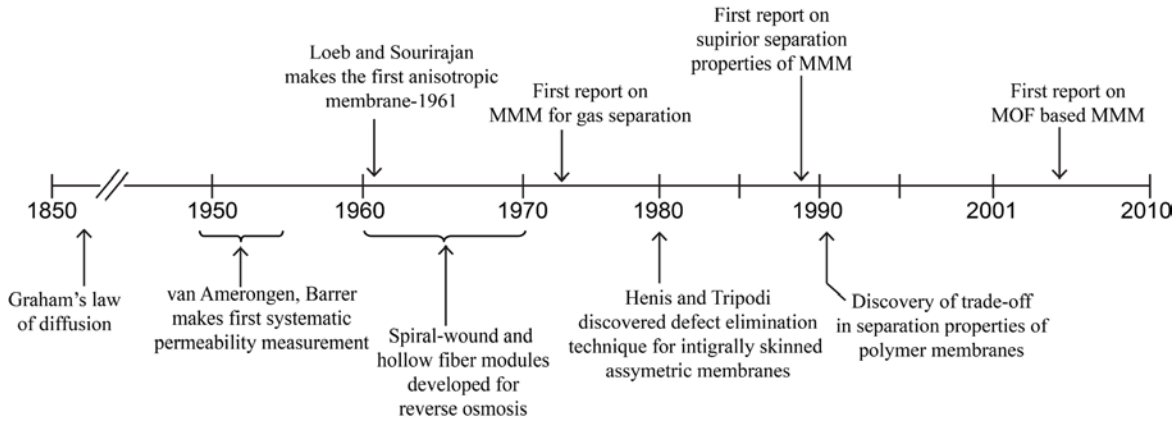

Figure 1.1 Chronology: Membrane development [Baker (2000)].

1.2 Advantages of membrane based gas separation

The conventional gas separation processes are cryogenic distillation, absorption and adsorption (pressure/temperature swing) technologies. Now a day's membrane systems are replacing these conventional technologies in many of the gas separation applications. The membrane technology is considered very promising due to the following advantages:

(i) Low capital and operational cost

The membrane systems having small hardware and minimal accessories, reduces the cost of installation as well as of operation. The only major cost is of membrane, which is a way lesser in comparison to the other technologies.

(ii) Low inherent energy cost of separation

Membrane separation does not require phase change during the separation of components, thus requires less energy for the separation in comparison to the conventional distillation process.

(iii) Environment friendly operation

The membrane life is significantly higher than the adsorbents and absorbents, which are required to be replaced frequently and are hazardous waste for the environment. Membranes for gas separation operate based on physical separation and can be used for much longer time.

(iv) Space and weight efficiency

The small size of the membrane skid makes it more space and weight efficient for the remote and off-shore applications.

(v) Design efficiency

The modular nature of the membrane makes it more flexible from the design perspective. It could be easily scaled up. The integration with other processes is also easy according to the requirements.

1.3 Applications of membrane technology: A brief survey

The membrane technology is gaining attention due to above mentioned advantages. It is already in use for many applications of gas separation. Due to stringent norms driven by better techno-economical feasibility, advanced membrane materials are being developed.

1.3.1 Established applications

The membranes based separation processes are devised for various industrial applications due to their advantages mentioned in section 1.2. Currently, membranes are practiced for following gas separation applications:

1.3.1.1 Air separation

(i) Oxygen enrichment of air

The O_2 preferentially passes through the polymeric membranes due its better sorption in polymers and relatively smaller size than N_2. The moderate O_2/N_2 selectivity

of 3-8 could be obtained by the commercial polymeric membranes. Thus, the membrane process could not be competed with the conventional cryogenic distillation and pressure swing adsorption for high purity O_2 (90-99%) production due to this limitation of selectivity. This moderate selectivity of the membranes renders their operation in the oxygen enrichment (up to 30-60%) applications like health care, fermentation and copper smelting. The first commercial *membrane oxygen enrichment system* was introduced in 1977 by the Oxygen enrichment company [Prasad (1994)]. The larger applications (oxy fuel) are still a matter of research as the membranes with high selectivity are to be produced. The membranes can also be useful in the hybrid systems where in the first stage the membrane enriches the O_2 which reduces the volume for second stage distillation.

(ii) Nitrogen enrichment of air

The O_2 permeates selectively through membrane leaving the N_2 enriched reject stream. Thus, commercial polymeric membranes with even moderate O_2/N_2 selectivity (3 to 8) can easily provide the 95 to 99% enriched nitrogen from air. As the enriched N_2 is produced at the reject stream, high productivity could be easily obtained. The enriched nitrogen finds applications in storage and handling of flammable materials for making the environment inert. It is also used for preservation of food materials and for inflation of automobile tyres.

1.3.1.2 Hydrogen separation

The first large scale application of the membrane for gas separation was H_2 separation from the ammonia purge stream containing argon, nitrogen and methane. In ammonia production, hydrogen and nitrogen reacts at high pressure to form ammonia. The reactor works in a loop where ammonia is condensed out continuously. In this process the impurities like CH_4 and Ar builds up with repeating cycles. These impurities must be continuously purged out to prevent them from exceeding a certain concentration. This purge stream contains valuable H_2 which need to be recovered. In 1980, Permea launched its PRISM membrane for the hydrogen recovery. This is an ideal application for the membrane as hydrogen show high flux and high selectivity over the other gases present in the purge stream. Additionally the feed stream to the membrane is free of

larger hydrocarbons which can cause plasticization of membrane reducing its selectivity.

Other similar but large application is synthetic gas ratio adjustment which requires partial separation of H_2 and CO. Syngas is produced by the reforming of hydrocarbons at high temperature. The H_2/CO ratio of the outcome varies with the source of production. This ratio needs to be adjusted according to the application. Syngas made via steam reforming has 3:1 H_2/CO ratio, whereas typical applications requires a ratio of between 0 and 2.1 [Zolandz (1992)]. Membranes are ideally suited for stripping H_2 out of the syngas in order to reduce the H_2/CO ratio.

The other lucrative application is hydrogen recovery from fuel gas streams, pressure swing adsorption (PSA) tail gas, Fluid catalyzed cracking unit (FCCU) gas, and hydrocracker/hydrotreater off-gas where hydrogen is present from 15 to 80%. The condensable hydrocarbon present in such streams could plasticise the membrane and destroy its separation performance, making the membrane process unreliable. In one such application, membrane is also used to recover H_2 from methanol plant purge gas. The recovered H_2 from the purge streams is recycled back to the reactor, leading to higher yield and lower operating costs [Zolandz (1992)].

1.3.1.3 Acid gas separation

The membrane based separation of acid gases (CO_2, H_2O and H_2S) finds application in the production of pipeline grade natural gas, CO_2 recovery and recycle in enhanced oil recovery (EOR), methane recovery from landfill, biogas up gradation and CO_2 separation from flue gases.

(i) Natural gas purification

The raw natural gas contains methane (30-90%), ethane, propane and other higher hydrocarbons. It also contains water, CO_2, H_2S, and N_2. The raw natural gas need to be processed in order to remove CO_2, H_2S, N_2 and water so that the pipeline specifications and increase calorific value of the gas can be met. The major technology for the CO_2 removal is amine absorption. It has limitations like, high cost, amine degradation and complex operation. These factors promote the membrane technology, especially in small and off-shore applications. At present, membrane has only <5% market share for natural gas purification [Baker (2008)]. This is due to the moderate selectivity of the membranes

causing loss of some amount of methane as permeate during the separation. To further improve its market share, there is a need for membranes with good selectivity and resistant to the plasticization caused by CO_2, water and higher hydrocarbons present in the raw natural gas, which causes reduction in the membrane performance.

(ii) Enhanced oil recovery (EOR)

In the EOR process, CO_2 is injected into the oil bearing strata at high pressures (~1000 psi), which help in easy displacement of oil to water [Zolandz (1992)]. The CO_2 need be recovered from the overhead off gas that consists of CO_2, N_2, H_2S, CH_4 and other hydrocarbons. The membrane technology is used for recovery of CO_2 (~ 95% purity to maintain its solvent power) from the off gas efficiently.

(iii) Biogas purification and land fill recovery

The membrane is very promising for this applications such as biogas plants and land fill gas, for which, sources are smaller in size. The small separation unit with low capital cost is more attractive for them, which membrane can easily meet. The other important advantage is that the membrane permeates CO_2 and H_2S leaving the reject stream methane enriched at high pressure, avoiding the cost of recompression.

1.3.1.4 Vapour separation

In this separation process, volatile organic compounds are recovered from the various industrial vent streams. For the separation, either rubbery polymer could be used as vapour permeating membrane or the glassy polymers air permeating (N_2, O_2) membrane. Most commonly rubbery polymer (silicon) membranes are used in combination with condensation process for the vapour recovery. The first plants were installed in 1990s to recover gasoline vapors or chlorofluorocarbon (CFC) vapours from industrial refrigeration plant [Baker (2002)]. Recently membranes are also used to recover hydrocarbons and processing solvents from petrochemical plant purge streams. One other successful application is vent recovery from the polyolefin plant. In polyolefin plant, the olefin, monomer, catalyst, solvent and other co-reactants are pressurised into the reactor. After polymerisation the obtained polymer contains unreacted monomer, which is removed by flash separation step. The recovered monomer is recycled. The

residual monomer is removed by stripping with nitrogen. The degassing vent composition varies greatly. It contains 20-50% of monomer, which represents 1% feed stock. This amount may seem small but the high value of the olefin monomer makes its separation promising. The membrane-condenser hybrid system is used to recover the monomer from this vent.

The glassy polymer membrane could be more promising where recovered vapour is recycled as these membranes only strip out the air and concentrate the vapour for direct reuse. Most of the glassy polymers get plasticised with the vapour stream and losses the selectivity drastically. The glassy fluoropolymer membranes show good resistant to the hydrocarbon vapour induced plasticization and are commercialized for the vapour recovery.

1.3.2 Future applications

The current membranes are either having moderate separation factors or issues of stable performance in the aggressive feed (high temperature, plasticizing impurities) conditions. New membrane material development with improving on these aspects may lead to their application in more challenging separation processes.

1.3.2.1 Olefin-paraffin separation

Olefin-paraffin separation is a highly energy intensive process by cryogenic distillation due to the close boiling point of the molecules to be separated. Membrane based separation of olefins (especially ethylene, propylene and isobutylene) from paraffins could be very promising as it does not require phase change. The current polymeric membranes show low selectivity (2-6) for C_2H_4/C_2H_6 [Rungta (2013)] and moderate selectivity (5-20) for C_3H_6/C_3H_8 [Burns (2003)]. Current polymeric membranes are also prone to plasticization, reducing their separation performance further. Thus membranes with high separation factor and good resistance to the plasticization are required to be developed for this application.

1.3.2.2 Natural gas dehydration

Membranes can also be used for gas dehydration. Most of the polymers show very high selectivity for the water permeation over the other gases. Thus, water can be easily

stripped out from the feed stream with the membrane permeating water preferentially. Currently the glycol absorption technology is used for the gas dehydration. It is well accepted industrially and suitable from the cost aspect. The major drawback of the membrane systems is some lose (~5%) of the methane to the permeate stream, which is not affordable. As the separation here is controlled by the pressure ratio, the improvement in the engineering aspects could make the membrane more competitive.

1.3.2.3 Inert gas separation from natural gas

The raw natural gas contains significant amount of inert gas (mostly N_2) in it. Many of the sources are not considered for economical production of natural gas due to the high inert gas content. The natural gas pipeline specification for the inert gas is ~4% [Baker (2008)]. The principle technology today for the inert gas removal from the natural gas is cryogenic distillation. Most of these plants also produce helium and natural gas liquids (NGL) as co-product. These co-products contribute significantly to the overall process economics. The cryogenic distillation is highly energy intensive is marginally economical at best. The membrane could be considered to separate nitrogen from the natural gas. The challenge is to make membrane with sufficient separation factor to achieve separation economically. According to Baker *et al.*, the membrane with CH_4/N_2 selectivity of 6 or N_2/CH_4 selectivity of 17 could be useful with the hybrid system containing cryogenic distillation to refine the gas stream containing 10% N_2 [Baker (2008)]. Unfortunately, current polymers have very low selectivity for these gases. The glassy polymers show N_2/CH_4 selectivity of 2-4 while the rubbery polymers show the reverse selectivity up to 2. Development of new membrane materials with higher selectivity could lead to their application for N_2 removal from natural gas.

1.4 Membrane materials

The present commercial membranes for gas separation are of polymeric nature. It is due to their higher selectivity and easy processing of polymeric materials into mechanically robust, defect free, ultrathin membranes at low cost. There are other materials which show highly selective transport behaviour and are also more resistant to aggressive thermal and chemical environment. All these membrane materials have their own advantages and limitations of stability, performance or processability.

1.4.1 Polymers

As stated above, polymers are the materials for the most of the present commercial membranes due to their easy fabrication in ultrathin membrane with high surface area configuration at low cost. A large number of the polymers are investigated for their gas separation properties [Robeson (2008)]. Among a large pool of polymers only few had achieved the commercial success. The gas separation properties of a polymer are not the sole factor for its choice as commercial membrane. Other important properties like its thermo-chemical stability in the actual feed environment, processability into ultrathin membrane at low cost are also as important. Both, the rubbery and glassy polymers can be used as membrane materials depending on the application. The common glassy polymers used in commercial membranes are cellulose acetate, polyimide, polyaramide, polysulfone, polycarbonate and polyphenylene oxide. Polydimethylsiloxane is the commonly used rubbery polymers for vapour/gas separation.

There is a lot of research carried out to improve the separation properties of the polymeric materials by structural variation [Yampolskii (2012)]. It was found that the polymeric materials show a trade off in the gas permeation properties [Robeson (1991, 2008)]. In other words, the improvement in the permeability comes at the cost of selectivity and *vice versa*. For example, we can see the trade off in the O_2 permeability and O_2/N_2 selectivity in the Figure 1.2.

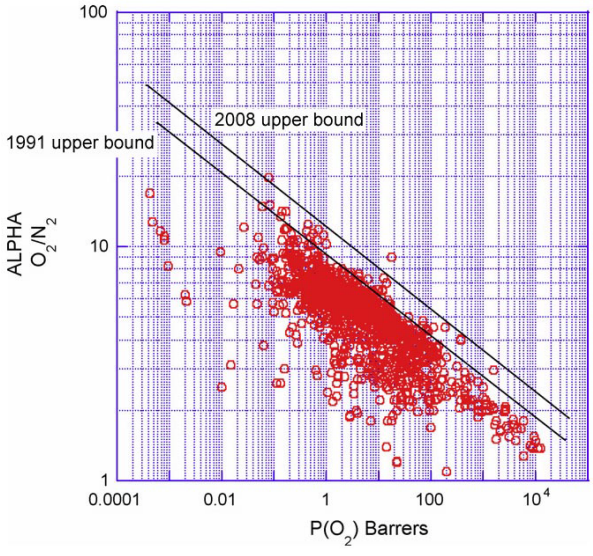

Figure 1.2 Trade off in the O_2 permeability and O_2/N_2 selectivity [Robeson (2008)].

The ultrahigh free volume glassy polymers have been the field of keen interest after the revelation of high permeability of poly(*1*- trimethylsilyl-*1*-propyne) (PTMSP) in 1983 [Masuda (1983)]. PTMSP though is glassy polymer, showed permeabilities more than 10 times higher than rubbery PDMS. Du pont's Teflon AF2400® and poly(*4*-methyl-*2*-pentyne) (PMP) also show very high permeability [Toy (1996), Morisato (1996)].

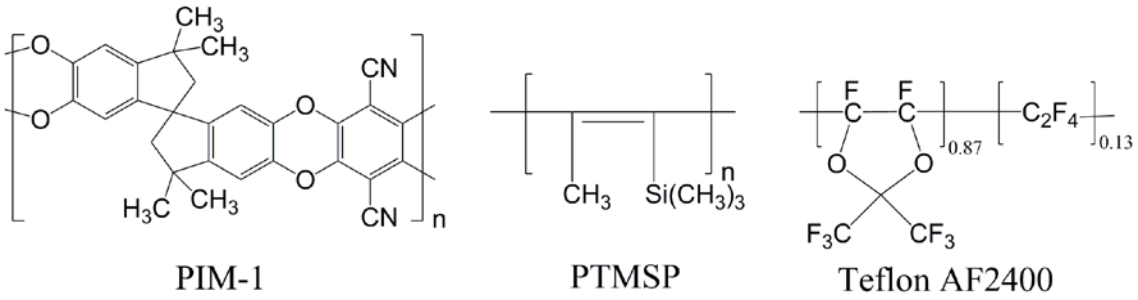

Figure 1.3 Chemical Structures of polymers containing high free volume

Recently the polymers of intrinsic microporosity (PIMs) are made which have rigid chain structure restricting the rotational freedom [McKeown (2010)]. The rigid structure (Figure 1.3) of these polymers halts their dense chain packing, resulting in high free volume and gas permeability. The PIMs show high permeability (due to high free volume) and good selectivity (due to rigid chains), putting their separation properties above the Robeson's upper bound [Ghanem (2014)]. Other than the permeability and selectivity limitation, polymeric membranes are also prone to loss of intrinsic separation performance in the presence of interactive gases [Baker (2000), Sanders (2013)]. The strong polymer-penetrant interactions reduce the inter-chain interactions and increase the mobility of polymer chains. This results in the increase in the gas permeability (Figure 1.4) with simultaneously loss of selectivity. This phenomenon is called plasticization [Horn (2011)].

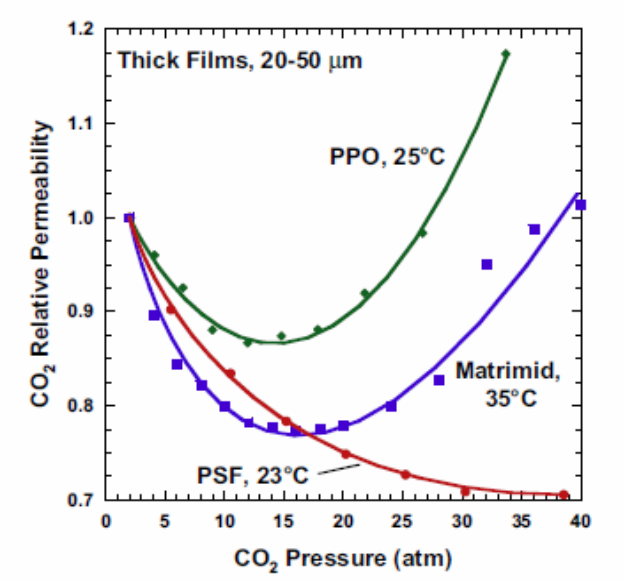

Figure1.4 Effect of CO_2 pressure on the permeability [Horn (2011)]

Aging is another problem with the glassy polymeric materials. Due to the nonequillibrium state of chain packing, the polymers contain extra free volume. In the long run, the polymer chains try to reach to the equilibrium state by the small segmental adjustments possible by the thermal motions of atoms. This process leads to reduction in the free volume and thus the gas permeability. The decrease in the gas permeability is accompanied by the some increase in the selectivity. The aging process is faster in the thin films (Figure 1.5) due to enhanced mobility near the surface of film [Rowe (2009)].

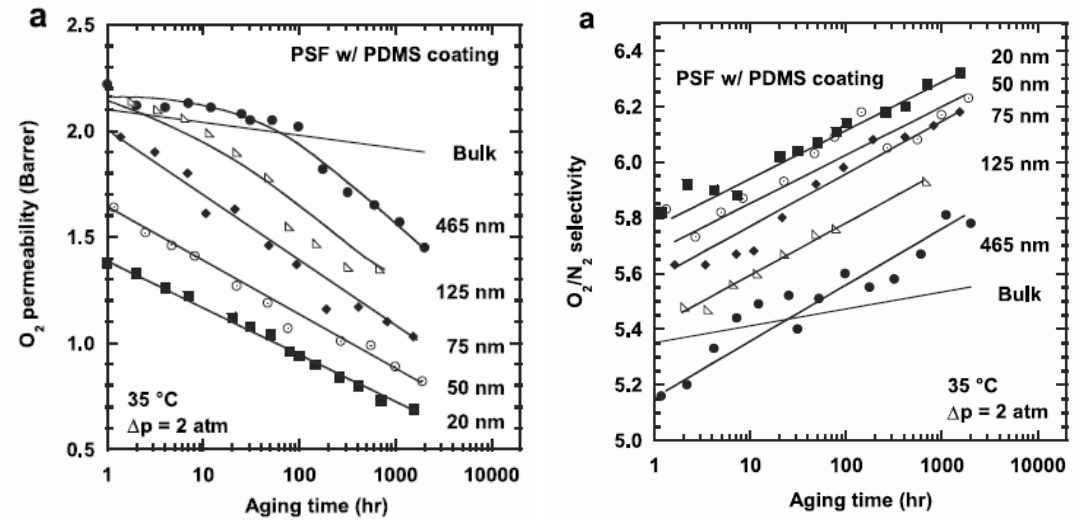

Figure 1.5 Aging of the polysulfone membrane with respect to time [Rowe (2009)].

1.4.2 Zeolites

Zeolites are aluminosilicates made of silica-oxygen network where some of the Si atoms are replaced by Al atoms. They have ordered porosity embedded in the structure. Their distinct size micropores could differentiate small gas molecules based on their size and shapes. For realising their high intrinsic separation properties there were immense attempts made to fabricate them into thin defect free membranes [Feng (2015), Rangnekar (2015)]. They are commercialized for the drying of the organic liquids due to their extreme hydrophilic nature, but till date there is no success obtained in gas separation application due to difficulty in defect elimination [Rangnekar (2015)].

1.4.3 Carbons

Carbon membranes are produced typically by the pyrolysis of the thermosetting polymers under controlled conditions. The pyrolysis converts the organic polymers into the amorphous carbon which have rigid random network. The amorphous carbon membranes having narrow distribution of pores could be achieved by controlling the pyrolysis conditions and selection of appropriate polymer [Ismail (2001)]. The carbon membranes with small pore size distribution (2-5 Å) show strong molecular sieving characteristics. Thus the molecules could be separated based on their size and shape difference. In the membranes with larger pore size distribution (>5 Å), diffusion based discrimination of gaseous molecules could not be obtained. In such membranes the interactions of molecules with membrane governs the selectivity. The molecules which sorb more (CO_2, NH_3, H_2S and hydrocarbons) could selectively permeate by surface diffusion mechanism. The carbon membranes are comparatively easy to fabricate than other inorganic membranes, they are formed by the polymeric materials which are easy to process in high surface morphology. Due to amorphous nature they do not have grain boundary (inter-crystalline) defects but still their brittle nature makes them susceptible to the crack formation.

Recently, graphene (two dimensional networks of sp^2 hybrid carbon atoms with mono-atomic layer thickness) has shown a great promise as membrane material. The graphene itself is not permeable to any gas, but the graphene oxide (GO) (which have precise defects due to controlled oxidation) has shown promising separation characteristics. The microporous GO membranes of 18 to 1.8 nm thickness are prepared

and have shown very high selectivity up to 3400 and 900 for H_2/CO_2 and H_2/N_2 respectively [Li (2013)]. In another study, submicrometer thick GO membrane shows the very unusual permeation behaviour. It is completely impermeable to the liquids, vapors, and gases, including helium, but allows unimpeded permeation of water (H_2O permeates through the membrane 10^{10} times faster than He) [Nair (2012)]. A different permeation mechanism works in this case. The molecules pass through the inter-layer spacing, which increase or decrease according to the interaction with penetrant molecules [Nair (2012)]. These studies show that graphene has very high potential as membrane material which could be taped by further advancement in the membrane preparation methods.

1.4.4 Ceramics

The ceramic membranes include the membranes made of silica, alumina, titanea, perovskites etc. These membranes could be categorized in two classes: (i) microporous and (ii) dense. These membranes are generally prepared by either chemical vapour deposition (CVD) or sol-gel synthesis method. The CVD method using standard silica precursors such as TEOS or tetramethyl orthosilicate (TMOS) generally result in a microporous or nonporous silica thin films showing good separation of small molecules like He and H_2 over the larger molecules like CO_2 [Mallada (2008)]. The use of silica precursors with larger organic groups gives membranes with grater permeance for the CO_2 [Sea (1997)]. The microporous membranes could also be prepared by sol-gel method. The fine control of the conditions gives membranes with well defined pore structure. The dense ceramic membranes are made of perovskites which permeate the gases in the form of their ions. Due to this mechanism these membranes give very high (almost infinite) selectivity. The O_2 and H_2 could be conducted in the ionic form through perovskite membrane [Leo (2006), Matsumoto (2006)]. These membranes generally have low flux and require high temperature (700-900 °C) for achieving significant flux. The difficult processing and brittle nature are major bottle neck for realising potential of these membranes.

1.4.5 Metals

Since Grahm first reported hydrogen sorption in the palladium [Graham (1866)], the metals were studied for their hydrogen sorption and subsequent phase changes. As the

palladium shows highest hydrogen sorption the research activities mainly focused on palladium based membranes. The hydrogen transport in these membranes occurs as shown in the Figure 1.6. The hydrogen molecules adsorb on the membrane surface and split into H^+ ions loosing the electrons to the metal lattice. The H^+ ions diffuse through the membrane and recombine on the permeate side of membrane to form H_2 molecule and desorbs from this surface.

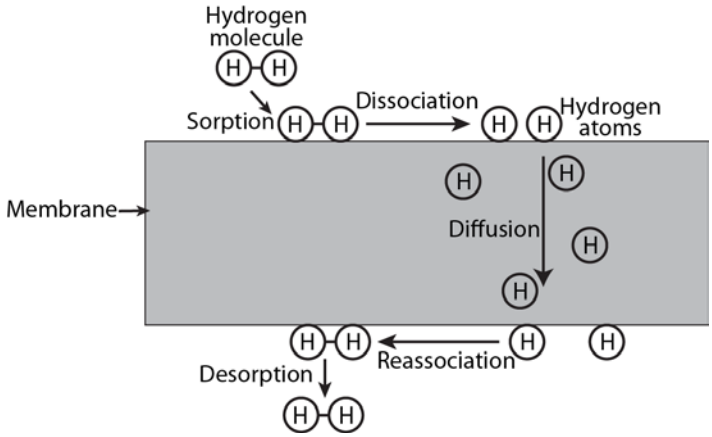

Figure 1.6 Hydrogen transport process in metal membranes [Baker (2000)].

The palladium/hydrogen system shows two phase behaviour below critical temperature (293 °C) and pressure (20 atm). This leads to phase separation by grain boundaries and results in the mechanical failure of the membrane [Paglieri (2002)]. The alloying with silver reduces this two phase system below ambient temperature (25 °C) resulting in stabilization of membrane [Hunter (1955)]. This discovery led to commercialization of palladium-silver alloy membranes for hydrogen separation developed by Johnson Metthey in 1964 [Uemiya, (1999)]. These membranes are used for production of very high purity H_2 for semiconductor industry.

The reduction of membrane thickness and mechanical stability are key issues to be addressed for greater applications. As the thicker membrane are costlier (due to very high cost of metal) and have low hydrogen flux. On the other hand thinner membranes are mechanically brittle and are susceptible to mechanical failure. The significant research efforts made to make these membranes robust and ultrathin. The multilayer composite membranes were made, where cheap materials are used as support on which a thin layer of selective metal is deposited.

1.4.6 Metal organic frameworks (MOFs)

MOFs are network structures, made of organic linkers connected to the metal based centre (Figure. 1.7). The organic linkers are ditopic or polytopic ligands, which connects to the metal containing unit to form architecturally crystalline framework with embedded microporosity [Furukawa (2013)]. As they are constituted of organic linkers, they have immense structural and functional diversity with more than 20,000 structures discovered in the last decade [Furukawa (2013)].

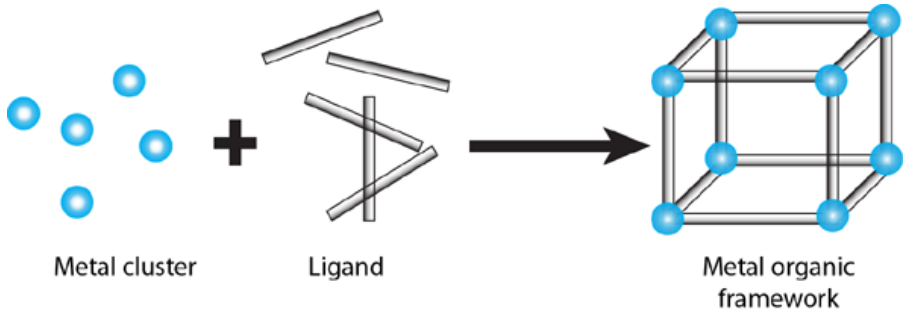

Figure 1.7 Schematic for the preparation of MOF.

These materials have high internal surface area in the range of 1000 to 10,000 m^2/g, exciding the conventional porous materials such as zeolites and carbon [Furukawa (2013)]. The high porosity and great structural and functional diversity of these materials makes them highly promising for the gas separation. These materials could separate the gas molecules either by size/shape selective diffusion or selective sorption. The beauty of these materials is that the porosity as well as functionality of material could be modified by both pre-synthetic as well as post-synthetic modifications of organic part, as shown in the following examples (Figure. 1.8) [Cohen (2011)].

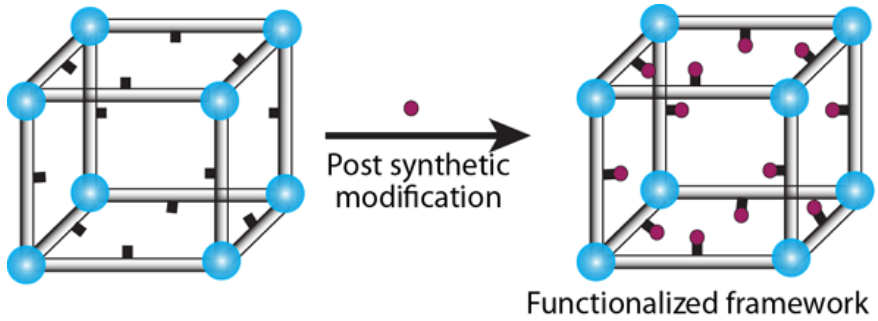

Figure 1.8 Schematic for the post synthetic modification of MOF.

Recently, thin continuous MOF membranes on organic/inorganic porous supports for gas and liquid separation have been reported by several research groups using MOFs such as MOF-5 [[a]Liu (2009), Yoo (2009)], HKUST-1 [Gascon (2008), Guo (2009), Guerrero (2010), Mao (2013)], CAU-1 [Zhou (2013)], $Zn_2(bdc)_2dabco$ [Huang (2014)], MIL-53 [Hu (2010)], NH_2-MIL-53(Al) [Zhang[a] (2012)], $Cu(bipy)_2(SiF_6)$ [Fan (2013)], Bio-MOF-13 and Bio-MOF-14 [Xie (2014)], Cu-(hfipbb)$(H_2hfipbb)_{0.5}$ [Ranjan (2009)], ZIF-8 [Bux (2009), Venna (2010), McCarthy (2010)], ZIF-7 [Li (2010)], ZIF-22 [Huang (2010)], ZIF-69 [Liu (2010, 2011)], ZIF-78 [Dong (2012)], ZIF-90 [Huang (2010)], SIM-1 [Aguado (2011)], UiO-66 [Liu (2015)], etc. The preparation of these membranes is easier than the zeolites due to easy synthesis at milder conditions. The major problem with these membranes is grain boundary defects which reduces their separation performance. In some of these studies where almost defect free films were obtained show the potential of MOFs as high performance membrane material [Kwon (2013), Shah (2013), Hara (2014)]. The poor mechanical stability of these membranes is another issue in their scale up for practical application.

1.5 Gas transport through membranes

Polymers and microporous materials are the principle materials used for the gas separation membrane preparation. Gas permeation mechanism in these materials is very different as described in the following sections.

1.5.1 Gas permeation through polymeric membranes

1.5.1.1 Mechanism

The permeability, which is the flux of a penetrant normalized by the pressure-driving force and thickness, is given by equation (1.1),

$$P_A = \frac{Q_A}{\Delta p_A / l} \tag{1.1}$$

where P_A is the permeability of component A, Δp_A is the pressure difference across the membrane as driving force, and l is the thickness of the membrane. This equation is valid for ideal components, which allows the driving force to be described by the difference in partial pressures. In nonideal cases, the difference in

partial pressure of components is replaced with their corresponding fugacity. Gas flux through the membrane normally follows Fick's first law.

$$Q_A = -D_A(dC_A/dx) \tag{1.2}$$

where D_A is the diffusivity and C_A is the local concentration of a gas in the membrane. The diffusivity is normally considered concentration independent with some deviations in the case of highly soluble gases.

Thus the permeability coefficient could be is given as the product of diffusivity and solubility coefficients,

$$P_A = D_A S_A \tag{1.3}$$

where, D_A and S_A are diffusivity and solubility coefficients for the component A, respectively. The S_A gives a measure of the amount of penetrant sorbed by the membrane under equilibrium conditions. Gas solubility is dependent on the properties of gas as well as of polymer [Ghosal (1994)]. The average diffusion coefficient D_A is a kinetic parameter, which indicates how fast the penetrant is transferred through a membrane and is determined by polymer-penetrant dynamics.

Selectivity is a membrane's ability to separate a desired component from the feed mixture. Selectivity is often calculated as permselectivity (ratio of permeation of pure gases) or as a separation factor 'α' for a mixture. The permselectivity ($\alpha_{A/B}$) is the product of the diffusivity selectivity and sorption selectivity as given in Equation 1.4.

$$\alpha_{A/B} = \frac{P_A}{P_B} = \left(\frac{D_A}{D_B}\right)\left(\frac{S_A}{S_B}\right) \tag{1.4}$$

The diffusivity selectivity term relates to the ability of polymer matrix to selectively separate penetrants based on their molecular size. As a result, it is governed by the chain backbone rigidity and intersegmental packing. The sorption selectivity favors more condensable penetrants and is affected by the relative affinity between the penetrants and the polymer matrix [Hellum (1989), Ghosal (1994)].

The diffusivity of the penetrants decreases with the increasing size of the molecules, while the sorption coefficients normally increase with the increasing size due to the increased van der Waals interaction. Thus, the diffusivity and solubility works in opposite direction in some cases like H_2/CO_2, H_2/N_2 and H_2/CH_4 separation. In case of rubbery polymers, the soft chains are not able to generate the large difference in the gas diffusivity based on their size, thus the solubility selectivity dominates the membrane selectivity. On the other hand the glassy polymers show strong diffusion selectivity due to their rigid chain structure which dominates the membrane selectivity.

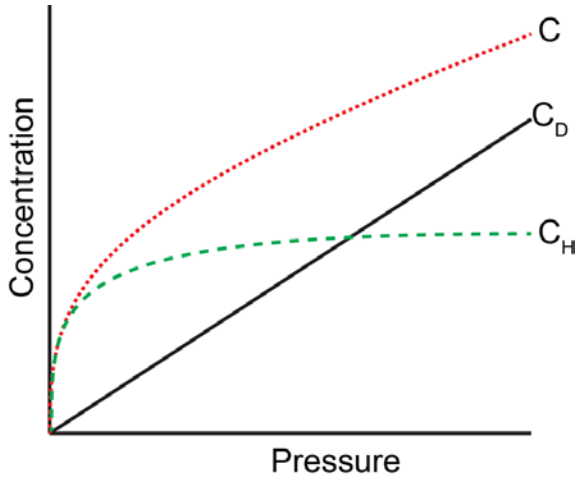

Figure 1.9 Schematic representation of the dual mode sorption.

Rubbery polymers show a typical Henery type sorption behavior, where the penetrant concentration in polymer increases with its increasing partial pressure as shown in the Figure 1.9. On the other hand, the glassy polymers show a very unusual sorption behavior which is partially Henery type and partially Langmuir type (Figure 1.9). Thus the sorption could be expressed as following equation:

$$C = C_D + C_H = k_D p + \frac{C'_H \, bp}{(1 + bp)} \qquad (1.5)$$

where, the C_D and C_H represents the Henry's Law concentration and the Langmuir concentration. Parameter k_D is Henry's Law coefficient, b is the Langmuir affinity constant, and C_H is the Langmuir capacity constant.

The thermodynamics of the polymer chain packing to be considered for understanding the unique sorption behavior of polymers. The polymer specific volume decreases linearly with decreasing temperature as shown in the Figure 1.10. As the temperature decrease below T_g, the slope of graph reduces. This happens due to the restriction of the segmental mobility of the polymer chains below T_g which do not allow the polymer chains to again achieve the thermodynamic equilibrium. Due to this nonequilibrium, some extra free volume (V_f) remains trapped between the chains. This frozen extra free volume is of microporous nature. Thus in the glassy state, polymers have partial liquid character and partial solid (microporous) character. The partial liquid character is responsible for the Henery type sorption behavior, while the solid character is responsible for the Langmuir type sorption.

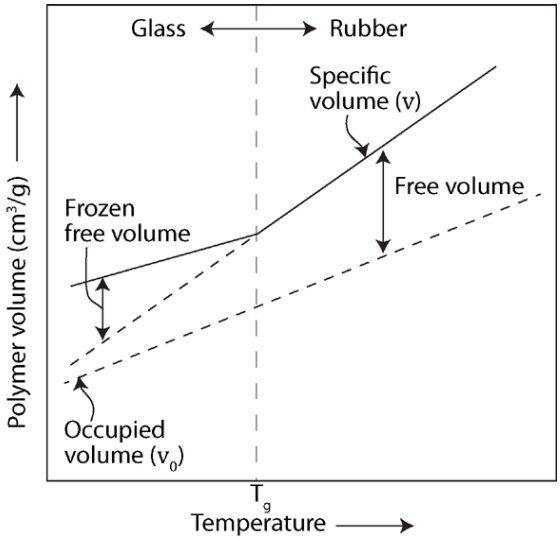

Figure 1.10 Polymer specific volume as a function of temperature [Baker (2000)].

There are various models were proposed to explain the gas permeation through this heterogeneous system. Two most commonly used models are discussed here.

(i) Dual mode model

This is very simple and most accepted model of the gas permeation in glassy polymers. In this model it is assumed that the gas molecules held at Langmuir

sights are completely immobilized, they remain in equilibrium with the Henery population of molecules. The one diffusion coefficient is defined for the mobile Henery population [Vieth (1976)].

(ii) Partial immobilization model

This model is based on the independent dual diffusion of the Henry and Langmuir modes [Paul (1976)]. Partial immobilization assumes that the Langmuir mode species can mobilize partly in glassy polymeric membranes, in contrast to the basic dual-mode model, where the Langmuir mode species is considered not to be mobile. The equation for partial immobilization model is

$$\overline{P} = k_D D_D \left[1 + \frac{FK}{1 + bp} \right] \tag{1.6}$$

$$K = \frac{bC'_H}{k_D} \text{ and } F = \frac{D_H}{D_D}$$

where, D_D is the diffusion coefficient due to the Henry mode species, D_H is the diffusion coefficient due to Langmuir mode species, F is the ratio of the two diffusion coefficients (D_H/D_D), or the mobile fraction of the Langmuir mode species and P is the average permeability coefficient. If we assume F=0, Equation 1.7 reduces to the immobilization model, which is represented by diffusion of the Henry mode species only. In such cases, $P=k_D D_D$ corresponds to the permeability coefficient of rubbery polymeric membranes. The theoretical pressure dependence of the permeability coefficient obeying the partial immobilization model is drawn for different F values in Figure 1.11. The permeability coefficient of the partial immobilization model decreases gradually with an increase in the applied pressure, and then it levels off to the value of $k_D D_D$, irrespective of the value of F.

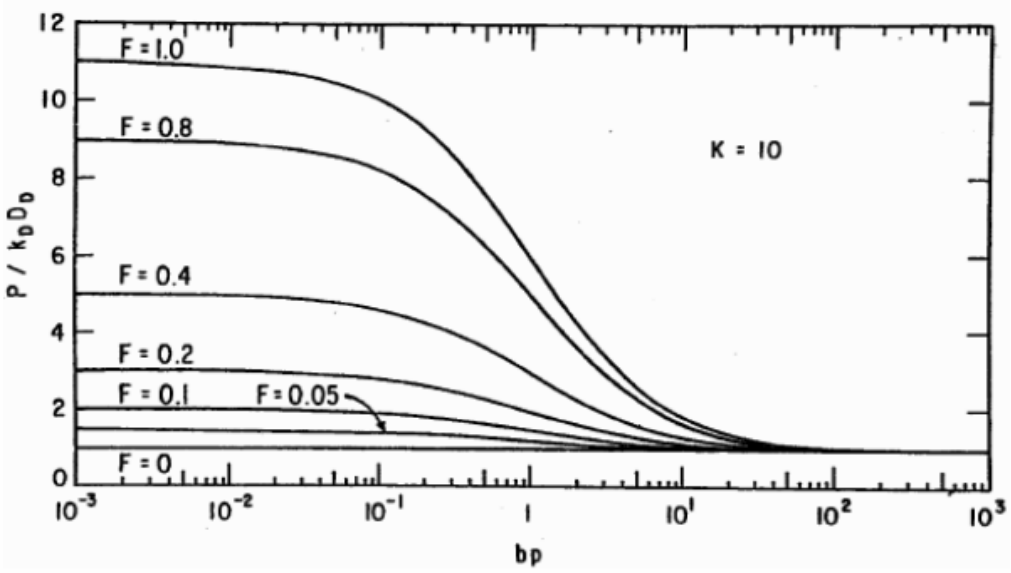

Figure 1.11 Theoretical pressure dependence of permeability in glassy polymers according to partial immobilization model [Paul (1976)].

1.5.1.2 Factors affecting the gas permeation properties of polymer membranes

As discussed above, the gas permeability depends on the diffusivity and solubility of the penetrant in the membrane. Both solubility as well as diffusivity is function of physical properties and structure of membrane material as well as of penetrant properties.

(i) Properties of gas

(a) Dimensions of gas molecules

The Diffusion coefficient of a molecule is inverse function of its size. The kinetic diameter (σ_{KT}) or Lennard-Jonnes collision diameter (σ_{LJ}) of gas molecules gives an approximate account of their size. The linear correlation of diffusion coefficients of gases with their σ_{LJ} values is observed [Tanaka (1996)].

The shape of molecule also play important role in diffusion process. Linear molecules show higher diffusion coefficients than the spherical molecules with similar volume. The ethylene (σ_{LJ} = 4.23) is much larger than the methane (σ_{LJ} = 3.82) but their diffusivity are almost similar due to the flat shape of ethylene which can diffuse easily than the spherical one [Bickel (2000)]. The van der Waals volumes of CO_2 and CH_4 are estimated to be 17.5 and 17.2 cm^3/mole. These

molecular volumes yield equivalent spherical diameters of 3.33 and 3.3Å for CO_2 and CH_4 respectively. Thus, kinetic diameter (3.3Å for CO_2 and 3.8 Å for CH_4) is frequently used to characterize the penetrant size [Ghosal (1994)].

(b) Condensability of gas molecules

The solubility coefficient of a gas in polymer matrix generally increases with increasing gas condensability. The condensability of a gas could be expressed in terms of its critical temperature (T_c), boiling temperature (T_b) or Lennard-Jones force constant (ε/k). These parameters are found to correlate well with the solubility coefficients of the gases in polymers [Tanaka (1996)] as seen in the Figure 1.12.

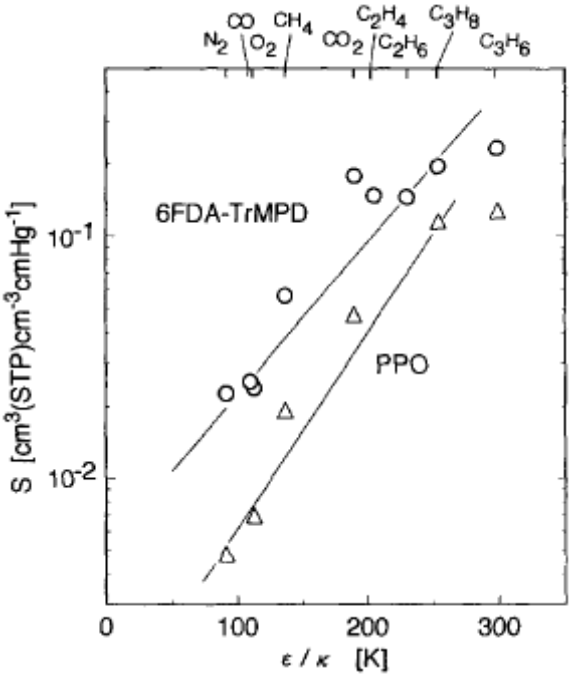

Figure 1.12 Correlation of gas solubility with their Lennard-Jones force constant [Tanaka (1996)].

(ii) Properties of polymer

(a) Chain packing

The polymer chain packing density is also a very crucial factor in determining the permeability of a gas in it. The densely packed chains have little

free volume between them and thus exert more resistance to the penetrating molecules. That's why the semi-crystalline polymers have very low gas permeability compared to the amorphous polymers due to their high packing density. The polymer chain packing density could be expressed in terms of density of polymer, average chain spacing (d_{sp}, determined by the X-ray scattering) and fractional free volume (V_f). V_f is the most approximate measurement of the polymer chain packing. Fractional free volume is a fraction of the total polymer specific volume that is not occupied by the polymer molecules. This excess free volume is due to the two reasons: (i) volume between the polymer chains not occupied due to the steric factor and (ii) a result of trapped non-equilibrium chain conformations due to extraordinarily long relaxation time for segmental motions in the glassy state. The fractional free volume is generally calculated by the group contribution method [Bondi (1964)]. The positron annihilation spectroscopy (PALs), photochromic and fluorescence technique are also used in the experimental determination of free volume and its distribution [Victor (1987)]. The increasing diffusion coefficients were correlated to the increasing V_f for many polymers, viz., polycarbonate [Hellums (1989)], polyimide [Coleman (1990)], polyarylate [Pixton (1995)], polysulfone [Mchattie (1991)] etc.

The diffusion coefficient (D) of a gas is related to V_f by the following equation,

$$D = A\exp(-B/v_f) \qquad (1.7)$$

where, constants A and B are characteristics of the polymer-penetrant system [Ghosal (1996)]. Constant A is related to size and shape of the diffusing molecule, while B is related to the minimum hole size necessary for a diffusion jump [Barbari (1997)]. The solubility of gas molecules is also known to increase with increasing free volume of polymers as the higher free volume accommodates larger number of sorbed molecules in it.

(b) Chain and subgroup mobility

The diffusivity of gas molecules is a strong function of polymer chain rigidity. In the Figure 1.13 diffusivity in a rubbery and a glassy polymer are plotted

to their kinetic diameter. It can be seen that the diffusion coefficients sharply decrease with increasing size in the gassy polymer while in the rubbery polymer a comparatively small change occurs.

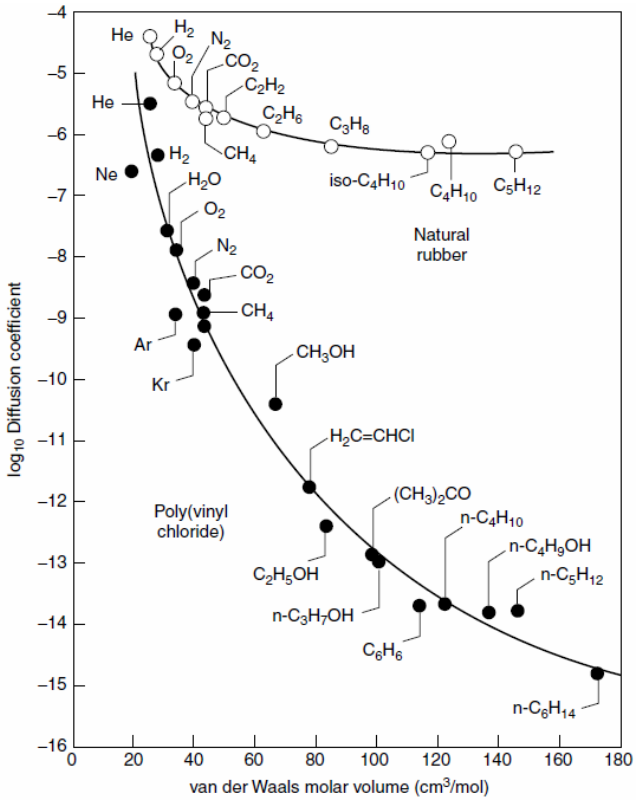

Figure 1.13 Diffusion coefficient as a function of molar volume for a variety of permeants in natural rubber and in PVC, a glassy polymer [Baker (2000)].

The rigid polymer chains create the high energy barrier for diffusion jump of a gas molecule from one free volume element to other in the polymer matrix. This leads to exponential decrease in the diffusivity of the lager molecules in such polymers. On the other hand in rubbery polymers soft chain segments makes very small energy barrier for the diffusion jump of molecule from one free volume element to other which could be easily overcome.

The glass transition temperature (T_g) of a polymer is generally considered as a measure of chain rigidity. Generally, the high T_g polymers show higher diffusion selectivity than the low T_g polymers [Ghosal (1994)]. Thus many efforts are reported in the literature for increasing rigidity of the polymers to achieve high

selectivity based size of permeating molecules. The rigidity of a polymer chain in the bulk polymer depends on the flexibility of the backbone and its interaction with the other chains. The polymer chain with the less flexible linkage in the backbone is generally more rigid and show higher T_g. The polymers of intrinsic microporosity (PIMs) are such polymers with high rigidity due to stiff backbone structure [McKeown (2010)]. The inter-chain interaction is also significantly affects the rigidity of chain in the bulk polymer. The greater interactions between the adjacent chains make them strongly oriented with respect to each other resulting in increased rigidity. The polybenzimidazoles with strong inter-chain hydrogen bonding are very rigid polymers and show high glass transition temperatures [Kumbharkar (2006)].

(c) Polarity

The polarity arises from the uneven distribution of the electrons in the chemical bonds. The more polar structure of polymer is expected to increase the selective sorption of the polymer in favor of the more polar molecule. The structural modifications to improve the solubility component via introducing polar groups are attempted [Van Amerongen (1950), Koros (1985), Ghosal (1992), Story (1991)]. Unfortunately, the more polar structure causes greater attraction between the adjacent chains, resulting in smaller V_f. As a result, polymer chain modification by polar groups like bromo, chloro, nitro, sulfonic/carboxylic acid group and their salts, etc. generally lead to a decrease in permeability and increase in selectivity [Bhole (2007), Ghosal (1992), Muruganandam (1987), Kharul (2002)]. Thus it is proving more advantageous to increase V_f in a polar and therefore selective polymer, than to increase selectivity in nonpolar polymer.

(iii) Operation conditions

(a) Temperature

The diffusivity and solubility both are function of temperature. The diffusion is kinetic process and could be correlated to temperature by the Arrhenius equation. Sorption a thermodynamic process could be correlated to temperature by Clausius Clapeyron equation.

$$D = D_0 e^{-E_a / RT} \quad (1.8)$$

$$S = S_0 e^{\Delta H / RT} \quad (1.9)$$

where E_a activation energy of diffusion; ΔH is the enthalpy of sorption; D_0 and S_0 are the pre-exponential factors for diffusivity and solubility; R is the universal gas constant; and T is the operating temperature.

The diffusion coefficient increases with temperature due to increased chain mobility and kinetic energy of the gas molecules. The decrease in diffusion selectivity occurs with increasing temperature due to the lowering of the activation barrier for larger molecules by reduced stiffness of polymer chain. On the other hand, solubility (exothermic process) decreases with the increasing temperature. Thus diffusivity and solubility factors counter each other with increasing temperature. For the permanent gases, the diffusivity increase is more dominant factor and leads to permeability increase with increasing temperature [Kim (1989), Costello (1994), Gülmüs (2007), de Sales (2008)]. On the other hand for condensable gases solubility reduction is more dominant factor in permeation and thus leads to permeability decrease with increasing temperature [[b]Liu (2009)].

(b) Pressure

As discussed in the section 1.8, glassy polymers show dual mode sorption behavior. Thus solubility decreases with increasing pressure due to saturation of Langmuir sites. The rubbery polymers do not show any significant change in solubility due to Henery type sorption mechanism. The diffusion coefficients are generally weak functions of penetrant pressure and do not change significantly till the penetrant concentration does not affect the polymer chain dynamics. The low sorbing small gases like He, H_2, N_2, and O_2 in either rubbery or glassy polymers show negligible change in permeability with an increase in the pressure [Ghosal (1994), Lin (2001), Merkel (2000), Bondar (2000)]. On the other hand, high sorbing penetrants like CO_2 and larger hydrocarbons show decrease in the permeability in glassy polymers due to decrease in solubility. At the high concentration of the interacting gases, polymer chain starts swelling and become more flexible resulting

in the decrease in the diffusion selectivity. This phenomenon is called plasticization.

1.5.2 Gas permeation through microporous materials

The gas permeation through a microporous material (pore size $\leq$10 Å) is more complex as the both diffusion as well as sorption is strong functions of the applied pressure. The sorption follows typical Langmuir mechanism expressed in the following equation.

$$\mathrm{C}(p) = \frac{C_s b p}{1 + bp} \tag{1.10}$$

where p is gas-phase equilibrium pressure (bar), $C(p)$ is the amount adsorbed (mmol/g), C_s is the capacity constant (mmol/g), and b is the affinity constant (1/bar).

The transport diffusivity of adsorbate molecules in the microporous material as given in the following equation is function of the adsorbate loading in the particle [Karger (1991)].

$$\mathrm{D} = D_0 \frac{d \ln p}{d \ln C(p)} \tag{1.11}$$

where D (cm^2/s) is the loading-dependent transport diffusivity, D_0 (cm^2/s) is the thermodynamically corrected diffusivity (the Maxwell-Stefan diffusivity) [Keil (2000)], $C(p)$ (mmol/g) is the amount adsorbed, and p (bar) is the gas-phase equilibrium pressure. Therefore, D/D_0 is dependent on the non-linearity of the adsorption isotherm. Generally, assuming that the adsorption isotherm can be described using the Langmuir model (equation 1.10); it will be easy to obtain the following relationship [Karger (1991)]:

$$\mathrm{D} = \frac{D_0}{1 - \theta} \tag{1.12}$$

Where $\theta = C(p)/C_s$, which is the surface fractional coverage.

Part B: Composite membranes: Brief literature survey

1.6 Composite/mixed matrix membranes: An Introduction

The polymeric membranes have moderate separation characteristics and are also facing the trade-off in the permeation properties as discussed in the section 1.5.1. On the other hand the ordered porous materials which have high inherent separation characteristics, but are not able to form the defect free membranes with high surface area. These limitations with the materials led to the concept of making blend/composite/hybrid/mixed matrix membrane (MMM) of polymer and ordered porous materials to combine the advantages of both the materials (Figure 1.14). In the ideal composite, polymer is expected to help in the easy processing into defect free membrane, while the porous filler will enhance the separation performance of the membrane. The right combination of permeation properties and chemical functionality is required for preparation of high performance composite membrane. The good compatibility between the two phases is proved very tedious. There are lot of literature reports on such composites and only few have shown the promising improvement in the separation performance. There are many types of porous filler like Zeolites, CNT, CNF, carbon molecular sieves and recently MOFs are used as fillers in the composite membranes [Chung (2007), Zornoza (2013)].

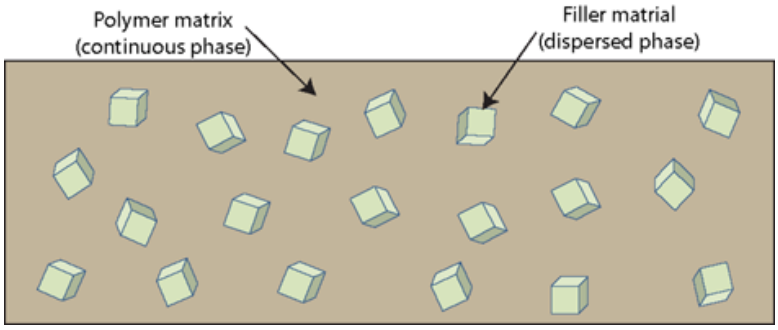

Figure 1.14 Schematic of composite membrane.

The first investigation on the composite membranes was reported by Paul *et al.* in 1973 when they observed the increased diffusion time lag for CO_2 and CH_4 with the addition of 5A zeolite into a rubbery polymer polydimethyl siloxane (PDMS) [Paul (1973)]. In this composite, though the change in time lag was significant, but the steady

state permeation was little affected. The achievement of superior gas permeation properties of MMMs to that of pure polymeric membrane was first reported in 1988 by UOP researchers [Kulprathipanja (1988)]. They observed an enhanced O_2/N_2 selectivity from 3.0 to 4.06 with 25% addition of silicalite in the cellulose acetate (CA) matrix. This work has stimulated further research in the area and led to many publications reporting incorporation of many kinds of fillers in the polymeric systems to improve their permeation properties [Chung (2007), Zornoza (2012), Jeazet (2012)].

1.7 Factors affecting gas permeation of composite membranes

The most of efforts to improve the separation performance had failed due to various non ideal effects. These non ideal effects could be either inhomogeneous distribution of filler particles or polymer-filler interfacial defects. There could be several reasons for these nonidealities which are discussed here.

1.7.1 Inhomogeneous distribution of filler particles

The inhomogeneous distribution of filler particles in composite membrane includes sedimentation and agglomeration of particles. The particle sedimentation could occur due to the various reasons. The large size filler particles can easily sediment during the solution casting of dilute solution. The heating or cooling of casted solution is also known to promote the uneven distribution of filler particles [Chung (2007)] in case of dilute solution casting. The fast solvent evaporation leads to formation of temperature gradient in the casted solution. This temperature gradient promotes formation of convection cells in the solution which takes the lighter filler particles on the top of solution and creates the inhomogeneity in the solution and resulting membrane. These issues could be solved by casting viscous composite solution. In the hollow fiber spinning of mixed matrix composite membranes, shear rate, and air gap have a very crucial role in determining filler particle distribution in the resulting membrane [Jiang (2005)]. The proper optimization of parameters is necessary to maintain the homogeneity of the particles into the separation layer. The filler particle agglomeration is another reason for the inhomogeneity of composite membranes. The filler particle agglomeration could happen be due to poor dispersion of the particles in the casting solution or due to the incompatibility of the filler with the polymer matrix. Normally high percent content of

the filler also causes agglomeration of its particles. The particle agglomeration could be more severe problem in case of the viscous solutions as the very small solvent amount is used to disperse high amount of filler which leads to incomplete dispersion of particles. This is one of the major issues in the fabrication of asymmetric composite membranes with high filler loading. In conclusion, the good dispersion of particles is dependent on both the process control as well as on the compatibility of filler and matrix.

1.7.2 Interface voids

The polymer filler interface morphology is also very crucial for the extracting full advantage of the filler particles. This depends exclusively on the polymer-filler interaction forces. The weak interaction could promote delamination of matrix from the filler surface and create nonselective voids. On the other hand strong adsorption of polymer chains could create high resistance layer between the two phases. The pore blockage of filler by the polymer chains could be another non ideal factor reducing the advantage of filler.

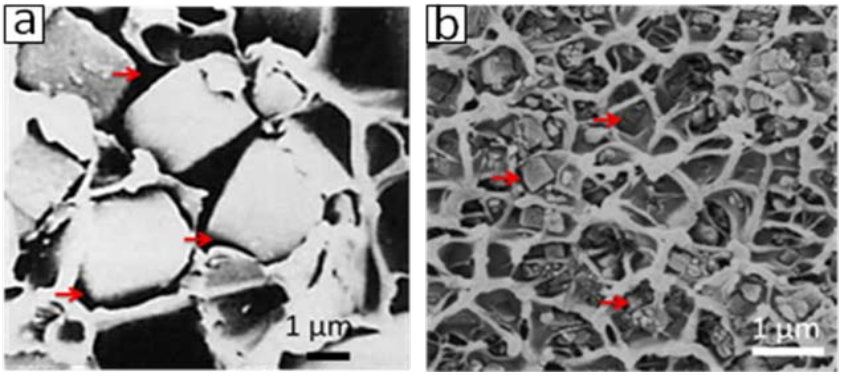

Figure 1.15 Sieve in cage morphology of the mixed matrix membranes: (a) PEI-silicalite composite [Duval (1994)] and (b) Cu-BPY-HFS/Matrimid composite [Zhang (2008)].

The formation of voids at polymer-filler interface is common among the glassy polymer based composite membranes [Chung (2007), Noble (2011), Goh (2011)]. The void formation is explained by the stress generation at interface during the membrane formation. The shrinkage in the volume of polymer chains occurs during the residual solvent removal from the vitrified membrane. It produces the stress, which is relieved by the local segmental movement of the chains. At some stage the polymer phase becomes

glassy and not able make the segmental motion to relieve the stress. Now if the polymer chains are not strongly adhered with the filler surface they can delaminate from the filler surface and create a void as shown in the Figure 1.15. The rubbery polymers maintain the flexibility even after the solvent removal, which can adjust the spatial configuration to reduce the effect of stress. Thus in the composite membranes of rubbery polymers usually have not shown such defects. The size of the filler crystals also significantly affects the void formation. The larger size crystals generally cause interface void formation. It is because (i) they have small contact surface for interaction and (ii) The stress also magnifies on the large facets of crystals.

To encounter the void formation various strategies are adopted in the literature reports. These approaches can be categorized into two parts:

(i) Covalent binding

The covalent bonding of the filler with the polymer was tried to encounter the stress problem [Vankelecom (1996), Pechar (2006), Guiver (2003), Li (2006)]. Zeolite surface was modified with the silane coupling agents as shown in the Figure 1.16. The –OEt groups present on the coupling agent condense with the –OH groups present on the surface of zeolite. The other end of silane coupling agents have primary amine group which could condense with the carboxylic acid group present in the polymer structure, leading to the covalent binding with polymer. These covalent linkage approaches were slightly successful as the voids were not appearing after covalent linking but significant improvement in the permeation properties was not observed in most of the cases. In some cases even the reduction in the permeability in comparison to the pristine polymers was observed [Duval (1994), Mahajan (2002)]. It was possibly due to the pore blockage by excess of binding agent.

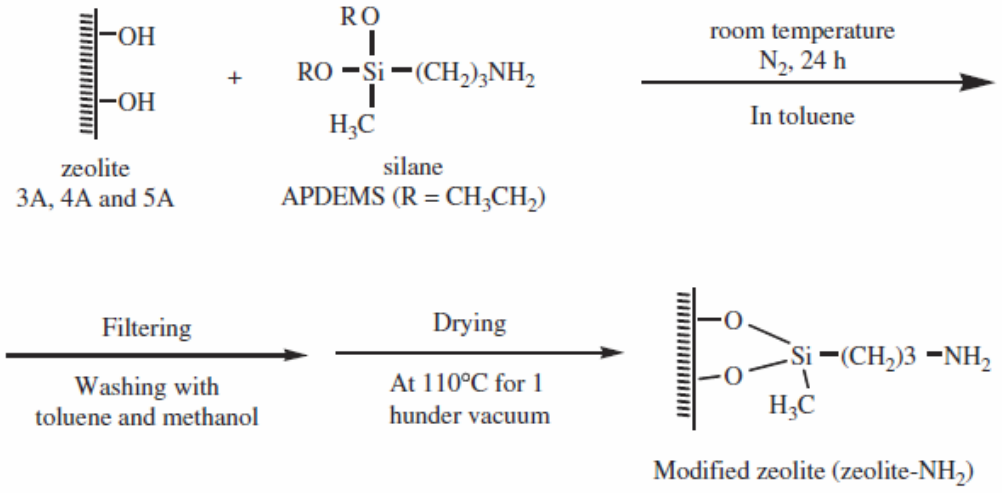

Figure 1.16 Surface modification of zeolites: A schematic representation [Li (2006)].

(ii) Addition of plasticizing agents

Plasticizing agents were mixed with polymer to soften the chains for reducing the void creating stress. But this approach compromises the permeation properties of the matrix with plasticization and was not proved so promising.

1.7.3 Polymer chain rigidification and sieve pore blockage

After formation of intimate contact between the polymer and filler, other non-ideal effects like pore blockage and polymer chain rigidification at the filler surface could also occur. These effects may leave the filler almost impermeable to the gases. The polymer chain rigidification near the filler surface is proved with the non-porous fillers. Moaddeb and Koros [Moaddeb (1997)] investigated the effect of addition of silica particles in the different polymer matrices. They found up to 56% increase in the O_2/N_2 selectivity of 6FDA-MDA with silica particle addition. The increased rigidity of polymer chains due to adsorption on the filler surface was assumed responsible for this improvement in the selectivity. This assumption was supported by the increase in the T_g of polymer matrix. But in case of porous filler addition such strong polymer chain adsorption on the filler surface may reduce the gas diffusivity in the interface region and make the filler practically impermeable. The blockage of molecular sieve pores near interface may also occur by the polymer chain intrusion inside these pores to render them impermeable for the gas permeation [Li (2005)]. It is hard to distinguish whether the barrier is created by

the pore blockage and rigid and dense polymer layer formation near the interface as there is no characterization to investigate it.

1.8 MOFs as filler in composite membranes

As discussed in section.1.5.6, MOFs are made of organic linkers connected with the metal based centre. They are considered more promising fillers over the conventional porous materials like zeolites and CMS due to the following three reasons:

(i) They have higher surface area then the other fillers, thus can be more effective in the flux improvement of polymeric materials.

(ii) Due to the organic part in their structure, it is easier to tune the structure and functionality according to the application.

(iii) The organic nature expected to be more compatible with the polymers for composite membrane fabrication.

(iv) Covalent linkage and surface modification intended for compatiblization is also much easier than the conventional fillers.

The incorporation of MOFs into a polymer matrix for gas separation was first explored by Yehia et al. [Yehia (2004)]. Since then, there are many studies conducted on preparation of MOF-polymer composites for gas separation. These are summarized in the Table 1.

In these studies various polymers and MOFs were mixed together to see the effect of MOFs on the gas permeation properties of composite membranes. In general it can be observed that addition of MOF particles of micron size is not improving the separation performance due to the poor interactions with the matrix [Nik (2012), Zhang (2008), Lin (2014)]. Ge et al have incorporated CuBTC particles of different size in the PPO matrix and observed that the small particles are showing better improvement in the gas permeation properties [Ge (2013)]. There are various methods were used to improve the adhesion of MOF particles with the polymer matrix. As the MOF particles contain the organic functionalities at their surface which could react with the complimentary group on the polymer chain or could be modified to do so. For better compatibility, MOFs with reactive functional group like –CHO and $–NH_2$ are tried. The good adhesion of particles

with polyimide matrix was observed in the SEM images of these composite membranes containing -NH_2 functionalized MOFs [Chen (2012), Nik (2012)]. Yet this good adhesion has not led to great improvement in the gas separation performance of the composite membranes.

Among the composites summarized in Table 1, ZIF-8/6FDA-DAM composite shows simultaneously high improvement in propylene permeability from 15.7 to 56.2 Barrer and selectivity from 12.4 to 31 [Zhang[b] (2012)]. ZIF-8/PBI composite shows high improvement in H_2 permeability from 3.7 to 105 Barrer without losing selectivity [Yang (2012)]. Bae et al. show that when Mg_2(dobdc) added to three different polymers (6FDA-DAM, XLPEO and PDMS), only 6FDA-DAM based composite shows improvement in permeability and selectivity simultaneously [Bae (2013)]. These studies shows that proper combination of MOF and polymer properties is essential for high performing composite membrane formation.

Table 1. MOF@polymer composite membranes and their gas separation performance

Sr. No.	MOF	Polymer	Permeation condition	MOF loading % (best performance)	Separation performance of composite (pristine polymer)	Reference
1	Cu(II) BPDC-TED	PAET	25 °C, 2 bar (pure gas)	10-30 (30)	P (CO_2) = 0.7 (1.4), α (CO_2/CH_4) = 32 (18)	[Yehia (2004)]
2	$[Cu_2(PF_6)(NO_3)(4,4'\text{-bpy})_4](PF_6)_2(H_2O)_2$	PSF	35 °C, 1 bar (pure gas)	2.5-5 (5)	P (H_2) = 10 (13), α (H_2/CH_4) = 203 (54)	[Won (2005)]
3	$(Cu_3(BTC)_2$	PDMS	-	10-40 (30)	P (CO_2) = 2900 (2500), α (CO_2/CH_4) = 3.6 (3.1)	[Car (2006)]
4	$(Cu_3(BTC)_2$	PSF		5-10 (5)	P (CO_2) =7.5 (6.5), α (CO_2/CH_4) = 25 (19)	
5	$Mn(HCOO)_2$	PSF		5-10 (10)	P (CO_2) =7 (6.5), α(CO_2/CH_4) = 9.5 (19)	
6	Cu-BPY-HFS	Matrimid	35 °C, 2.7 bar (pure gas)	10-40 (40)	P (H_2)=26.7(17.5), α (H_2/N_2) = 54.8 (79.5); P (CO_2)=15.6(7.3), α (CO_2/CH_4) = 25.5 (34.7)	[Zhang (2008)]
7	$(Cu_3(BTC)_2$	Matrimid	50 °C, 7 bar (pure gas)	30	P (CO_2) =22.1 (10), α(CO_2/CH_4) = 29.8 (28.2)	[Liu[c] (2009)]
8	IRMOF-1	Matrimid		20	P (CO_2) =38.8 (10), α(CO_2/CH_4) = 29.2 (28.2)	
9	IRMOF-1	Ultem		10-20 (20)	P (CO_2) =2.97 (1.95), α(CO_2/CH_4) = 23.6 (30.3)	
10	CuTPA	PVAc	35 °C, 4.42 bar (pure gas)	15	P (CO_2) = 3.3 (2.4), α(CO_2/CH_4) = 40.4 (34.9)	[Adams (2010)]

Sr. No.	MOF	Polymer	Permeation condition	MOF loading % (best performance)	Separation performance of composite (pristine polymer)	Reference
11	ZIF-90	6FDA-DAM	35 °C, 4.5 bar (mixed gas, 1:1)	15	P (CO_2) = 720 (390), α(CO_2/CH_4) = 24 (37)	[Bae (2010)]
		Ultem			P (CO_2) = 2.9 (1.4), α(CO_2/CH_4) = 39 (38)	
		Matrimid		15	P (CO_2) = 10.5 (7.5), α(CO_2/CH_4) = 35 (34)	
12	ZIF-8	Matrimid	35 °C, 2.63 bar (pure gas)	20-60 (40)	P (H_2) = 71.2 (28.8), α(H_2/CO_2) = 3.03 (2.96), P (CO_2) = 24.5 (9.5) α(CO_2/CH_4) = 35 (27.6)	[Ordõnez (2010)]
13	ZIF-7	PBI	35 °C, 7 bar (mixed gas 1:1)	10-50 (50)	P (H_2) = 13.3 (2.9), α(H_2/CO_2) = 7.2 (7.1)	[Yang (2011)]
14	ZIF-20	PSF	35 °C, 2 bar	8	P (O_2) = 1 (1.6), α(O_2/N_2) = 6.7 (4.7)	[Seoane (2011)]
15	ZIF-8	PEES	30 °C, 1 bar (pure gas)	10-30 (30)	P (CO_2) = 50 (5.72), α(CO_2/CH_4) = 20.8 (22.9)	[Diaz (2011)]
16	MIL-101	PSF	30 °C, 3 bar (pure gas)	8-24 (24)	P (O_2) = 5.25 (1.47), α(O_2/N_2) = 5.42 (5.89)	[Jeazet (2012)]
17	ZIF-8	6FDA-DAM	35 °C, 2 bar (pure gas)	15-50 (50)	P (C_3H_6) = 56.2 (15.7), α(C_3H_6/C_3H_8) = 31 (12.4)	[Zhang[b] (2012)]
18	ZIF-8	PBI	35 °C, 3.5 bar (pure gas)	15-60 (35)	P (H_2) = 238.6 (3.7), α(H_2/CO_2) = 7 (8.6)	[Yang (2012)]

Sr. No.	MOF	Polymer	Permeation condition	MOF loading % (best performance)	Separation performance of composite (pristine polymer)	Reference
19	UiO-66	6FDA-ODA	35 °C, 10 bar	25	P (CO_2) = 50.4 (14.4), α(CO_2/CH_4) = 46.1 (44.1)	[Nik (2012)]
	NH_2UiO-66			25	P (CO_2) = 13.7 (14.4), α(CO_2/CH_4) = 51.6 (44.1)	
	MOF-199			25	P (CO_2) = 21.8 (14.4), α(CO_2/CH_4) = 51.2 (44.1)	
	NH_2MOF-199			25	P (CO_2) = 26.6 (14.4), α(CO_2/CH_4) = 59.6 (44.1)	
	UiO-67			25	P (CO_2) = 20.8 (14.4), α(CO_2/CH_4) = 15 (44.1)	
20	NH_2-MIL-53	Matrimid	35 °C, 3 bar (mixed gas 1:1 mol ratio)	25	P (CO_2) = 2.4 (3.3), α(CO_2/CH_4) = 117 (55)	[Rodenas (2013)]
21	ZIF-90	PBI	35 °C, 3.5 bar (pure gas)	10-45(45)	P (H_2) = 24.5 (4.1), α(H_2/CO_2) = 25 (8.9)	[Yang (2013)]
22	ZIF-8	Copolyimide	35 °C, 10-3.5 bar (pure gas)	5-40 (40)	P (CO_2) = 779 (256), α(CO_2/CH_4) = 20.3 (19.5), P (C_3H_6) = 47.3 (13.2), α(C_3H_6/C_3H_8) = 27.4 (11.7)	[Askari (2013)]
23	ZIF-8	RTIL (P[vbim][NTf_2]/ [emim][NTf_2]/ZIF-8)	35 °C, 3.5 bar (pure gas)	10-25 (25)	P (CO_2) = 693.6 (300.1), α(CO_2/CH_4) = 12.1 (14.8)	[Hao (2013)]
24	ZIF-8	PIM-1	20 °C, 1 bar (pure gas)	11-43 (43)	P (H_2) = 6680 (1630), α(H_2/CH_4) = 15.5 (5.3)	[Bushell (2013)]

Sr. No.	MOF	Polymer	Permeation condition	MOF loading % (best performance)	Separation performance of composite (pristine polymer)	Reference
25	Mg_2(dobdc)	6FDA-TMPDA	25 °C, 2 bar (pure gas)	10	P (CO_2) = 850 (650), α(CO_2/N_2) = 23 (14)	[Bae (2013)]
		XLPEO	25 °C, 2 bar (pure gas)	10	P (CO_2) = 250 (380), α(CO_2/N_2) = 25 (27)	
		PDMS	25 °C, 2 bar (pure gas)	20	P (CO_2) = 2100 (3100), α(CO_2/N_2) = 12 (9.5)	
26	Cd-6F	6FDA-ODA	-	10	P (CO_2) = 38 (21), α(CO_2/N_2) = 35 (26)	[Lin (2014)]
27	MOP	PSF	25 °C, 3 bar (mixed gas 1:1)	8-18 (18)	P (CO_2) = 15.2 (7), α(CO_2/CH_4) = 34 (28)	[Ma (2015)]
28	ZIF-11	Matrimid	35 °C, 3.3 bar(mixed gas 1:1)	10-25	P (H_2) = 95 (20), α(H_2/CO_2) = 4.5 (3.2)	[Láınez (2015)]

1.9 Aims and objective of this thesis

The aim of this work was to investigate the MOFs as fillers in systematically chosen polymers for improving the separation properties of the resultant composite membranes. For preparation of high performance composite membranes, there is a need for understanding the factors affecting homogeneity and gas permeation properties of these membranes. In the compatiblization of filler with the matrix, the role of chemical nature of two phases is very crucial. Thus, the main objective of this work was to understand effects of polymer structural architecture on the gas permeation of the composite membranes. The other objective of the work was to investigate the ZIF-8 based composite membranes for the olefin/paraffin separation performance. The objectives of this work are achieved by the following methodologies.

a) Investigating effects of PBI structural variation on the gas permeation of CuBTC based composite membranes

The objective of this part of the work was to investigate CuBTC as filler material with polybenzimidazoles (PBIs). The CuBTC having the open metal sites is expected to improve the sorption selectivity of the membranes as well as diffusivity due to its high internal free volume. Four structurally different PBIs were blended with the CuBTC in order to understand the role of chemical nature of the polymers on the gas permeation properties of the resultant composite membranes.

b) Investigating effects of PBI structural variation on the gas permeation of ZIF-8 based composite membranes

ZIF-8, a MOF with small aperture size (3.4 Å) and having chemical analogy with PBIs was investigated as the filler material for composite membrane preparation. In this study also, three structurally different PBIs were blended with the ZIF-8 to understand the role of chemical nature of the polymers on the gas permeation properties of the resultant composite membranes. The asymmetric composite membrane preparation was also attempted to improve the MOF loading in matrix and to understand the issues related to thin selective membrane preparation.

c) Investigating olefin/paraffin separation properties of ZIF-8 based composite membranes

Knowing the high kinetic selectivity of ZIF-8 for propylene/propane, the ZIF-8 based composite membranes of the DBzPBI-BuI and PPO (polymers having good propylene permeability) were fabricated and studied for the olefin/paraffin permeation properties. The thin film composite membranes of ZIF-8@DBzPBI-BuI composite material were also fabricated aiming at their evaluation for practical application.

1.10 Organization of the thesis

The work carried out to prepare the MOF@polymer composite membranes and study their gas permeation is organized in the following chapters.

Chapter 1: This chapter reviewed the state of art membrane materials and their mechanism of separation. The issues related of the membrane fabrication and separation performance are discussed in this chapter.

Chapter 2: Experimental procedures for synthesis of materials (MOFs and polymers), fabrication of membranes and method of evaluation of their physical properties are described in this chapter.

Results and discussion is divided into 3 chapters as follows.

Chapter 3: The chapter contains small introduction of the CuBTC and PBIs and the objective of composite membrane preparation. The results and discussion on the preparation of CuBTC, PBIs, their structural modification is given. The composite membrane preparation, their physical characterizations and gas permeation analysis are presented. The effect of structural variation of the PBIs on the gas permeation of the composite membranes is discussed.

Chapter 4: The chapter begins with a brief introduction of the ZIF-8 and the motive behind the composite membrane fabrication. The results and discussion of the preparation of ZIF-8, based composite membrane preparation; their physical characterizations and gas permeation analysis are presented. The effect of structural variation of the PBIs on the gas permeation of the composite membranes is discussed.

Chapter 5: The chapter have first small introduction about the olefin/paraffin separation by the membranes and the related issues. The olefin/paraffin separation performance of the ZIF-8@DBzPBI-BuI composite membranes is presented first, following their transformation into the thin film composite (TFC) morphology. In the end, the preparation of ZIF-8@PPO composite membranes with their physical and gas permeation properties is presented.

Chapter 6: This chapter summarizes the conclusions of MOF@polymer composite membranes preparation, effect of the polymer structure on their gas permeation properties and applicability of these membranes for the olefin/paraffin separation.

Chapter 2

Material syntheses and characterizations

2.1 Monomers and materials

The $Cu(OAc)_2.3H_2O$ and $Zn(NO_3)_2.6H_2O$ were procured from the Loba Chemie. The *1,3,5*-benzene tricarboxilic acid, *2*-methyl imidazole, *3,3'*-diaminobenzidene (DAB), *4,4'*-(hexafluoroisopropylidene)bis(benzoic acid) (HFA), *5-tert*-butylisopthalic acid (BuI), methyl iodide, *4-tert*-butylbenzyl bromide, *2,6*-dimethylphenol and *N,N'*-Dimethylacetamide (DMAc), pyridine and decahydronaphthalene (decalin, a mixture of cis and trans isomer) were procured from Sigma Aldrich. Ethanol, methanol, isopropyl alcohol (IPA), *N,N'*-dimethylformamide (DMF), toluene, tetrahydrofuran (THF) and dimethyl sulfoxide (DMSO) were procured from Thomas Baker. Chloroform and *1,1,2,2*-tetrachloroethane (TCE) were procured from Merck. Polyphosphoric acid was procured from Alfa Aesar.

The gases used, viz. He, H_2, N_2 with 99.9% purity were procured from Vadilal Chemicals Ltd. The CH_4 and CO_2 with 99.995% purity were procured from the Praxair India Pvt. Ltd. The C_2H_4 and C_2H_6 with 99.9% and C_3H_6 and C_3H_8 with 99.5% purity were procured from the Deluxe industrial gases.

2.2 Synthesis of MOFs

2.2.1 Synthesis of CuBTC

The CuBTC was synthesized by following a reported method [Tranchemontagne, 2008]. The BTC (5.00 g, 0.0238 mol) was dissolved in 120 ml of the solvent mixture containing DMF:EtOH:H_2O (1:1:1). A solution of $Cu(OAc)_2.3H_2O$ (8.62 g, 0.0431 mol) in 120 ml of the same solvent mixture was added to the BTC solution while stirring. The TEA (5 ml) was added to this reaction mixture and stirred for 24 h. It was then centrifuged and the sediment was collected. It was washed twice with 200 ml of DMAc and then dispersed in 200 ml of DMAc while stirring and sonicating four times (10 min for each cycle, with an interval of 1 h, while stirring). This suspension remained stable for several days. This suspension was used as a stock solution of CuBTC for further use.

Its concentration was determined by gravimetric estimation. Solvent from two samples (~10 ml each) was removed by evaporation; obtained solid was vacuum dried at 100 °C for a day and weighed.

2.2.2 Synthesis of ZIF-8

The ZIF-8 nanocrystals were synthesized by following a reported method [Cravillon, 2009]. A solution of *2*-methylimidazole (16.22 g, 0.197 mol) was prepared in 500 ml of methanol. A separate solution of $Zn(NO_3)_2 \cdot 6H_2O$ (7.33 g, 0.024 mol) in 500 ml of methanol was prepared. Both, the ligand and metal ion solutions were mixed together and stirred for an hour. It was then centrifuged and the sediment was collected. It was washed twice with 200 ml of DMAc and then dispersed in 200 ml of DMAc while stirring and sonicating four times (10 min for each cycle, with an interval of 1 h, while stirring). This protocol resulted into a suspension which remained stable for several days. This was used as a stock suspension for further use. Its concentration was determined by gravimetric estimation as used for CuBTC.

2.3 Synthesis of Polymers

2.3.1 Synthesis of PBIs

The PBI synthesis is carried out by solution polycondensation at 200 °C in PPA (Scheme 2.1) as reported earlier [Kumbharkar (2006)]. Typically, a three-necked flask equipped with a mechanical stirrer, N_2 inlet and $CaCl_2$ drying tube was charged with 60 g of PPA, 2 g (0.0093 mol) of DAB and the temperature was elevated to 120 °C. A 0.0093 mol of corresponding dicarboxylic acid (HFA or BuI) was added; temperature was elevated to 170 °C and maintained for 5 h under constant flow of nitrogen. The temperature was further raised to 200 °C and maintained for another 8 h. The highly viscous reaction mixture was then precipitated in stirred water. The polymer was treated with saturated sodium bicarbonate solution followed by water washing till neutral to pH. The crude polymer was then soaked in acetone for 5 h and then dried in oven at 100 °C for 12 h. The polymer was further purified by dissolving in DMAc (5% w/w), removing undissolved material, if any, by centrifugation; followed by re-precipitation in water. The precipitated polymer was then soaked in acetone (5 h) and then dried at 100 °C for 12 h.

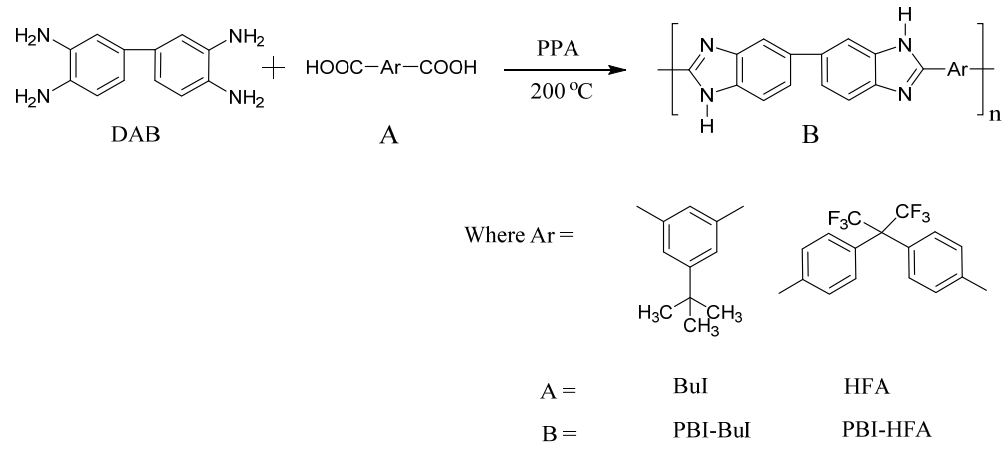

Scheme 2.1 Synthesis of PBIs

2.3.2 *N*-substitution of PBI-BuI

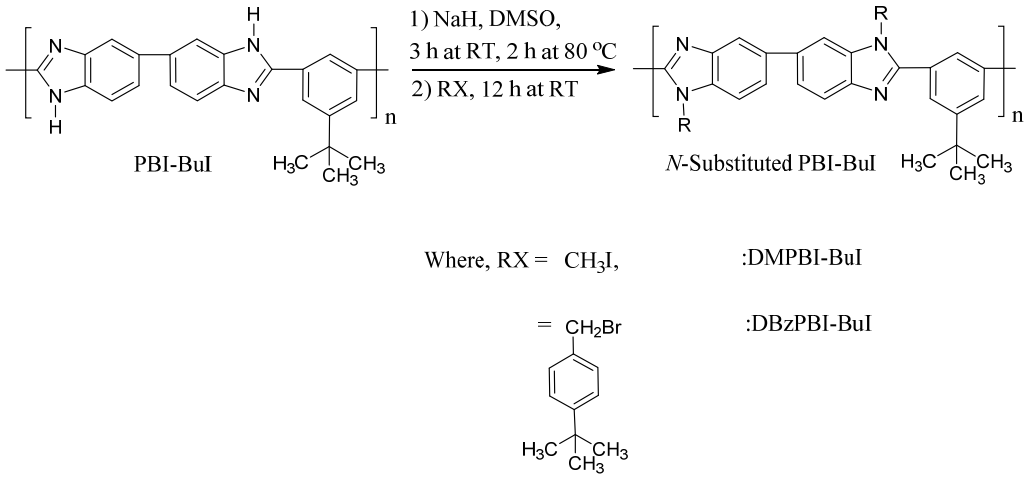

Scheme 2.2 *N*-Substitution of PBI-BuI

The *N*-substitution reaction of PBI-BuI (Scheme 2.2) was carried out as reported earlier [Kumbharkar (2009)]. Typically, in a three-necked round-bottomed flask, PBI-BuI (10.0 g, 0.0275 mol) was dissolved in 300 ml of dry DMSO and 2.1 equivalents of NaH (2.31 g, 0.0576 mol, 60% dispersion in mineral oil) was added under inert atmosphere. The solution was stirred at ambient for 3 h and then at 80 °C for 2 h. The reaction mixture was cooled to the ambient and 2 molar equivalents of alkyl halide (methyl iodide or *4-tert*-butylbenzyl bromide dissolved in 10 ml of dry DMSO) were added in a drop wise manner for a period of 15 min. The reaction mixture got precipitated indicating formation of the *N*-substituted PBI. It was stirred further at ambient temperature for 12 h

and precipitated in acetone. Obtained polymer was separated and vacuum dried at 100 °C for 3 days. It was further purified by dissolving in DMAc and reprecipitation in acetone.

2.3.3 Synthesis of polyphenylene oxide (PPO)

The PPO was synthesized by oxidative coupling of *2,6*-dimethyl phenol as shown in Scheme 2.3; while following the reported procedure [Penczek (1986)]. In a 500 ml three necked round bottom flask, 20 gm of *2,6*-dimethyl phenol (0.164 moles) was added to 10 ml of morpholine and stirred until solution became clear at ambient temperature. The 0.34 gm of $CuCl_2$ (0.00253 mol) and a mixture of toluene-ethanol (160 ml + 40 ml) was added. The oxygen was bubbled into the reaction mixture continuously with stirring. After ~ 6 hours the reaction mixture was precipitated on to stirred methanol, filtered and washed thrice with methanol. The crude polymer was first air dried and then in vacuum oven at 60 °C for 12 hours. For purification, the crude polymer was dissolved into chloroform (4% w/v), filtered and then precipitated in methanol with subsequent drying in vacuum oven at 100 °C.

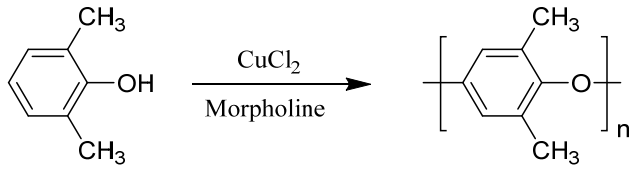

Scheme 2.3 Synthesis of poly-2,6-dimethylphenylene oxide (PPO).

2.4 Membrane preparation

2.4.1 Preparation of dense MOF@polymer composite membrane

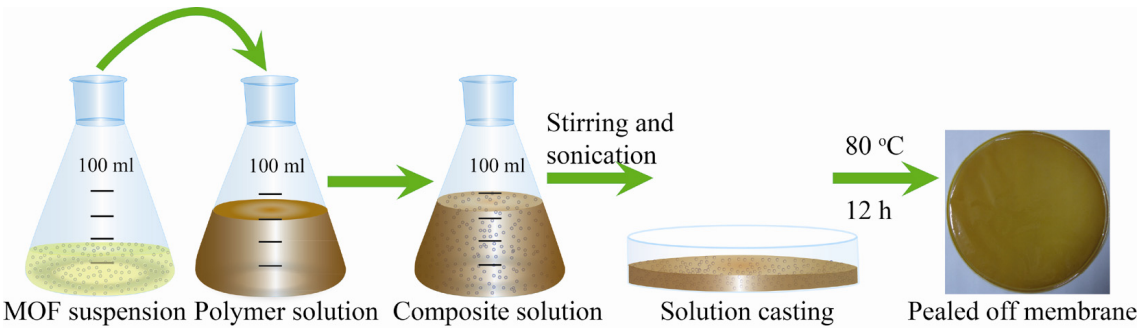

Figure 2.1 Membrane preparation by solution casting method: A schematic representation.

The solution casting method was employed to make dense composite membranes as shown in the Figure 2.1. The polymer solution (3% w/v) was made by dissolving it in a suitable solvent (the DMAc was used as solvent in case of PBI-based membranes while chloroform was used for PPO based membranes). The solution was filtered to remove undissolved particle, if any. This solution was mixed with calibrated amount of stock suspension of the MOF particles, and stirred for 24 h (bath sonicating intermittently for 4 times) in order to obtain a homogeneous suspension. It was then poured on a flat glass Petri dish kept inside a dust free oven with maintained temperature (40 °C for $CHCl_3$, while 80 °C for DMAc as the solvent) in order to evaporate the solvent. The fused calcium chloride was kept inside oven to maintain the dry atmosphere. The membrane was peeled off from the glass surface after 24 h and was kept in the vacuum oven at 100 °C for a week in order to remove traces of the solvent. The obtained membranes were named Z_n@P, where 'Z' refers to ZIF-8, 'n' represents the percentage of ZIF-8 loading (w/w) into the composite membrane, while 'P' represents the name of the polymer.

2.4.2 Preparation of asymmetric MOF@polymer composite membrane

(a) Dual layer casting

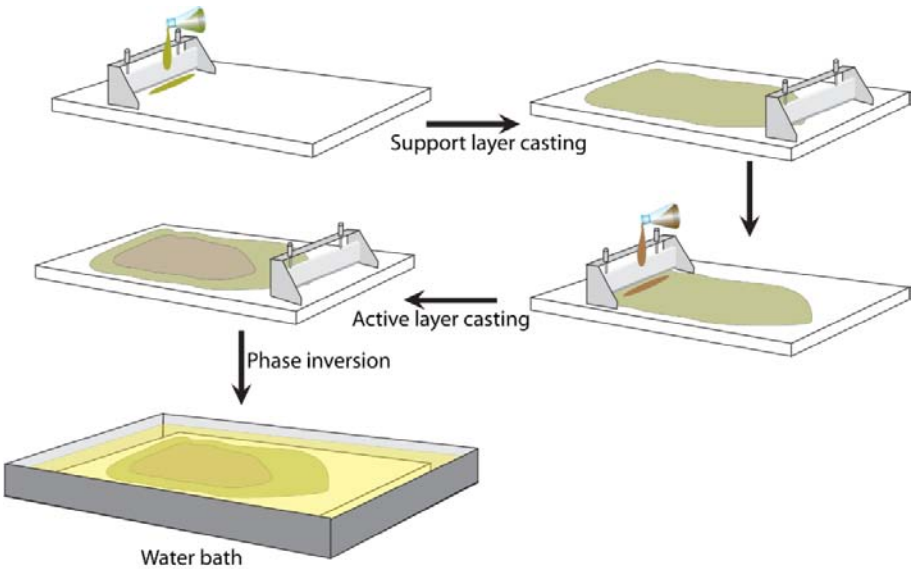

Figure 2.2 Schematic of preparation of the dual layer asymmetric membrane by the phase inversion method

The dual layer asymmetric membrane preparation method is shown in the Figure 2.2. The bottom layer dope solution is 14% PBI-BuI solution prepared in the NMP. The top layer dope suspension has 20% (w/v) concentration (20% w/w PBI-HFA and 80% w/w ZIF-8 nanoparticles) in a solvent mixture, where the solvent mixture composition is varied as given in the Table 2.1. In the first step, the bottom layer dope solution is poured on the clean glass plate and spread evenly by the doctor blade (knife gap = 250 μm) as shown in the Figure 2.2. Immediately, the top layer dope solution is poured on the existing layer and again spread using the doctor knife while setting the knife at additional gap. The casted solutions were kept in air for the defined period of time (Table 2.1) and then dipped into the water for the phase inversion process. The water is changed after every 3 h in order to remove the solvents from the membrane. The membrane was taken out from water after 24 h and first dried in air and then in vacuum oven at ambient for another 24 h. The circular coupons of 3 cm diameter were cut from the dried membrane and used for the gas permeation analysis. These membranes were named as Z_n@P ($Py_xT_yN_z$) where 'Z' refers ZIF-8, 'n' represents content of ZIF-8 in total solid, 'P' is polymer name. The solvent composition is written in the bracket after membrane name, where the initial letter of solvent (Py for pyridine, T for THF and N for NMP) is written with the subscript (x, y and z) representing percentage of the solvent.

Table 2.1 Parameters for the dual layer membrane preparation.

Membrane name	Top layer dope composition	Air drying time
Z_{80}@PBI-HFA ($Py_{50}T_{50}$)	1 g solid (80% ZIF-8 + 20% PBI-HFA) + 4 g solvent (50% Pyridine + 50% THF)	0, 30, 60 , 90, 120 and 300 sec
Z_{80}@PBI-HFA ($Py_{45}T_{45}N_{10}$)	1 g solid (80% ZIF-8 + 20% PBI-HFA) + 4 g solvent (45% Pyridine + 45% THF + 10% NMP)	30, 60 , 90, 120 and 300 sec
Z_{80}@PBI-HFA ($Py_{35}T_{35}N_{30}$)	1 g solid (80% ZIF-8 + 20% PBI-HFA) + 4 g solvent (35% Pyridine + 35% THF + 30% NMP)	30, 60 , 90, 120 and 300 sec

(b) Thin film composite membrane preparation

The thin film composite membranes were prepared by coating of ZIF-8@DBzPBI-BuI composite solution on the pre-dried polyacrylonitrile (PAN)

ultrafiltration membrane and subsequent drying. The coating solution concentration was 4% w/v.

The ultrafiltration type of PAN membrane support with required porosity was made by the phase inversion process already described elsewhere [Lohokare (2011)]. The 17% PAN dope solution in DMF was casted on the nonwoven fabric by a pilot scale membrane casting machine. The prepared membrane roll was kept in water for 24 h in order to remove the traces of solvent and then preserved in the formalin solution in refrigerator at 4 °C till used. The wet membrane was first washed with the deionised water in order to remove the formalin from membrane and then immersed into isopropyl alcohol (IPA) for solvent exchange. After 2 h, the membrane was taken out from the IPA and immersed into the hexane for 2 h to exchange IPA with hexane. Finally the membrane was taken out from hexane and air dried for a day. This membrane was cut into the 14 x 7 cm^2 pieces, and fixed on the glass plate with the cello tape. The clear coating solution (without any dust particle) was spread on the film by dropper and then the film was kept tilted vertically (45°) in order to remove the extra coating solution. The thin dense film forms on the top of PAN membrane after drying of coating solution layer in the air. Thus prepared TFC membranes were dried in the vacuum oven at 60 °C for 12 h in order to remove traces of the solvent. These dried membranes were used for gas permeation and further physical characterization.

2.5 Physical characterization methods

The synthesized polymers were analyzed for their inherent viscosity, ^{1}H-NMR and IR spectra. The inherent viscosity of the 0.2% (w/v) polymer solutions was measured using the Ubbelohde viscometer. The PBI-HFA, PBI-BuI, DMPBI-BuI and DBzPBI-BuI were dissolved in the DMAc for the viscosity measurement, while the PPO solution was made in the TCE. The ^{1}H-NMR spectra were recorded on Bruker AC-200 using DMSO-d_6 as the solvent for PBI-HFA, PBI-BuI and DMPBI-BuI. The DBzPBI-BuI was dissolved in $CDCl_3$ for NMR characterization. The FT-IR spectra of polymers in thin film form (~ 10 μm) were recorded at ambient temperature on Perkin Elmer-16-PC FT-IR spectrophotometer.

Wide angle X-ray diffraction (WAXD) spectra of the MOFs and polymers films were recorded using Rigaku X-ray diffractometer (D-max 2500) with Cu-Kα radiation. The average inter-segmental *d*-spacing (d_{sp}) for the amorphous peak maxima was calculated using Bragg's equation ($n\lambda = 2d\sin\theta$). Thermo gravimetric analysis (TGA) was performed on Perkin Elmer TGA-7 and TGA-5000 (TA instruments, USA) in air with a heating rate of 10 °C/minute.

Scanning electron microscopy (SEM) was performed on a FEI Quanta 200 3D ESEM (dual beam) instrument with a field emitter as an electron source. The powder samples were first dispersed in the methanol by bath sonnication for 10 min. and then drop casted on the silicon wafer for imaging. To image the membrane cross sections, the membranes were fractured in the liquid nitrogen and then mounted on the brass stub vertically. All the samples were gold coated using a sputter coater. Whole area EDAX of the composite membrane was taken on an instrument of resolution 130.2 eV with a voltage of 20 kV.

For the transmission electron microscopy (TEM) images, the MOF samples were prepared by the drop-casting the suspension onto a 200-mesh copper grid coated with carbon film (Ted Pella, INC) and drying under an IR lamp. The membrane samples were prepared by the microtomy. The small membrane pieces were mixed with epoxy resin and cured in a rubber mold to make a solid block. The cured epoxy piece containing the membrane samples is taken out from the mold and was cut into thin slices (100 nm) with diamond razor fitted in the microtome. The thin slice containing membrane piece is mounted on the 200-mesh copper grid and dried for 24 h before the imaging.

The density (ρ) measurement of dry membranes was performed using specific gravity bottle. For this purpose, organic solvent, having adequate density and negligible sorption in membranes was selected. The maximum sorption of decalin in any membrane was ≤ 2 wt % for the exposure of 2 h at 35 °C. Five samples of each membrane were analyzed and variation in the density was found to be ≤1 %.

The mechanical property of the polymer and composite films was measured using Linkam TST-350 microtensile testing instrument. The five film samples were tested for the each material and average values were considered. The samples were analyzed at the low strain rate of 5 $\mu m.s^{-1}$, due to brittle nature of the composite membranes.

2.6 Gas sorption analysis

Pure gases sorption of C_2H_4, C_2H_6, C_3H_6 and C_3H_8 in DBzPBI-BuI and its composite membranes with the ZIF-8 was analyzed at 35 °C and at the incremental pressures up to 4 atm. The gas sorption equipment consisted of dual volume single-transducer set up based on the pressure decay method [Vieth (1966), Karadkar (2006)]. The schematic of sorption equipment is given in Figure 2.3a, while the photograph is given in Figure 2.3b.

The membrane sample was placed in the sorption cell, and then the system was evacuated to 0.00001 mbar using oil diffusion pump. The pure gas is first introduced in the reference volume, after attaining the constant temperature and pressure the gas is released to the cell volume. As the sorption occurs in the sample, gas pressure decreases till the equilibrium attained which is monitored by the pressure transmitter and the data is recorded on PC through Lab-view software. The amount of gas sorbed in the sample at each equilibrium pressure was determined from the initial and final pressure.

The gas solubility coefficient (S), for a gas in these glassy polymers is described by the dual-mode model [Vieth (1976)];

$$S = \frac{C}{P} = k_D + \frac{C'_H b}{(1 + bp)}$$

where, C is gas concentration in polymer, p the applied gas pressure, k_D is the Henry's solubility coefficient, C'_H is the Langmuir capacity constant and b is the Langmuir affinity constant, i.e. the ratio of rate constants of sorption and desorption process [Vieth (1976)]. These constants were obtained by the nonlinear regression analysis of experimentally determined gas sorption by genetic algorithm, an optimization technique capable of searching global optima [Kumbharkar (2006)].

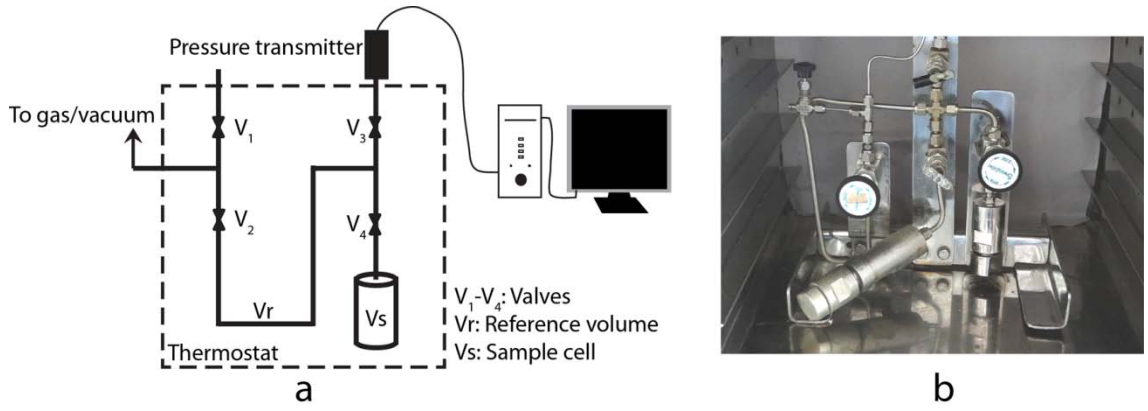

Figure 2.3 (a) Schematic and (b) photograph of gas sorption equipment.

2.7 Gas permeation analysis

2.7.1 Pure gas permeation

The two techniques are used for the pure gas permeability measurement. Basically, the gas flux through the membrane could be measured either as change of the volume in the permeate chamber at atmospheric pressure or as a change of pressure into the closed constant chamber with calibrated volume attached on the permeate side.

(i) Variable volume method

Variable volume method [Stern (1963)] was used for determination of the gas permeability at upstream gas pressure of 20 atm and at 35 °C, while maintaining the permeate side at the atmospheric pressure. A schematic and photograph of permeation equipment are shown in Figure 2.4. One end of the feed side of the cell was connected through valve V_1 to the feed gas cylinder outlet and a WIKA pressure gauge (0-550 psi range). The valve V_2 was placed on the vent and used to control the feed pressure and for flushing of cell. On the permeate side of the permeation cell, a calibrated borosilicate glass capillary (I. D. = either 1.0 or 1.5 mm) containing a small mercury slug (~ 4-6 mm in length) was connected. The membrane cell assembly was kept in thermostat maintained at 35 °C. Displacement of the mercury slug was monitored against time using cathetometer. The permeability (P) was calculated using the following equation.

$$\mathrm{P} = \frac{14.7 \times d \times F.C. \times l}{76 \times A \times t \times \Delta p}$$

where, d = distance traveled by mercury slug (cm), F.C. = flow meter constant [volume of the flow meter capillary per unit length (cm^3/cm)], ℓ= thickness of the membrane (cm), A= effective membrane area (cm^2), t = time (sec), Δp = pressure difference across the membrane (psi). The permeation measurements were repeated with at least 3-5 different membrane samples prepared under identical conditions and the data was averaged. The variation in permeability measurement was up to $\pm$ 15% for different gases studied.

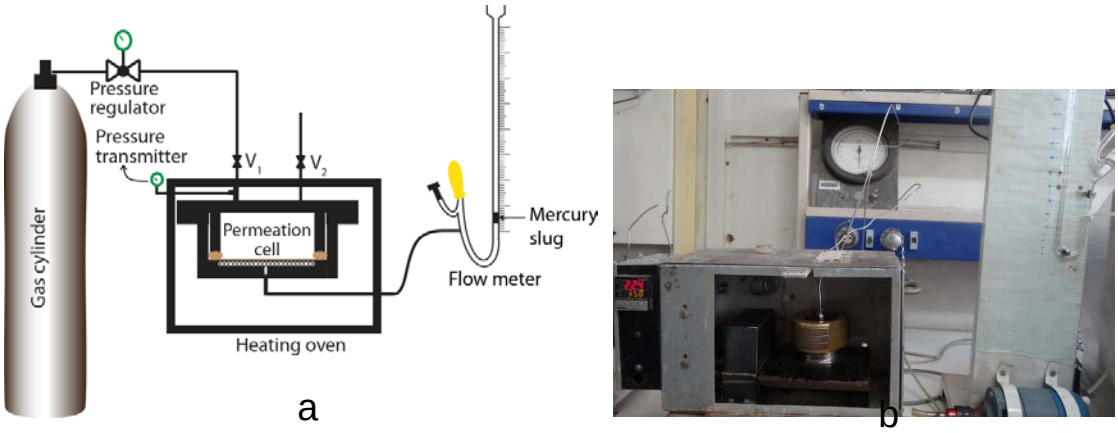

Figure 2.4 (a) Schematic and (b) photograph of gas permeation equipment based on variable volume method.

(ii) Variable pressure method

A schematic and photograph of the variable pressure based gas permeation apparatus is given in Figure 2.5. The film is mounted in the cell as shown in Figure 2.5a. Pure gas is fed to the upstream side of the film by opening the valve (V_1). The WIKA pressure transmitter is attached to the feed side for the pressure measurement. The downstream half of the system consists of an MKS Baratron model 626A pressure transducer with full-scale range of 1-1000 mm Hg with a resolution of 0.001 mm Hg. The permeate side volume was kept small (32 ml) in order to obtain the high sensitivity for the low gas fluxes. In the permeate side, the extra volume of (40.10 ml) can also be attached for the measurement of occasional high fluxes. To avoid any possible interference of permeation through gasket, the permeation cell was specially designed with an inside step. The permeation cell and most of the permeate volume was kept inside the convection oven to maintain the temperature accurately. Feed side pressure

transmitter and permeate side transducer are kept outside the oven due to temperature limitations of transmitters (temperature limit 50 °C).

To minimize stress on the membrane due to the mounting, the membrane was masked with aluminum foil on the edges and sealed with epoxy as shown in the Figure 2.5a. The exposed area of the film was of 5.6 cm^2. The mask gives precise definition of the diffusion area and protects the brittle film from cracking by gasket pressing. The membrane is supported by a smooth and highly porous sintered metal disc on downside to protect the film from rupture.

The calibration volume is determined by careful liquid filling and weighing of the cylinder. Filling the cylinder with low gas pressures permits accurate determination of the volume of the complicated tubing network by simple gas expansion calculations. The Swagelok tube fittings were used to minimize the leaks. On the permeate side Swagelok bellows-sealed valves (V_3 and V_4) have been used. This system is sufficiently leak proof and the minimum leak rate is ~$1x10^{-5}$ torr/sec. were negligible compared to the flux of the lowest permeability component. The gas permeability was measured by determining using the following equation:

$$P = \frac{273\times10^{10}}{760}\,\frac{Vl}{AT(p_2\times76/14.7)}\,\frac{dp}{dt}$$

where P is the membrane gas permeability in Barrer (1 Barrer = $1x10^{-10}$ cm^3 (STP) cm cm^{-2} s^{-1} $cmHg^{-1}$), V represents the volume of the downstream reservoir (cm^3), A is the effective membrane area (cm^2), ℓ refers to the membrane thickness (cm), T is the operating temperature (K) and p_2 indicates the upstream pressure (psi). The ideal selectivity was calculated based on the following equation:

$$\alpha_{a/b} = \frac{P_a}{P_b}$$

where α(a/b) is the selectivity of gas **a** over the gas **b**, while P_a and P_b are permeability of gas **a** and gas **b** respectively.

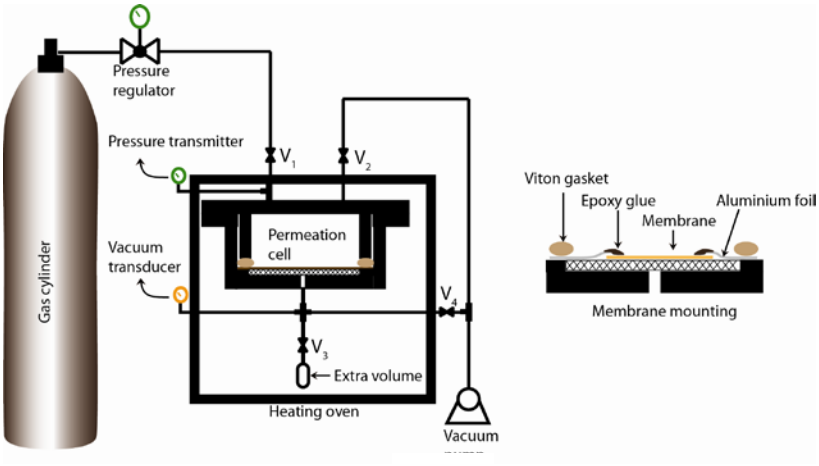

(a)

(b)

Figure 2.5 (a) Schematic of the gas permeation equipment based on variable pressure method, (b) photograph of the equipment used in present work.

2.7.2 Mixed gas permeation

The mixed gas permeation system (Figure 2.6) was similar to the Wicke-Kallenbach technique [Huang (2012)]. The mixed gas was fed to the membrane mounted in the cell. The sufficiently large feed volume (530 ml) was taken to avoid any significant change in the feed composition by membrane permeation. On the permeate side of membrane, the pure nitrogen was swept continuously in order to avoid the concentration polarization. The permeated gases swept out with nitrogen were analyzed with gas chromatograph (GC) to determine their quantity and ratio.

The Haysep-Q packed column of 3 meter length was used for the hydrocarbon analysis. First, the different known amounts of pure gases were injected into the GC and their corresponding peak area was determined to construct the calibration plots. Now in

the further experiments, the unknown gas samples were quantified by determining their peak area and placing that on the calibration plot.

The mixed gas selectivity is calculated from the mole fraction ratio of gas '**a'** and gas '**b'** in the downstream to the upstream as expressed by the following equation:

$$\alpha_{a/b} = \frac{P_a}{P_b} = \frac{y_a / y_a}{x_b / x_b}$$

where P_a and P_b represent the permeabilities of gas '**a'** and gas '**b'**, respectively. The '*x*' and '*y*' refer to the volume fractions of the indicated gas in the feed and permeate, respectively.

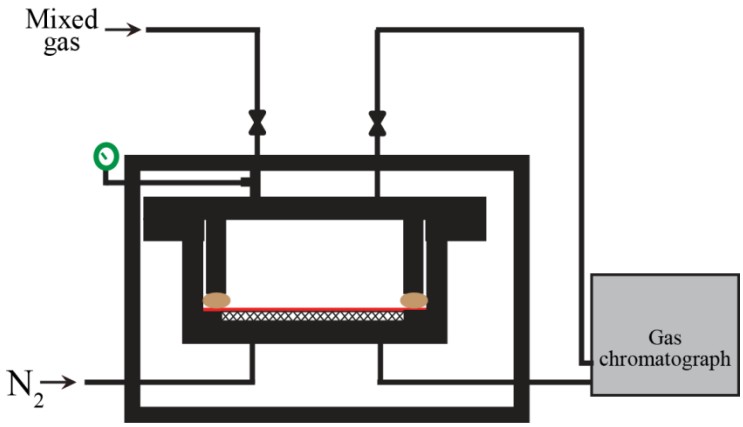

Figure 2.6 Schematic: Mixed gas permeation analysis

Chapter 3

Effect of polymer structural features on gas permeation properties CuBTC@PBI composite membranes

3.1 Introduction

The MOF, viz., HKUST-1, or $Cu_3(btc)_2$ or CuBTC (btc/BTC = *1,3,5*-benzenetricarboxylate) was first synthesized by Chui et al. [Chui (1999)]. It has a three-dimensional network with main channels of 9 Å diameter surrounded by the tetrahedral pockets of 5 Å diameter. The tetrahedral pockets and main channels are connected by triangular windows of 3.5 Å diameter [Keskin (2009)]. The diverse methods of synthesis for CuBTC are reported. It has been synthesized by solvothermal [Kim (2012)], microwave assisted synthesis [Seo (2009)], sonochemical [Khan (2009)], electrochemical [Mueller (2012)] and mechano-chemical [Klimakow (2010)] methods. It was also synthesized by some novel techniques like interfacial synthesis [Ameloot (2011)] and spray drying method [Sánchez (2013)] with precise control on crystal size and morphology. The bulk syntheses of HKUST-1 have also been carried out by hydrothermal approach as well as from mechano-chemical and electrochemical methods using cheap metal source (Cu and $Cu(OH)_2$) [Mueller (2012), Crawford (2015), Majano (2013)]. The salt-free electrochemical methodology using Cu-electrodes is applied in large scale by BASF [Czaja (2009)]. The large scale solvent free continuous synthesis of CuBTC by twin screw extruder is also promising for commercial production of CuBTC [Crawford (2015)]. The CuBTC has shown good performance for gas storage and separation [Panella (2006), Karra (2010)] due to its high surface area and open metal sights. In a comparative study, it is established that CuBTC could outperform the 13X zeolite in selective sorption of CO_2 [Liang (2009)]. The researchers have also made efforts to fabricate dense CuBTC films on the porous supports for gas separation analysis [Guo (2009), Ben (2012), Nan (2011),

Nagaraju (2013), Zhou (2012)]. Though the limited success is achieved in these approaches due to the weak mechanical stability of the crystalline films, these studies demonstrate the potential of CuBTC as the membrane material. The other approach was to add it as fillers in polymeric materials to improve the film formation ability. At the beginning of present work, only a couple of reports were available on such composite methodology utilizing the commercial polyimides, polysulfone and PDMS as the matrix polymer [Basu (2010), Car (2006)]. The addition of the CuBTC as the filler improved permeability to some extent, but the voids at polymer-filler interface led to defective morphology of the membranes. This indicates that customized polymer matrix is required for the composite membrane preparation, and became the objective of this work.

The aromatic polybenzimidazoles have very rigid molecular structure with strong inter-chain H-bonding. They posses excellent thermo-oxidative stability, high glass transition temperature and retain its mechanical properties at high temperature [Vogel (1961, 1963)]. Thus, the conventional PBI (based on isopthalic acid and diaminobenzedene) finds applications in protective coating against heat [Belohlav (1974)]. It is used for making apparels of fire fighters, gear, spacesuit of astronauts, and aircraft wall fabric [Belohlav (1974)]. The good thermo-chemical properties also make PBIs as potential membrane material for gas and vapour separation with high stability in the aggressive feed conditions like high temperature, high pressure and reactive components which can reduce the separation performance or degrade the membrane [Baker (2002)]. Unfortunately, the low gas permeability of the conventional PBI is the main bottleneck in its application as the membrane material. In our lab, PBIs with varying chemical structures are synthesized and considerable improvement in the gas permeability (comparative to the commercial membrane materials) is obtained without losing the thermo-mechanical properties [Kumbharkar (2006, 2010)]. We here intend to improve permeation properties further by addition of highly porous CuBTC in selected members of PBI family.

In this work, we have studied the blend formation and compatibility between CuBTC and polybenzimidazoles with variation in structural architecture of the polymer

matrix. The CuBTC was chosen as the MOF filler due to its easy synthesis and high selective sorption properties. It was blended with four different polymers of polybenzimidazole family. PBI-HFA (based on *4,4′*-(hexafluoroisopropylidene) bis(benzoic acid) and *3,3′*-diaminobenzidene (DAB)) and PBI-BuI (based on *5-tert*-butylisopthalic acid (BuI) and DAB are synthesized. Two *N*-substituted derivatives of PBI-BuI (substitution by methyl and *4-tert*-butylbezyl) were also synthesized. These four polymers were used as matrix for the preparation of composite membranes. Physical properties of the composites were also studied in order to understand the microscopic composite structure.

3.2 Synthesis of CuBTC and polymers

3.2.1 Synthesis of CuBTC

The WAXD pattern of synthesized CuBTC powder matched well with the simulated pattern, confirming the structure of MOF (Figure 3.1a). SEM and TEM images of CuBTC showed particles of 40-80 nm size (Figure 3.1b and c).

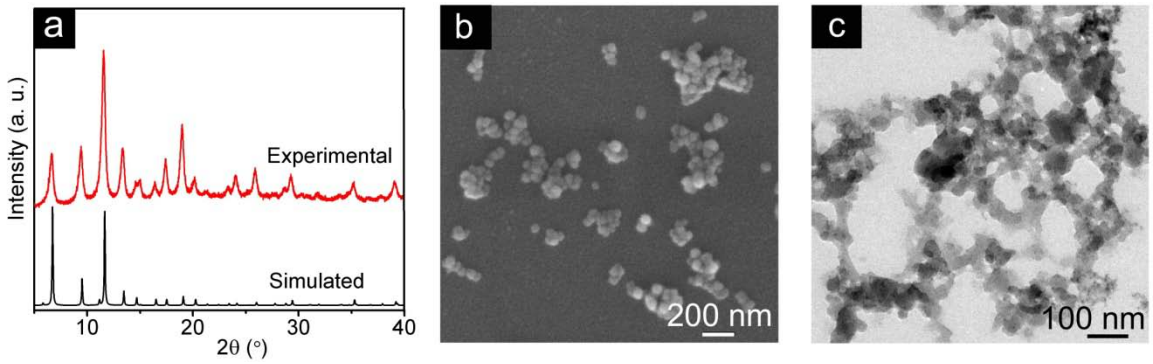

Figure 3.1 (a) The XRD spectra of the synthesized CuBTC in comparison to the simulated spectra, (b) SEM image and (c) TEM image of the CuBTC particles.

3.2.2 Synthesis of polymers

The synthesized PBI-HFA and PBI-BuI exhibited good inherent viscosity of 0.68 and 0.84 dL/g, which indicates high degree of polymerization. FT-IR spectra of the polymers (Figure 3.2) showed peaks of the in-plane ring vibration characteristic of substituted benzimidazole moiety at 1490-1530 cm^{-1}, imidazole ring breathing at 1270-1290 cm^{-1} and imidazole-ring vibration at 800-810 cm^{-1}. These bands confirm completion of the imidazole ring formation during PBI synthesis [Musto (1993)]. After *N*-

substitution, the broad peak at 3000-3400 cm^{-1} due to the –N-H group disappeared, as the proton is replaced by the alkyl group. The ^{1}H-NMR spectra of DMPBI-BuI (Figure 3.3a) showed peaks at 7.78-8.18 ppm for aromatic protons, 4.04 ppm for methyl protons and at 1.47 ppm for *tert*-butyl protons. It confirms the substitution of imidazole proton by methyl group. The ^{1}H-NMR spectra of DBzPBI-BuI (Figure 3.3b) showed peaks at 7.08-8.54 ppm for aromatic protons, 5.83 ppm for methylene protons and at 1.14 ppm for protons belonging to the *tert*-butyl groups. The presence of peak for methylene protons in the spectrum confirms the *N*-substitution by the *4-tert*-butylbezyl groups. The degree of *N*-substitution of the PBI-BuI was quantified by the integration of the peaks of ^{1}H-NMR spectra of the substituted polymers. It was found to be ~99% for both, DMPBI-BuI and DBzPBI-BuI.

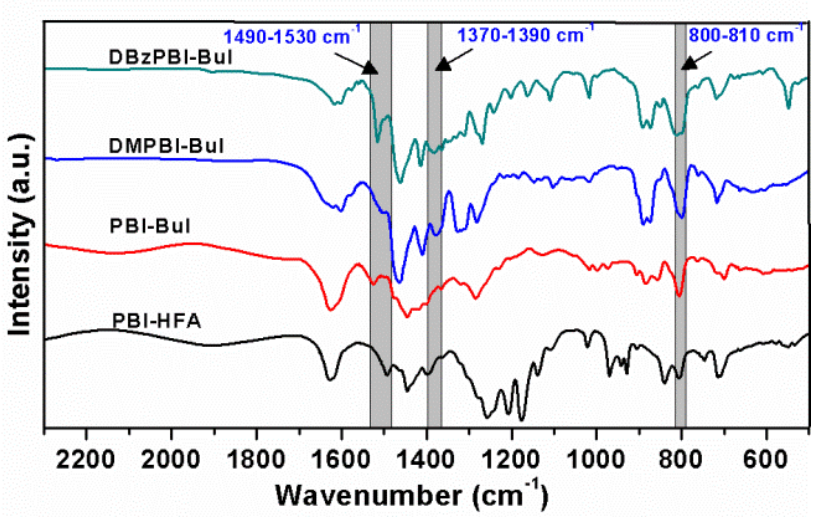

Figure. 3.2 FT-IR spectra of the synthesized polymers

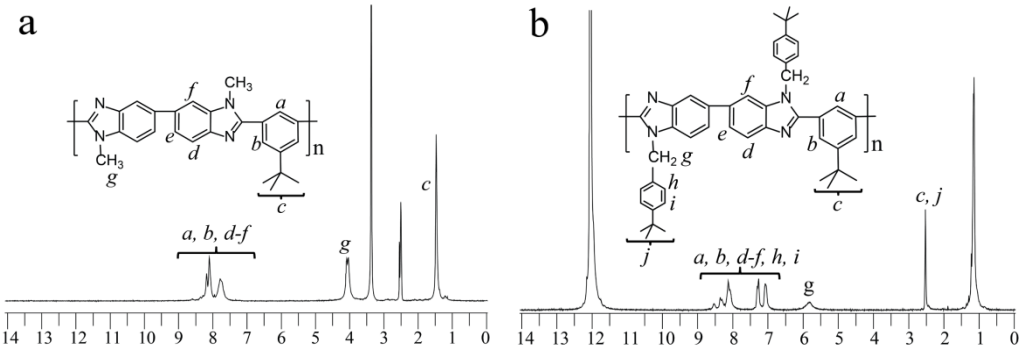

Figure 3.3 ^{1}H-NMR spectra of (a) DMPBI-BuI and (b) DBzPBI-BuI.

The WAXD spectrums of all polymers showed a broad hollow, a characteristic of their amorphous nature (Figure 3.4), which corresponds to the average inter-chain separation (d_{sp}) in the polymer matrix. The d_{sp} calculated from the Bragg's equation was 4.76 Å, 4.56 Å, 4.64 Å and 5.27 Å for PBI-HFA, PBI-BuI, DMPBI-BuI and DBzPBI-BuI; respectively. Higher d_{sp} value for DBzPBI-BuI indicates its more open polymer matrix, leading to increase in its gas permeability [Kumbharkar (2010)].

3.3 Physical properties of membranes

In the WAXD pattern of composite membranes, sharp multiple peaks belonging to CuBTC in addition to the characteristic amorphous hollow of host polymers were present (Figure 3.4). Presence of all the sharp peaks belonging to CuBTC in the spectra of composite membranes confirms that the structure of MOF remained intact.

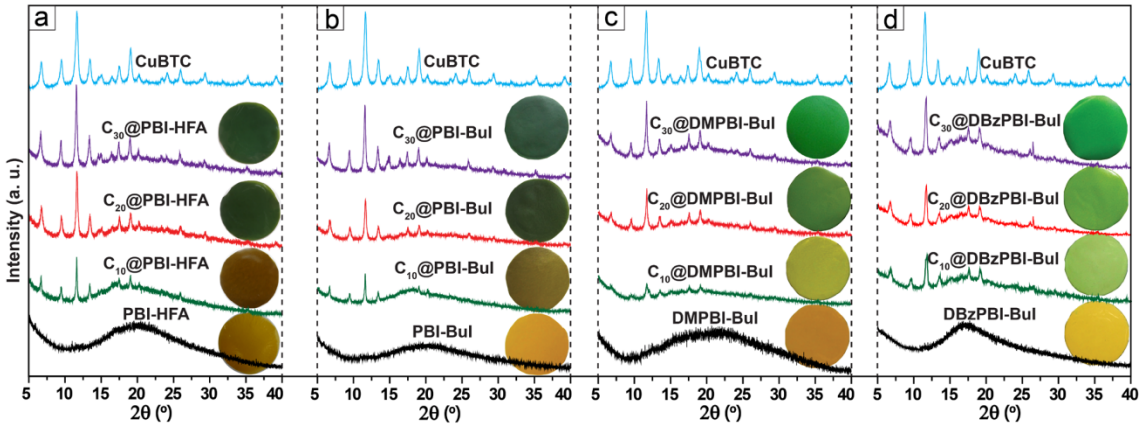

Figure 3.4 WAXD patterns of the composite membranes based on (a) PBI-HFA, (b) PBI-BuI, (c) DMPBI-BuI and (d) DBzPBI-BuI.

The MOF nanoparticles into the membrane cross sections are visible in the SEM images (Figure 3.5). The distribution of particles throughout the composite membrane cross section looks even as no sedimentation of particles was observed. It is also proved by the further elemental mapping of membranes as shown in the Figure 3.6. The intensity of Cu is uniform throughout the membrane cross section. This could be the result of adopted membrane preparation methodology, in which the MOF nanoparticles were added to a polymer solution in the form of their stock suspension. This avoided MOF drying and thus particle agglomeration.

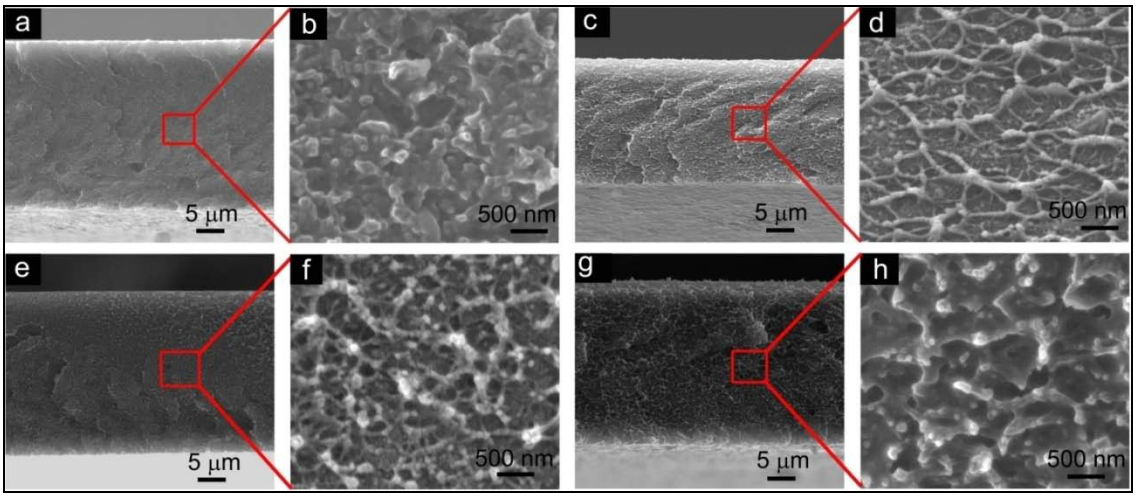

Figure 3.5 SEM images of cross section of CuBTC based composite membranes with; PBI-HFA (a, b), PBI-BuI (c, d), DMPBI-BuI (e, f), and DBzPBI-BuI (g, h).

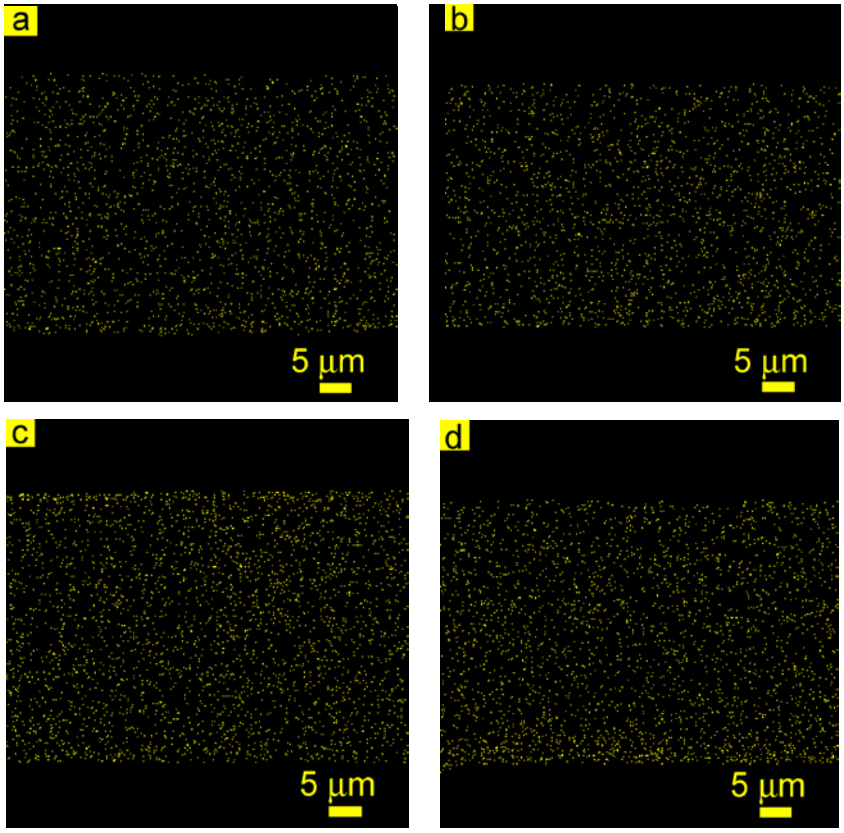

Figure 3.6 Cu mapping of (a) C_{30}@PBI-HFA, (b) C_{30}@PBI-BuI, (c) C_{30}@DMPBI-BuI and (d) C_{30}@DBzPBI-BuI composite membranes.

SEM images of membrane cross section did not show any voids at MOF- polymer interface. This indicates a good compatibility between the MOF and polymer. The voids present in earlier reported composite membranes at Matrimid/$[(Cu)_3(BTC)_2]$ [Basu

(2010)] and Cu-BPY-HFS-Matrimid [Zhang (2008)] interface were absent in the present cases. Polymers chosen for the present work belong to the PBI family possessing two imidazole groups per repeat unit. Absence of any voids in the present composite membranes indicates that PBI and its structural variants have good compatibility with CuBTC. This could be correlated to the imidazole moiety of PBI, which could have interactions with the metal ion at the MOF surface.

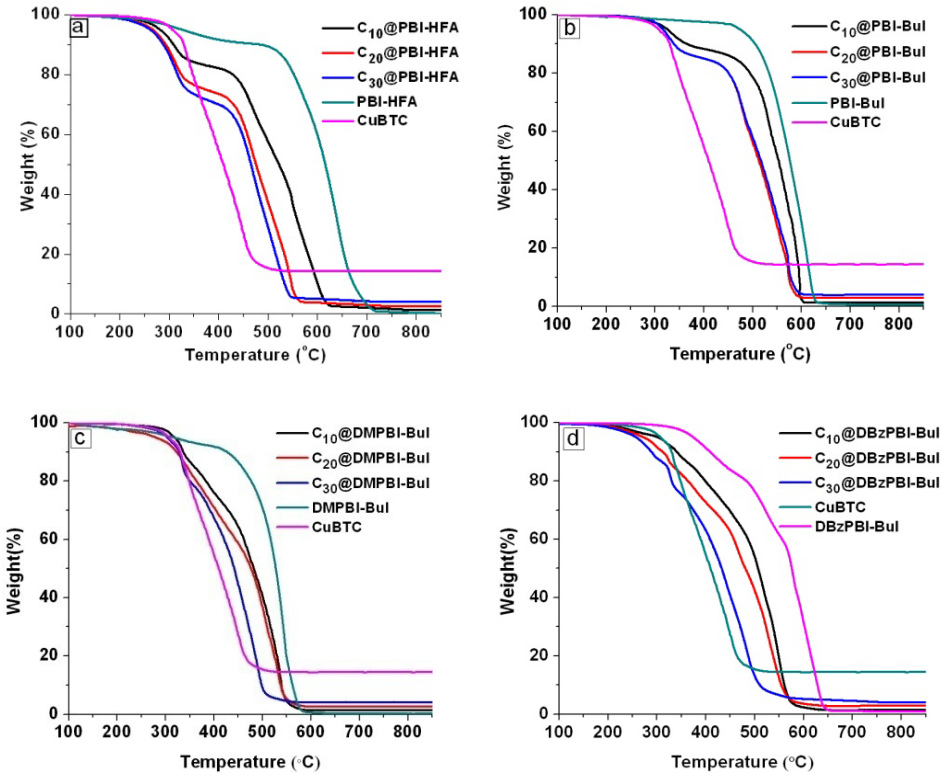

Figure 3.7 TGA thermograms of PBIs, CuBTC and composites: (a) PBI-HFA, CuBTC and their composites, (b) PBI-BuI, CuBTC and their composites, (c) DMPBI-BuI, CuBTC and their composites and (d) DBzPBI-BuI, CuBTC and their composites.

In the TGA analysis in air, the CuBTC showed degradation at the 300 °C (Figure 3.7) that is according to the reported literature [Ge (2013). The PBI-HFA, PBI-BuI, DMPBI-BuI and DBzPBI-BuI are thermally stable up to 520 °C , 500 °C, 450 °C and 350 °C, respectively, in air (Figure 3.7). The DBzPBI-BuI showed comparatively lower thermal stability than other polymers, possibly due to the presence of benzylic group (*tert*-butylbenzyl) in it. The composite membranes started degrading around 300 °C due to the early degradation of CuBTC. The degradation of composite membranes in air

yielded only metal oxides as a char. From this data, accurate estimation of the MOF content in the membrane was made. It matched well with the MOF quantity taken during the preparation of composite membranes (Table 3.1).

Analysis of mechanical properties of composite membranes showed decreasing tensile strength for all the composite membranes with an increase in MOF loading (Table 3.1 and Figure 3.8). This could be attributed to the increased rigidity of membranes due to CuBTC. The small decrease in the modulus for CuBTC@PBI-BuI and CuBTC@DMPBI-BuI composites was observed. The CuBTC@PBI-HFA and CuBTC@DBzPBI-BuI composites did not show any significant change in the modulus which indicates good interaction between the polymer and MOF in these composites. It is worthy to note that all the present membranes were sufficiently flexible and could withstand 20 atm upstream pressure, when mounted in the gas permeation cell.

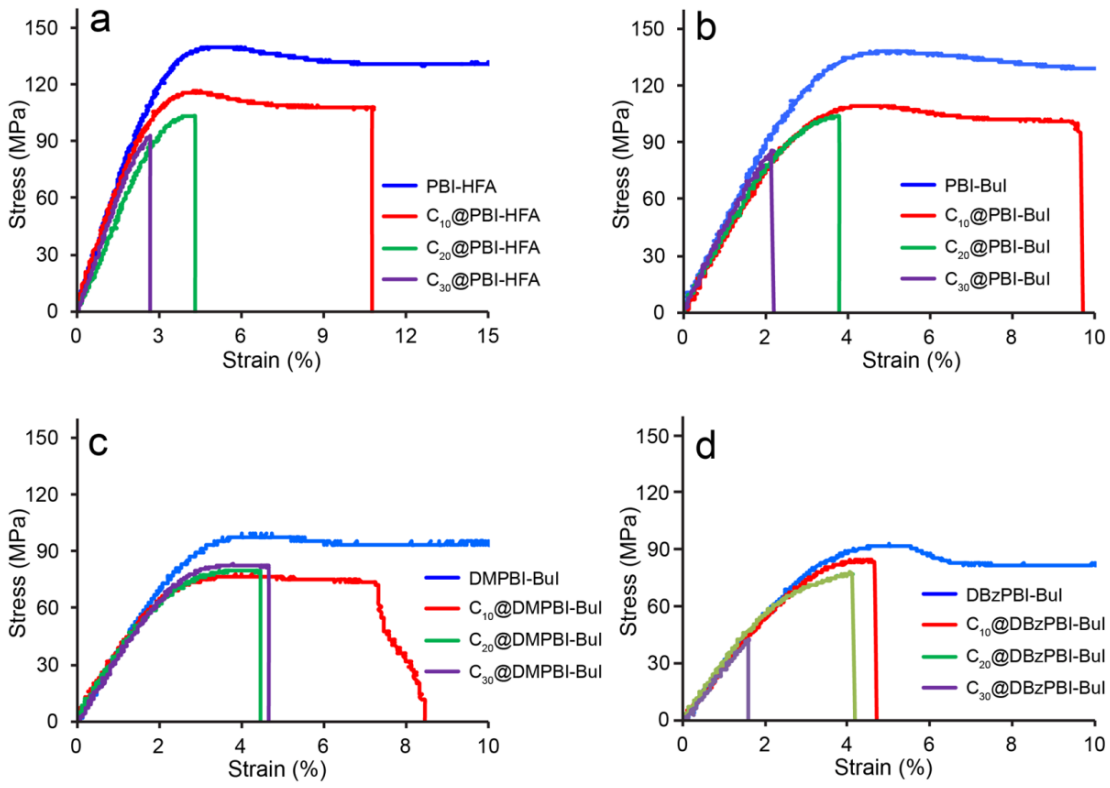

Figure 3.8 The stress-strain curve of the polymer and composite membranes; (a) CuBTC@PBI-HFA composites, (b) CuBTC@PBI-BuI composites, (c) CuBTC@DMPBI-BuI composites and (d) CuBTC@DBzPBI-BuI composites.

The experimental value of density of composite membranes matched well with the theoretically calculated value (Table 3.1). The theoretical density of the composite membranes was calculated by the addition method. The similar values of experimental and theoretical density of composite membranes indicate that CuBTC did not cause any alteration in the polymer matrix. This could be an indirect evidence of absence of voids in the matrix of the composite membranes.

Table 3.1 Physical properties of the polymer and composite membranes.

Membrane	MOF content in membrane (%,)[a]	[b]Density (calc.) ($g.cm^{-3}$)	Density (expt.) ($g.cm^{-3}$)	Mechanical properties		
				Young's Modulus (GPa)	Tensile strength (MPa)	Elongation at break (%)
PBI-HFA	-	-	1.371	4.1	124.3	31.6
C_{10}@PBI-HFA	12.6	1.355	1.351	4.0	115.8	7.2
C_{20}@PBI-HFA	23.4	1.340	1.334	3.9	104.3	4.2
C_{30}@PBI-HFA	34.6	1.325	1.312	3.9	92.7	2.1
PBI-BuI	-	-	1.193	4.2	131.2	26.1
C_{10}@PBI-BuI	9.9	1.196	1.227	3.9	112.1	8.0
C_{20}@PBI-BuI	22.3	1.198	1.242	3.6	101.9	3.7
C_{30}@PBI-BuI	29.9	1.201	1.222	4.0	88.8	2.4
DMPBI-BuI	-	-	1.196	3.3	90.2	53.04
C_{10}@DMPBI-BuI	9.9	1.198	1.200	3.2	78.7	17.9
C_{20}@DMPBI-BuI	20.0	1.201	1.203	3.2	82.0	8.4
C_{30}@DMPBI-BuI	31.0	1.203	1.211	3.2	85.8	5.4
DBzPBI-BuI	-	-	1.097	2.8	92.3	12.6
C_{10}@DBzPBI-BuI	9.8	1.109	1.115	2.9	85.6	5.0
C_{20}@DBzPBI-BuI	23.2	1.122	1.126	2.9	82.0	3.8
C_{30}@DBzPBI-BuI	28.5	1.134	1.138	2.7	52.8	2.0

a: based on char yield observed in TGA spectra; b: Theoretical densities for both type composites were calculated using CuBTC density[1] as 1.22 $g.cm^{-3}$.

3.4 Gas permeability analysis

Pure gas permeation analysis of CuBTC@PBI-HFA composite membranes revels that with increasing CuBTC loading gas permeability of small gases (H_2 and CO_2) increased significantly (Figure 3.9a). The CO_2 permeability of the pristine polymer was 4.4 Barrer, which increased to 8.1 Barrer in composite membrane with 30% CuBTC

content. On the other hand the larger gases like N_2 and CH_4 did not show any significant change in permeability (Table 3.2). As a result, both CO_2/N_2 and CO_2/CH_4 selectivity increased in composite membranes with increasing CuBTC content (Figure 3.9a). As CuBTC is known for its selective CO_2 adsorption, it could be assumed that its addition improved the selective CO_2 permeation by enhancing the sorption properties of the composite membranes (Figure 3.9a). Thus, it can be concluded that the CuBTC as filler has improved the gas permeation of PBI-HFA based membranes. It could be attributed to the good compatibility of the polymer with the CuBTC filler particles, as observable in SEM image of membrane cross section (Figure 3.5b). Though the diffusion based selectivity of H_2/N_2 and H_2/CH_4 showed no significant change in composite membranes, it may be due to nonselective diffusion of the molecules inside large pores (9 Å) of CuBTC.

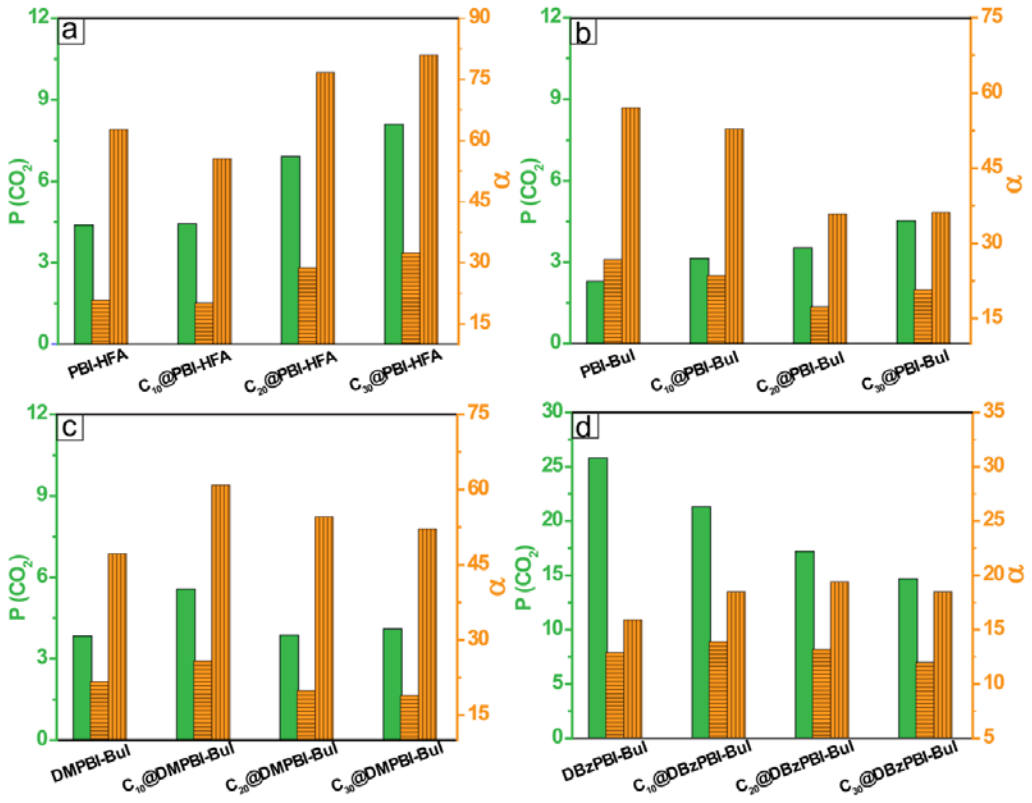

Figure 3.9 Variation in CO_2 permeability (▬) and its selectivity over CH_4 (▬) and N_2 (▬) with CuBTC loading in (a) CuBTC@PBI-HFA, (b) CuBTC@PBI-BuI, (c) CuBTC@DMPBI-BuI and (d) CuBTC@DBzPBI-BuI composite membranes

CuBTC/PBI-BuI composite membranes also showed increase in CO_2 permeability from 2.3 Barrer to the 4.5 Barrer but with the sharp decrease in selectivity over the N_2 and CH_4 (Figure 3.9b). The CO_2/N_2 and CO_2/CH_4 selectivity of the pristine polymer was 26.8 and 57 respectively. Addition of 30% CuBTC led to the decrease in the CO_2/N_2 and CO_2/CH_4 selectivity to 20.8 and 36.2 respectively (Table 3.3). This was against the expectation as the selective CO_2 sorption by CuBTC should have increased the selectivity as seen in the CuBTC@PBI-HFA composites. Such behavior of composite membranes is also reported in the literature and is attributed to the defective morphology of the membrane [Moore (2005)]. The addition of 4A zeolite in the Matrimid caused the reduction of selectivity of the membrane with small increase in the permeability. Any voids between the polymer and CuBTC crystals are not observable in SEM image but some particle agglomeration is visible (Figure 3.5d). These agglomerates may have the inter-crystalline voids which are possibly causing the non selective passage of the gas molecules leading to the loss of separation performance.

In methyl substituted PBI-BuI with addition of CuBTC, a small increase in permeability of CO_2 at 10% CuBTC loading with simultaneous increase in selectivity for CO_2/CH_4 and CO_2/N_2 pairs was observed (Figure 3.9c). By further increase in the loading to 20 and 30%, no significant change in either permeability or selectivity occurred. Thus it could be assumed that at small loading of CuBTC of ~10%, enhancement in the permeation properties could be due to good particle dispersion and polymer-filler adhesion. Beyond this concentration of CuBTC, particle agglomeration predominates as visible in the SEM image of C_{30}@DMPBI-BuI (Figure 3.5f). Similar kind of behavior was also seen in PDMS and CuBTC based composites, where separation performance improved at 10% MOF loading and beyond this, there was no significant effect of increasing MOF loading [Car (2006)]. This type of composite phase could be considered slightly better than the CuBTC@PBI-BuI phase, where defects were not so sever to lead to non selective passes of the gases.

In the case of DBzPBI-BuI composites with CuBTC, it was surprising to note a consistent reduction in CO_2 permeability with no significant change in selectivities (Figure 3.9d). This kind of behavior is similar to case (V) defined by Koros *et al*. [Moore (2005)], where porous filler led to reduced permeability. The decrease in permeability

was associated with either similar selectivity (CO_2/N_2) or some small improvement (CO_2/CH_4). This is a typical phenomenon of addition of impermeable fillers to a polymer matrix, where the gas permeability decreases due to the tortuous path followed by the penetrants [Ryu (2005)]. As a result, more permeable gases are affected less due to the tortuous path, increasing their selectivity. In the present case, it may be possible that the polymer chains rigidified at the MOF particle surface and their pendent large alkyl groups blocked the entry of penetrants into the opening of CuBTC pores, making them almost impermeable as showed in the Figure 3.10.

3.5 Effect of polymer structure on gas permeation properties

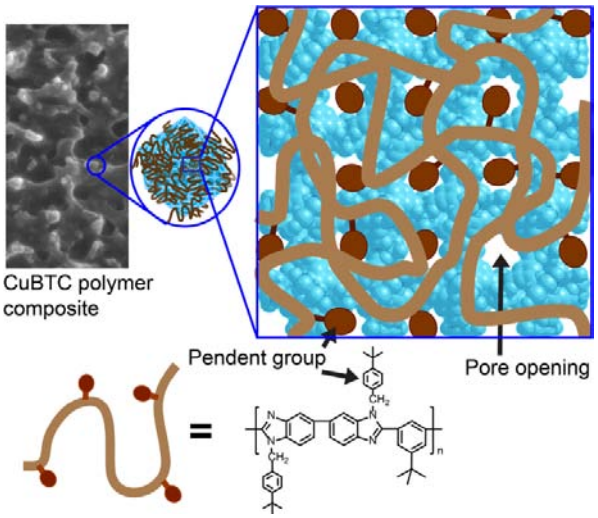

Figure 3.10 Schematic of CuBTC pore blockage by polymer chain pendent groups

The effect of change in the polymer backbone structure as well as side group functionalization on the permeation properties of the CuBTC based composite membranes is significant. Though the benzimidazole group is assumed to be the main interacting functionality of the PBIs, the rest of the groups on polymer chain are also significantly affecting the composite membrane performance. The PBI-HFA with a polar $–C(CF_3)_2$ group showed the simultaneous improvement in the permeability as well as selectivity in the CuBTC based composite membranes. On the other hand, the PBI-BuI with non-polar $–C(CH_3)_3$ group was leading to the reduction of separation performance in the CuBTC based composite membranes. The *N*-substitution of the PBI-BuI reduces the inter-chain hydrogen bonding and thus is thought to indirectly strengthen the CuBTC@PBI interactions. The *N*-substituent is also known to plays significant role in

the polymer properties [Kumbharkar (2010)]. The DMPBI-BuI with methyl group substituent has almost same chain packing parameters (also gas permeability) as of PBI-BuI. On the other hand, the DBzPBI-BuI has low chain packing due to steric factor of large t-butyl benzyl side group. The permeability (H_2) of the DBzPBI-BuI is also six fold higher than the PBI-BuI. These substituents were also thought to have different amount of interactions with CuBTC. As the DMPBI-BuI showed improvement in the permeation properties at only 10% loading, at higher loading of 20 and 30% it also lost the advantage possibly due to the particle agglomeration. The DBzPBI-BuI based composite membranes unexpectedly show a decrease in the permeability with increasing CuBTC content. It means that the CuBTC is acting as impermeable filler in this case. It can be only explained by assuming that the CuBTC pores are blocked by the polymer chains surrounding it. The possibility is of large *tert*-butylbenzyl substituent getting adsorbed at the pore opening of the MOF, leaving it inaccessible to the gaseous molecules as showed in the Figure 3.10.

Table 3.2 Gas permeability (P*) of the composite membranes.

Permeability	P_{He}	P_{H_2}	P_{N_2}	P_{CH_4}	P_{CO_2}
CuBTC@PBI-HFA composite					
PBI-HFA	13.1	12.6	0.21	0.07	4.39
C_{10}@PBI-HFA	15.3	13.5	0.24	0.08	4.44
C_{20}@PBI-HFA	15.4	14.6	0.25	0.11	6.91
C_{30}@PBI-HFA	16.9	18.4	0.25	0.10	8.10
CuBTC@PBI-BuI composite					
PBI-BuI	6.5	6.22	0.09	0.04	2.30
C_{10}@PBI-BuI	7.6	7.88	0.13	0.06	3.14
C_{20}@PBI-BuI	7.3	7.95	0.20	0.10	3.53
C_{30}@PBI-BuI	9.6	9.65	0.22	0.13	4.53
CuBTC@DMPBI-BuI composite					
DMPBI-BuI	11.0	12.8	0.18	0.08	3.84
C_{10}@DMPBI-BuI	11.2	13.20	0.22	0.08	5.58
C_{20}@DMPBI-BuI	11.6	13.19	0.20	0.07	3.87
C_{30}@DMPBI-BuI	11.5	12.87	0.23	0.08	4.10
CuBTC@DBzPBI-BuI composite					
DBzPBI-BuI	44.5	61.35	2.00	1.63	25.8
C_{10}@DBzPBI-BuI	35.7	49.75	1.53	1.54	21.3
C_{20}@DBzPBI-BuI	29.3	40.53	1.30	0.90	17.2
C_{30}@DBzPBI-BuI	22.3	37.05	1.22	0.80	14.7

*****Permeability is expressed in Barrer (1 Barrer = 10^{-10} cm^3 (STP).cm/cm^2.s.cm Hg).

Table 3.3 Ideal gas selectivity of the composite membranes.

Selectivity	P_{He}/P_{N_2}	P_{H_2}/P_{N_2}	P_{He}/P_{CH_4}	P_{H_2}/P_{CH_4}	P_{H_2}/P_{CO_2}	P_{CO_2}/P_{N_2}	P_{CO_2}/P_{CH_4}
CuBTC@PBI-HFA composite							
PBI-HFA	62.4	60.0	187.1	180.0	2.9	20.9	62.7
C_{10}@PBI-HFA	63.7	56.2	191.2	168.7	3.0	18.5	55.5
C_{20}@PBI-HFA	61.6	58.4	154.0	146.0	2.1	27.6	69.1
C_{30}@PBI-HFA	67.6	73.6	169.0	184.0	2.3	32.4	81.0
CuBTC@PBI-BuI composite							
PBI-BuI	76.2	72.9	162.1	154.7	2.7	26.8	57.0
C_{10}@PBI-BuI	57.3	59.5	128.0	132.9	2.5	23.6	52.8
C_{20}@PBI-BuI	36.1	39.3	74.5	81.1	2.3	17.4	35.8
C_{30}@PBI-BuI	39.3	44.3	68.2	77.0	2.1	20.8	36.2
CuBTC@DMPBI-BuI composite							
DMPBI-BuI	61.9	72.1	135.1	157.5	3.4	21.7	47.2
C_{10}@DMPBI-BuI	51.0	60.3	142.9	166.0	2.8	25.8	60.9
C_{20}@DMPBI-BuI	59.3	67.5	163.8	182.9	3.4	19.9	54.6
C_{30}@DMPBI-BuI	50.5	56.9	129.6	152.9	3.0	19.0	52.1
CuBTC@DBzPBI-BuI composite							
DBzPBI-BuI	22.3	30.7	27.5	37.6	2.4	12.9	15.9
C_{10}@DBzPBI-BuI	23.5	32.6	32.4	33.6	2.4	13.9	18.5
C_{20}@DBzPBI-BuI	22.5	31.1	33.4	45.2	2.4	13.2	19.4
C_{30}@DBzPBI-BuI	22.3	30.4	34.2	46.5	2.5	12.0	18.5

3.6 Conclusions

In CuBTC@PBI composite membranes, good compatibility and homogeneous filler distribution were obtained by blending of as synthesized nano-sized filler with polymers. In the composite membranes, MOF pore blockage led to the reduction in gas permeation properties; wherein effects of PBI molecular structure played a crucial role. The CuBTC based composites with PBI-HFA showed a significant improvement in gas permeability as well as in selectivity. PBI-BuI based composites showed a small increase in permeability, DMPBI-BuI showed no significant change, while DBzPBI-BuI showed decrease in the permeability with increasing MOF loading. Thus, molecular structure of polymer used for making composites is important in governing gas permeation properties of resulting composites. By appropriate selection of the polymer and MOF, excellent combination of high permeability and selectivity can be achieved.

Chapter 4

Effect of polymer structural features on gas permeation properties ZIF-8@PBI composite membranes

4.1 Introduction

A new class of MOFs was discovered having topology similar to that of zeolites [Banerjee (2008), Phan (2010), Eddaoudi (2014)]. They are made of metal ions (Zn, Co, etc.) and imidazole type of ligands (imidazole, benzimidazole, purine, indole etc.) Thus, they were named as zeolitic imdazolate frameworks (ZIFs). These MOFs have the tuneable pore size and chemical functionality coupled with exceptional thermal stability [Park (2006)]. The ZIF-8 is a member of this sub-family of MOFs, made up of Zn and *2*-methylimidazole. It has the sodalite topology with pores of 11.6 Å size connected through the aperture diameter of 3.4 Å [Park (2006)]. It shows thermal stability up to 400 °C in air [Huang (2006)]. Although MOFs are known for poor stability in the presence of water [Huang (2003), Li (2007), Kaye (2007)], ZIF-8 exhibit structural integrity even in the boiling water [Park (2006)]. It possesses high porosity with surface area of 1947 $m^2.g^{-1}$ [Park (2006)]. The ZIF-8 has shown selective CO_2 sorption [Pellitero (2010)]. The small pore aperture is also expected to differentiate gas molecules based on their size and shape. The easy synthesis of ZIF-8 is another advantage of it. The ZIF-8 has been synthesized by various methods with good particle size control [Cravillon (2009, 2011), Nune (2010), Pan (2011), Beldon (2010), Crawford (2015)]. The nanocrystals with narrow size dispersion could be easily prepared at the room temperature [Cravillon (2011)]. The cost effective large scale production by mechano-chemical methods is also demonstrated [Crawford (2015)].

In recent time, ZIF-8 is actively perused as a membrane material due to its easy synthesis and good thermo-chemical stability. There are literature reports on the preparation of dense crystalline ZIF-8 film on the porous supports for the gas

separation application [Yao (2014)]. Although these membranes were not free of defects, they showed potential of ZIF-8 for the separation of gaseous molecules. The ZIF-8 is also used as filler in the polymeric membranes for the enhancement of the permeability and selectivity [Yao (2014)]. At the beginning of present study, there were only two reports available on the ZIF-8@polymer composite membranes. In these, ZIF-8 was added to the polysulfone [Díaz (2010)] and Matrimid [Ordõnez (2010)] as a polymer matrix to make composite membranes. These reports though claim improvement in the separation properties, they showed heavy agglomeration of ZIF-8 particles and voids at MOF-polymer interface in the cross section SEM images [Díaz (2010), Ordõnez (2010)].

In the present study, we have blended ZIF-8 with three different polymers of polybenzimidazole family in order to enhance their separation properties and to know the effect of polymer structure on the gas permeation properties of resulting composite membranes. The polybenzimidaole (PBI) as a family of polymers is very promising membrane materials due to their good thermo-chemical properties as discussed in the chapter 3. The ZIF-8 was selected as filler due to the high porosity and small pore aperture size of it. The small aperture size is expected to improve the molecular sieving properties of the membrane. Another advantage of choosing this pair is the chemical analogy of ZIF-8 and PBIs (both contain imidazole groups), which may help in good compatiblization of two phases. The PBI-BuI and its two *N*-substituted derivatives are used as the matrix to make ZIF-8@polymer composite membranes. A PBI-BuI, one of the members of PBI family, has excellent combination of high thermal stability and gas permeability (10-14 times higher permeability for different gases than that of base PBI-I) [Kumbharkar (2010)]. The *N*-substitution of PBI-BuI further elevates its gas permeability without serious threats to its thermal stability [Kumbharkar (2009)]. Composite membranes of these polymers with ZIF-8 were prepared and evaluated for requisite characteristics (thermal, spectral and gas permeation). This approach of blending high permeability PBIs with ZIF-8 as composite membranes for gas separation would provide an insight towards structural aspects of a polymer to be used for blending with ZIFs.

4.2 Synthesis of ZIF-8 and polymers

The synthesis of ZIF-8 was carried out by the simple room temperature method reported earlier [Cravillon (2009)]. The WAXD analysis of dry ZIF-8 powder showed the typical crystalline spectrum. The spectrum matched well with the simulated spectrum for ZIF-8 (Figure 4.1a), confirming successful formation of ZIF-8. As synthesized ZIF-8 nanocrystals were also analyzed by the dynamic light scattering (DLS), SEM and TEM for determining size, shape and distribution of particles. The DLS analysis showed the bimodal size distribution of particles (Figure 4.1b), the one around 50-60 nm size and other at 100-130 nm. The SEM and TEM images show the particles with 60-80 nm with rhombic dodecahedral shape (Figure 4.1c, d). Thus, the second distribution at around 120 nm particles appearing in DLS analysis could be possibly due to agglomerates of particles [Yang (2012)]. The as synthesized ZIF-8 nanocrystals were used after solvent exchange for blending with polymer for better dispersion of particles. The discussion on synthesis of three polymers used is already presented in the section 3.2.2 of chapter 3.

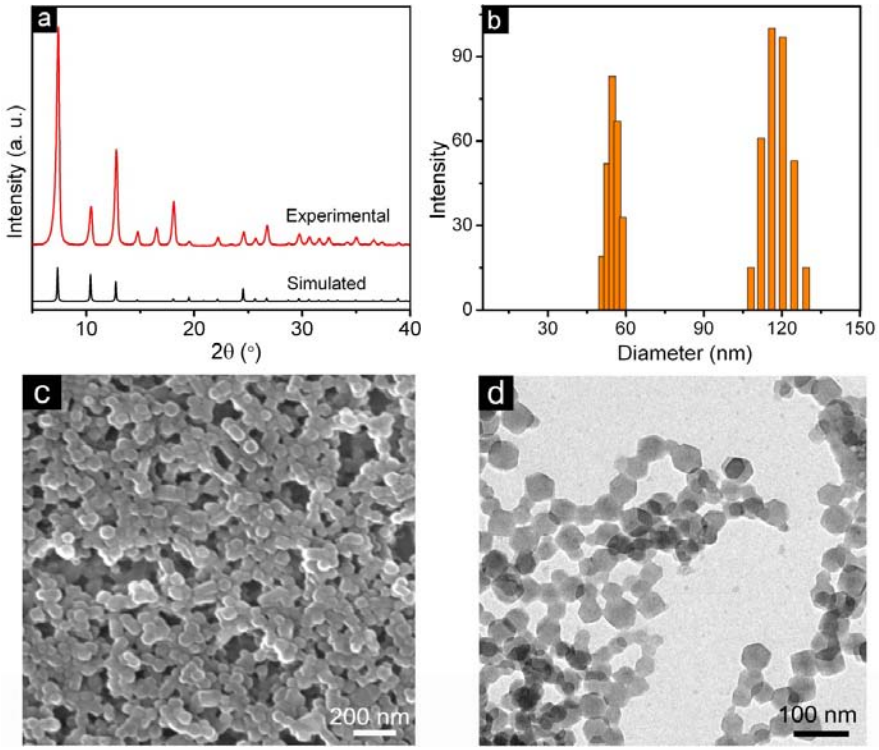

Figure 4.1 (a) Comparison of WAXD patterns of synthesized ZIF-8 nanoparticles with simulated one, (b) Dynamic light scattering of ZIF-8 nanoparticles, (c) SEM image and (d) TEM image of ZIF-8 nanoparticles.

4.3 Characterization of dense composite membranes

4.3.1 Physical properties

The ZIF-8 based composite membranes with PBI-BuI and DMPBI-BuI with good mechanical strength could be successfully prepared up to 30% (w/w) of ZIF-8 loading. They could also be analyzed easily for the physical properties and gas permeability investigations. Beyond 30% ZIF-8 content, the membranes were brittle and broken into small pieces during the drying of film. Unfortunately, composite membranes based on DBzPBI-BuI and ZIF-8 with good mechanical strength could be prepared only up to 20% of ZIF-8 loading. The membrane with 30% ZIF-8 loading was brittle and could not be used for the gas permeation analysis. The brittleness of the membrane could be due to the lower intrinsic strength (related to molecular weight) of the matrix polymer.

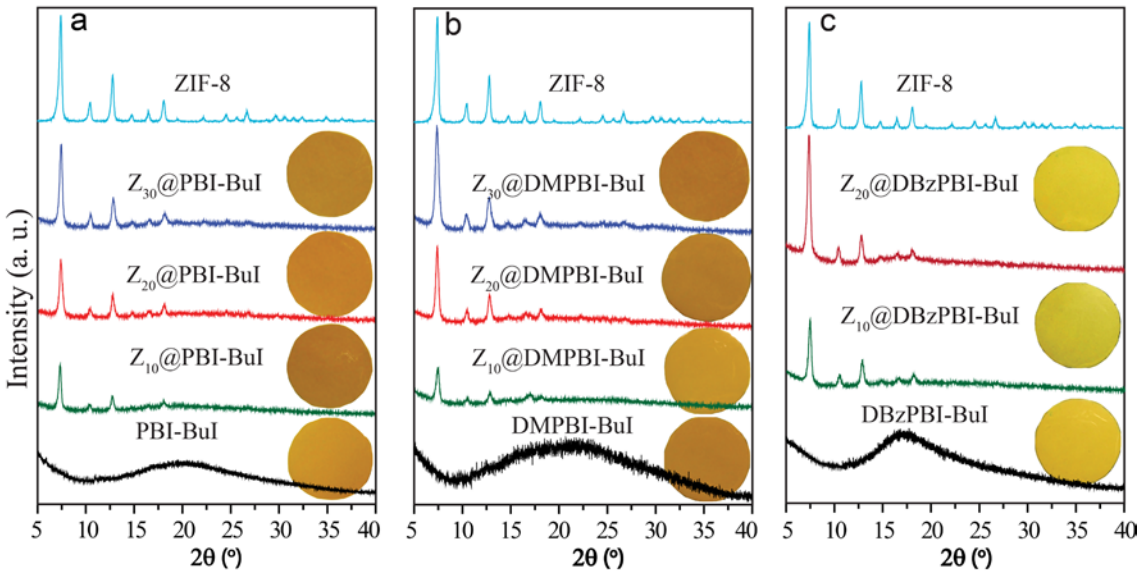

Figure 4.2 WAXD patterns with photograph of ZIF-8 composites.

In the WAXD pattern of composite membranes, sharp multiple peaks belonging to ZIF-8 in addition to the characteristic amorphous hollow of matrix polymers were present (Figure 4.2). This indicates that the structure of ZIF-8 is intact in the composite membranes.

SEM images of the cross section of composite membranes (Figure 4.3) showed a nice homogeneous distribution of the ZIF-8 nanoparticles throughout the membrane cross sections. There was no agglomeration of the particles observed in the SEM images as

visible in the previous studies [Ordõnez (2010)]. The nanoparticles seem to be well adhered with the polymer phase as no phase boundary or voids are observable in any of the membrane. The even distribution of particles was further supported by the Zn mapping of the membrane cross sections (Figure 4.4). The even intensity was observed throughout the membrane cross sections in all the three composites. This success in obtaining highly homogeneous membranes was a combined result of adopted membrane methodology and good compatibility between the filler and polymer.

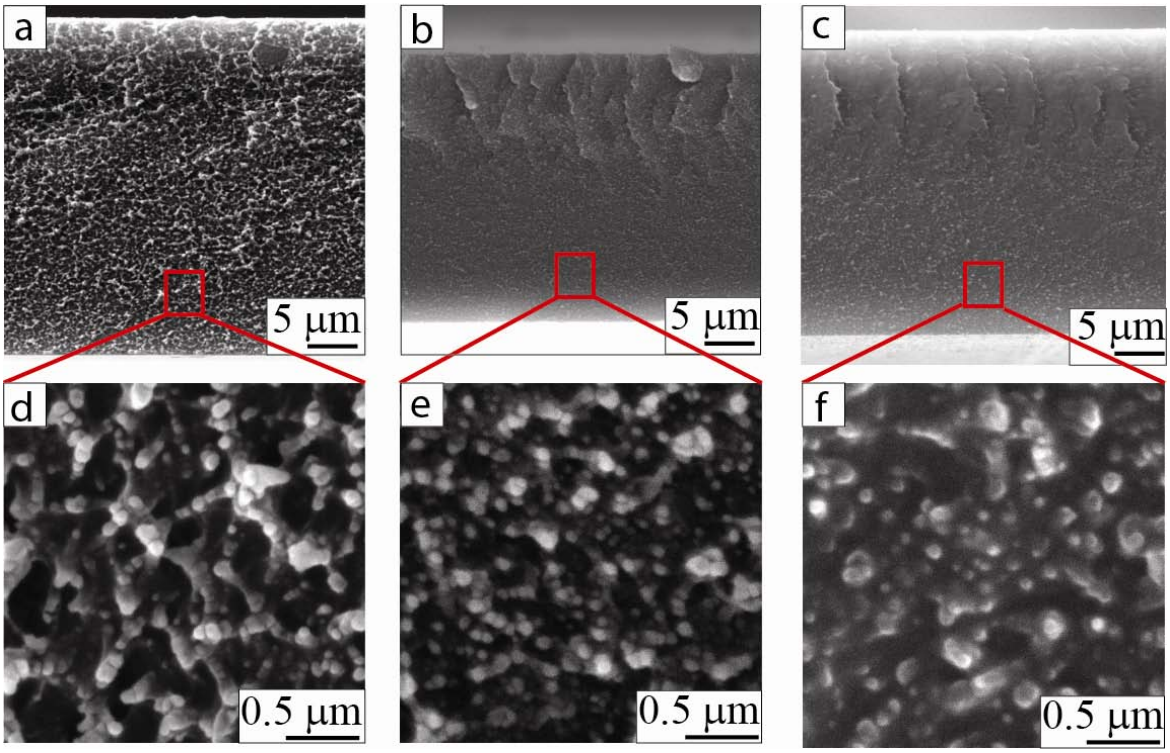

Figure 4.3 SEM images of (a) Z_{30}@PBI-BuI, (b) Z_{30}@DMPBI-BuI and (c) Z_{20}@DBzPBI-BuI composite membranes.

The previous literature reports use the dried ZIF-8 powder for making blend membranes [Díaz (2010, 2011), Ordõnez (2010)]. The powder was dispersed in the solvent by the sonnication. In a recent report, it was noted that after drying, nanoparticles agglomerate and could not be redispersed completely with sonnication treatment [Cravillon (2009)]. Thus, we used the as synthesized ZIF-8 nanoparticles (without drying) for mixing with polymer and membrane formation. As synthesized ZIF-8 nanoparticles make a nice homogeneous suspension in the DMAc (solvent used) and did

not settle down even after 2-3 weeks. Thus, they did not settle down during the casting process and remained dispersed homogeneously in the composite solution and in the resultant membranes. This may be a primary reason why the particles did not show any agglomeration in the composite membranes. This way of blending also eliminated void formation at the interface. This also indicates a good compatibility between the polymer and ZIF-8. Polymers chosen for the present work belong to the PBI family possessing two imidazole groups per repeat unit. The good observed compatibility could be correlated to the electron donor '*N*' present in the imidazole moiety of PBI, which could have positive interactions with the metal ion at the MOF surface.

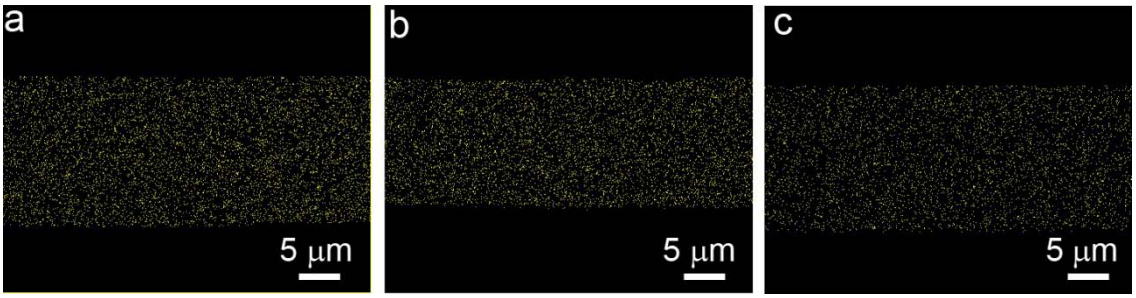

Figure 4.4 Zn mapping of (a) Z_{30}@PBI-BuI, (b) Z_{30}@DMPBI-BuI and (c) Z_{20}@DBzPBI-BuI composite membranes.

The TGA analysis showed that ZIF-8 is stable up to 450 °C in air (Figure 4.5). This value is in the agreement with the literature report [Cravillon (2009)]. The thermal stability of the polymers used is already discussed in the section 3.3 of chapter 3. The ZIF-8@PBI-BuI and ZIF-8@DMPBI-BuI composite membranes showed the good thermal stability with initial degradation temperature (IDT) at 465 °C, where the ZIF-8 starts degrading. On the other hand, the ZIF-8@DBzPBI-BuI composite membranes showed the IDT around 370 °C where the DBzPBI-BuI starts degrading. Still, the thermal stability of these membranes was high enough for their application as membrane materials for gas separation. The degradation of composite membranes in air yielded only metal oxides as char. From the char yield the accurate content of ZIF-8 in the composite membrane can be easily determined. It matched well with the ZIF-8 quantity taken during the preparation of composite membranes (Table 4.1).

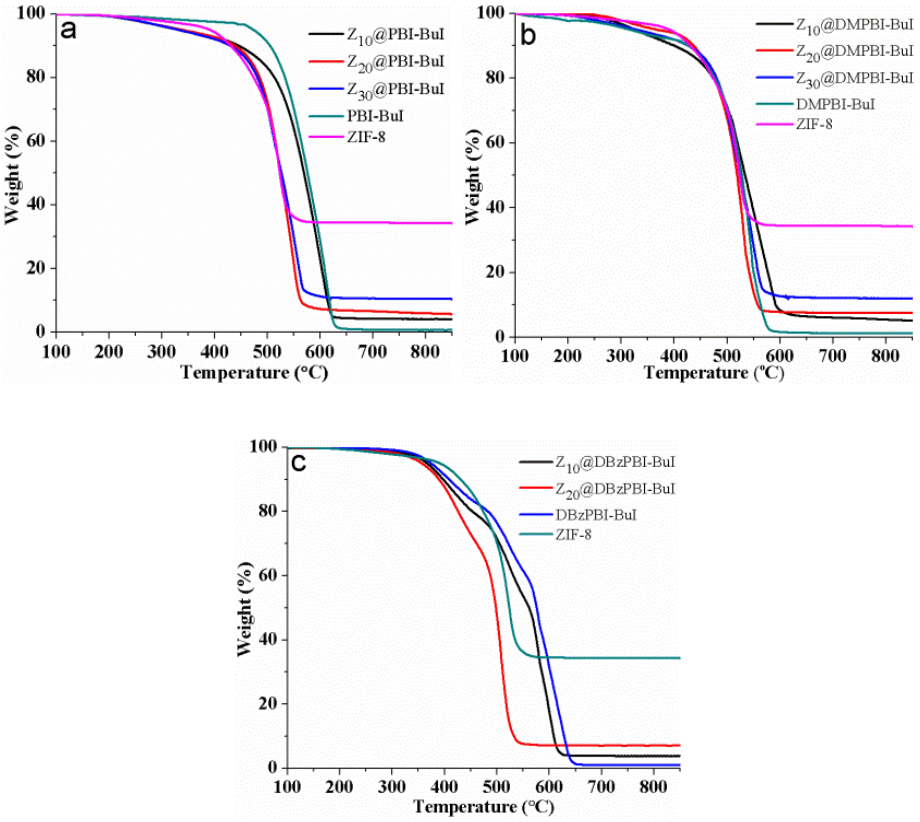

Figure 4.5 TGA thermograms of PBIs, ZIF-8 and composites: (a) PBI-BuI, ZIF-8 and their composites, (b) DMPBI-BuI, ZIF-8 and their composites and (c) DBzPBI-BuI, ZIF-8 and their composites.

The density of the polymer and composite membranes were determined in order to analyse any effect of the ZIF addition on the free volume of the polymer. For this, the experimentally determined density was compared with the theoretically calculated density. The theoretical density was calculated by the additive method with the assumption of volume additivity. It was found that composite membranes showed lower density than the corresponding theoretical values (Table 4.1). The percent change in the density [Δρ (%)] was calculated by following equation:

$$\Delta\rho\ (\%) = \frac{\rho_T - \rho_E}{\rho_T} \times 100$$

where, ρ_T is the theoretical density and ρ_E is the experimental density.

As could be seen from Figure 4.6, Δρ (%) increased with the ZIF-8 loading in the composite membranes based on all the three PBIs. The decrease in density qualitatively

indicates increase in the free volume in the composite membranes. It is known in the literature that the nano-fillers can significantly affect the polymer chain packing as their dimensions are in the same range. For example, addition of fumed silica caused significantly change in the PMP chain packing arrangement [Merkel (2003)]. Song *et al.* also have observed similar extra free volume creation in the Matrimid based composites [Song (2012)] by addition of ZIF-8 as a filler.

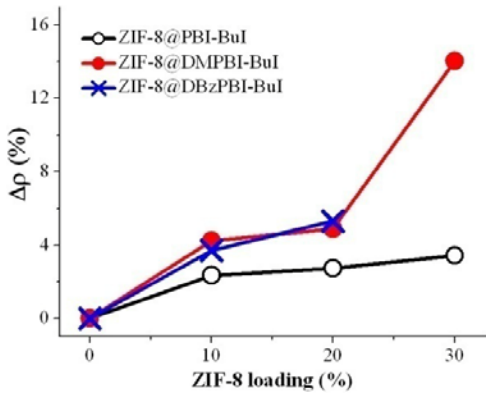

Figure 4.6 The Density variation of composite membranes with ZIF-8 loading.

Analysis of mechanical properties of composite membranes was also performed. The decrease in tensile strength (Figure 4.7) and modulus with increasing ZIF-8 loading was observed (Table 4.1). The decrease in modulus than that of the respective pristine polymer means lower toughness of the composite membranes. At 30% loading, significant decrease in the tensile strength was observed. The decrease in the tensile strength is expected, as the addition of crystalline filler makes the composite membrane more brittle.

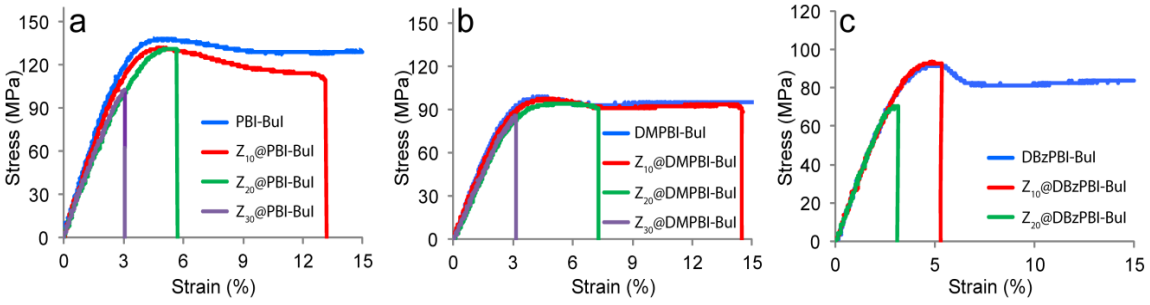

Figure 4.7 The stress-strain curve of the polymer and composite membranes: (a) ZIF-8@PBI-BuI composites, (b) ZIF-8@DMPBI-BuI composites and (c) ZIF-8@DBzPBI-BuI composites.

It is noteworthy that all the present membranes could withstand 20 atm upstream pressure, when mounted in the gas permeation cell, indicating their strong mechanical robustness. To our knowledge, this is the highest ever pressure tested for the MOF-polymer composite membranes and thus showed the success of choosing PBI as a family of polymers to make the composite membranes with ZIF-8.

Table 4.1 Physical properties of the polymer and composite membranes

Membrane	% MOF content in membranes (%)[a]	[b]Density (calc.) ($g.cm^{-3}$)	Density (expt.) ($g.cm^{-3}$)	Mechanical properties		
				Young's Modulus (GPa)	Tensile strength (MPa)	Elongation at break (%)
PBI-BuI	-	-	1.193	4.2	131.2	26.1
Z_{10}@PBI-BuI	11.5	1.169	1.141	3.8	130.4	13.8
Z_{20}@PBI-BuI	18.1	1.144	1.113	3.5	129.7	5.0
Z_{30}@PBI-BuI	33.9	1.120	1.082	3.5	104.8	2.4
DMPBI-BuI	-	-	1.196	3.3	90.2	53.04
Z_{10}@DMPBI-BuI	9.2	1.171	1.122	3.2	94.9	15.5
Z_{20}@DMPBI-BuI	18.1	1.147	1.091	3.2	95.1	7.0
Z_{30}@DMPBI-BuI	27.6	1.122	0.965	3.0	65.4	2.3
DBzPBI-BuI	-	-	1.097	2.8	92.3	12.6
Z_{10}@DBzPBI-BuI	10.7	1.082	1.042	2.6	92.3	5.3
Z_{20}@DBzPBI-BuI	20.2	1.068	1.011	2.7	79.3	4.6

a: based on char yield observed in TGA spectra; b: Theoretical densities for both type composites were calculated using ZIF-8 density[1] as 0.94 $g.cm^{-3}$.

4.3.2 Gas permeability analysis

The PBI-BuI based composite membranes showed a linear increase in the gas permeability with the increasing ZIF-8 content [Figure 4.8a, b]. The H_2 permeability of the pristine PBI-BuI was 6.2 Barrer, which increased to 11.4 Barrer with 10% ZIF addition and to further 14 Barrer with 20% ZIF addition in PBI-BuI. For 30% ZIF content (Z_{30}@PBI-BuI), H_2 permeability increased up to (for pristine PBI-BuI) 22.1 Barrer (Table 4.2). This was accompanied by increase in H_2/CH_4 selectivity from 155 to 184 and H_2/N_2 selectivity variation from 73 to a small decrease up to 67 (Table 4.3). The CO_2 permeability also showed an increase from 2.3 Barrer to 5.3 Barrer (Table 4.2). Although CO_2 based selectivities (Figure 4.8b) were slightly decreased, the CO_2/CH_4 selectivity remained appreciable even with 30% of ZIF-8 loading as 43.6. This is higher than the

selectivity for commonly used gas separation membrane materials such as Matrimid [36, Yong (2012)], polysulfone [22, McHattie (1992)] and polycarbonate [19, Hellums (1989)].

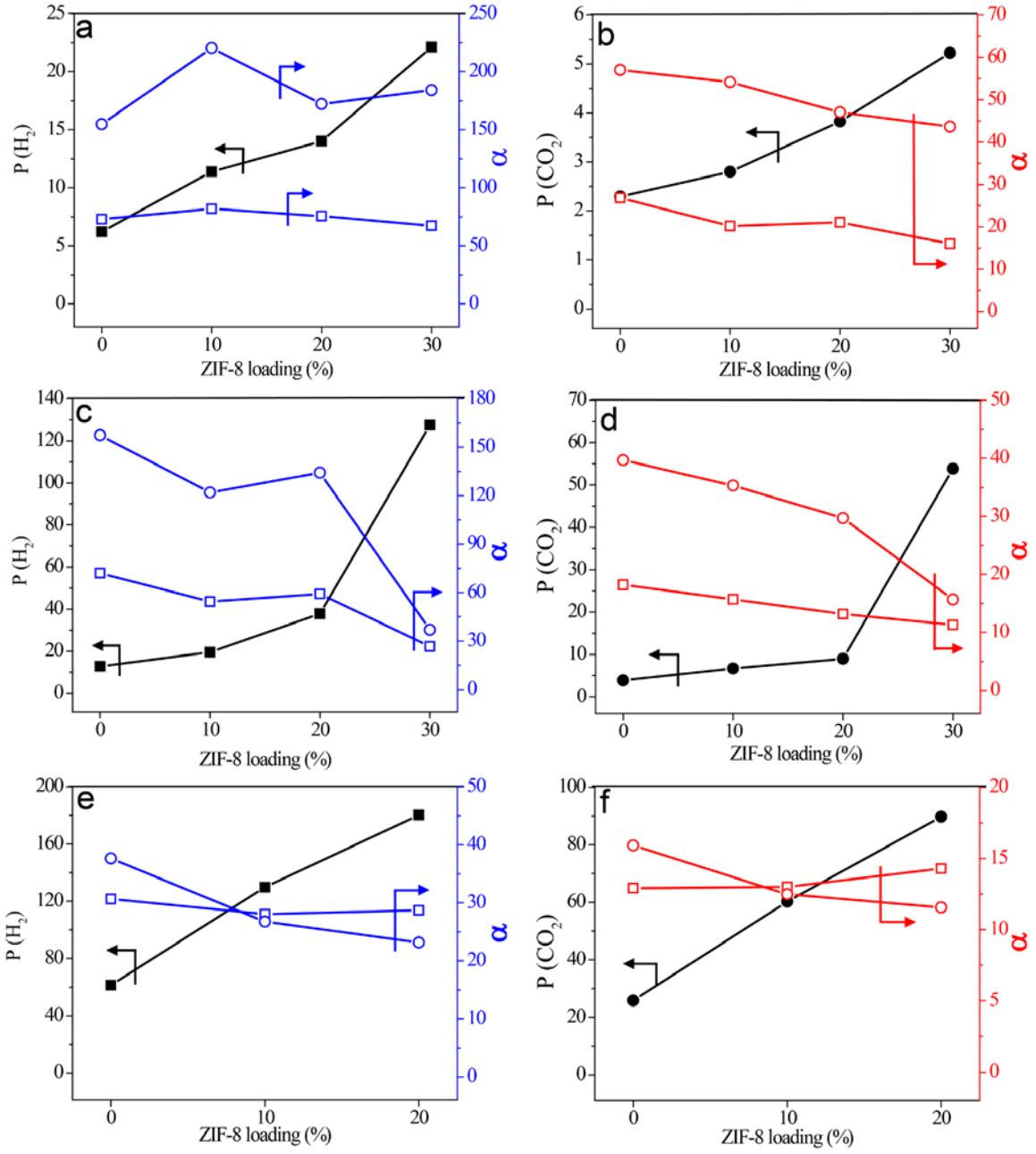

Figure 4.8 Variation in H_2 (■) and CO_2 (●) permeability and their selectivity over CH_4 (round symbol) and N_2 (square symbol) with ZIF-8 loading in ZIF-8@PBI-BuI (a, b), ZIF-8@DMPBI-BuI (c, d) and ZIF-8@DBzPBI-BuI (e, f) based composite membranes.

The ZIF-8@DMPBI-BuI composite membranes also showed the linear increase in the gas permeability with increasing ZIF-8 loading up to 20%. The H_2 permeability increased from 12.8 Barrer to the 37.8 Barrer with addition of 20% ZIF-8 (Table 4.2). Simultaneously the H_2/N_2 and H_2/CH_4 selectivity showed a small decrease from 72.1 to 59.3 and 157.5 to 134.3, respectively (Table 4.3). At 30% ZIF loading sharp increase in the gas permeability of all gases coupled with significant lowering in the gas selectivity was observed. The H_2 permeability increased up to 127.5 Barrer (Table 4.2) with H_2/N_2 and H_2/CH_4 selectivity reduced to only 26.7 and 37, respectively (Table 4.3). This is unexpected behavior which was not observed with the PBI-BuI case. The membranes were completely transparent and no defect or pinhole was present that would reduce the selectivity to such a large extent. The SEM image also showed nice homogeneous membrane (Figure 4.3b). As the permeation is repeated with three membranes showing consistent data, the possibility of defect could be ruled out. This anomaly could be understood by the observation of density data. The experimental density of the Z_{30}@DMPBI-BuI composite membranes is significantly lesser than the theoretical density. This means that the matrix polymer's chain packing is heavily altered in the composite membrane and so is with the gas permeability and selectivity.

In case of DBzPBI-BuI, the increasing ZIF-8 content in the composite membrane led to similar high improvement in the gas permeability (Figure 4.8 e, f). The H_2 permeability increased from 61.4 Barrer to 129.8 Barrer with 10% ZIF content and further to 180.3 Barrer with 20% ZIF content in the composite membrane (Table 4.2). This was coupled with no significant change in the H_2/N_2 selectivity and small decrease in the H_2/CH_4 selectivity from 37.6 to 23.2 (Table 4.3). The CO_2 permeability also improved from 25.8 Barrer to the 89.8 Barrer (Table 4.2) with small increase in CO_2/N_2 selectivity from 12.9 to 14.3 and small decrease in the CO_2/CH_4 selectivity from 15.9 to 11.6 (Table 4.3).

4.3.3 Effect of polymer structure on gas permeability of composite membranes

The effect of structural variations in PBI-BuI was prominently seen in DMPBI-BuI based composites. An order of magnitude elevation in H_2 permeability than the pristine case was achieved with 30% loading (Figure 4.8c). This was coupled with ~70% decrease in H_2/N_2 and H_2/CH_4 selectivity than that of unloaded DMPBI-BuI. In the case

of DBzPBI-BuI composites, the ZIF-8 loading could be successfully achieved only till 20%. When the elevation in permeability at this level is compared with that of unsubstituted PBI-BuI case, the effect of bulky substituent, -DBz, is prominently evident. The rise in H_2 and CO_2 permeability in DBzPBI-BuI composites occurs up to 3 and 3.5 times, respectively, than the pristine DBzPBI-BuI. On the other hand, the similar enhancement in the PBI-BuI based composite membranes was just 2.2 and 1.7 times, for H_2 and CO_2, respectively. Improved permeation properties of all the three PBI based composite membranes concludes that benefits of ZIF-8 porosity can be better drawn with the polymers of low diffusion resistance (high permeability), provided that they have good compatibility with the MOF. These results show that ZIF-8 contributed to a significant increase in the permeability in all three polymer cases. It can thus be concluded that ZIF-8 elevates permeability, rather than affecting size based discrimination of penetrants. This could be concluded since the selectivity is not affected to a large extent as that of permeability.

Table 4.2 Gas permeability (P*) of the polymer and composite membranes.

	P_{He}	P_{H_2}	P_{N_2}	P_{CH_4}	P_{CO_2}
ZIF-8@PBI-BuI composite					
PBI-BuI	6.5	6.22	0.09	0.04	2.30
Z_{10}@PBI-BuI	11.6	11.37	0.14	0.05	2.80
Z_{20}@PBI-BuI	13.3	14.01	0.18	0.08	3.83
Z_{30}@PBI-BuI	21.6	22.11	0.33	0.12	5.23
ZIF-8@DMPBI-BuI composite					
DMPBI-BuI	11.0	12.8	0.18	0.08	3.8
Z_{10}@DMPBI-BuI	15.1	19.5	0.36	0.16	6.7
Z_{20}@DMPBI-BuI	29.9	37.8	0.64	0.28	9.0
Z_{30}@DMPBI-BuI	69.3	127.5	4.77	3.51	53.9
ZIF-8@DBzPBI-BuI composite					
DBzPBI-BuI	44.6	61.4	2.0	1.6	25.8
Z_{10}@DBzPBI-BuI	86.3	129.8	4.6	4.8	60.2
Z_{20}@DBzPBI-BuI	116.4	180.3	6.3	7.8	89.8

*****Permeability is expressed in Barrer (1 Barrer = 10^{-10} cm^3 (STP).cm/cm^2.s.cm Hg).

Table 4.3 Ideal gas selectivity of the polymer and composite membranes.

	P_{He}/P_{N_2}	P_{H_2}/P_{N_2}	P_{He}/P_{CH_4}	P_{H_2}/P_{CH_4}	P_{H_2}/P_{CO_2}	P_{CO_2}/P_{N_2}	P_{CO_2}/P_{CH_4}
ZIF-8@PBI-BuI composite							
PBI-BuI	79.6	72.9	162.2	154.7	2.7	26.8	57.0
Z_{10}@PBI-BuI	83.9	82.0	225.6	220.4	4.1	20.2	54.2
Z_{20}@PBI-BuI	75.5	75.6	176.4	172.2	3.6	21.1	47.0
Z_{30}@PBI-BuI	65.6	67.3	179.5	184.1	4.2	16.0	43.6
ZIF-8@DMPBI-BuI composite							
DMPBI-BuI	61.9	72.1	135.1	157.5	3.4	21.7	47.2
Z_{10}@DMPBI-BuI	42.1	54.4	94.3	121.9	3.4	18.7	42.2
Z_{20}@DMPBI-BuI	46.9	59.3	106.2	134.3	3.8	14.0	31.4
Z_{30}@DMPBI-BuI	14.6	26.7	20.27	37.0	2.4	11.3	15.7
ZIF-8@DBzPBI-BuI composite							
DBzPBI-BuI	22.3	30.7	27.5	37.6	2.4	12.9	15.9
Z_{10}@DBzPBI-BuI	18.6	28.0	18.0	27.0	2.2	13.0	12.5
Z_{20}@DBzPBI-BuI	18.5	28.7	15.0	23.2	2.0	14.3	11.6

4.4 Characterization of dual layer composite membranes

4.4.1 Preparation of dual layer composite membranes

As observed in the dense composite membranes, the mechanical strength of membranes reduced with the increasing MOF loading. The dense composite membranes with above 30% MOF loading were very brittle and could not be studied for the gas permeation. The content of MOF in the composite membrane should be high to draw better advantage of the MOFs separation properties. Thus, we tried another way to prepare the composite membrane with high MOF loading as asymmetric composite membranes, where the ZIF-8@PBI composite film was supported on the porous substructure as shown in the schematic Figure 4.9.

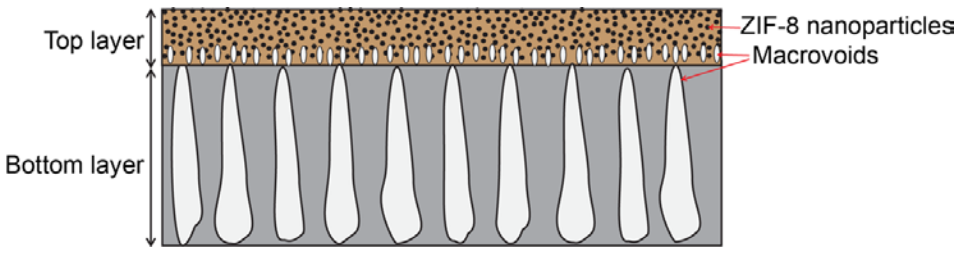

Figure 4.9 Schematic of dual layer composite membrane.

The membrane preparation procedure is described in the section 2.4.2a of chapter 2. In the dual layer composite membranes, there are two important issues to be addressed: (i) Good adhesion between the lower support layer and top composite layer, which is essential for the good mechanical strength of the resulting composite membrane, (ii) thin selective skin formation at the top surface. To achieve good adhesion, we have used the polybenzimidazole polymers for both the support layer and top layer to avoid any compatibility issue between the two layers. The support layer material was PBI-BuI, while the top layer material was ZIF-8 blended with the PBI-HFA. The PBI-HFA was chosen as the matrix material for the composite preparation due to its solubility in the low boiling solvents like pyridine and THF. The dope solution after casting were kept in air for some defined time and then dipped in water in order to allow phase inversion. During the exposure to air, solvent evaporates making the top layer dense (Figure 4.10a). The bottom layer is fully porous due to phase inversion (Figure 4.10c, d) and does not cause any resistance to the gas permeation.

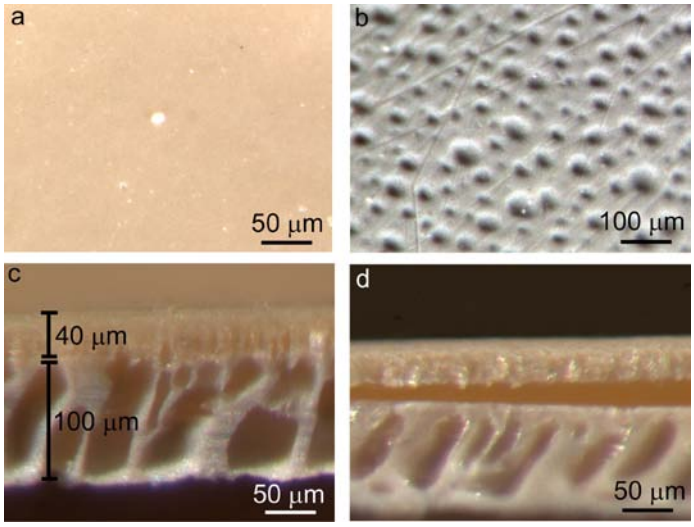

Figure 4.10 Dual layer composite membrane (a) top surface, (b) bottom surface, (c) cross section and (d) delamination of the two layers.

4.4.2 Gas permeation properties of the dual layer membranes

It was observed that the Z_{80}@PBI-HFA ($Py_{50}T_{50}$) composite membranes are not showing any significant gas selectivity (H_2/N_2) at small air exposure time during membrane making. On the other hand, membrane with higher air exposure time started delaminating.

Table 4.4 Gas permeance and ideal selectivity of the dual layer membranes.

Z_8@PBI-HFA ($Py_{50}T_{50}$) membranes						
Air drying time	0	30	60	90	120	300
P (H_2)	19736	13948	11394	3209	-	-
P (N_2)	9183	4932	3044	832	-	-
P (H_2/N_2)	2.15	2.83	3.74	3.86	-	-
Z_{80}@PBI-HFA ($Py_{45}T_{45}N_{10}$)						
Air drying time	-	30	60	90	120	300
P (H_2)	-	20913	15394	4832	1735	-
P (N_2)	-	7283	4953	832	493	-
P (H_2/N_2)	-	2.87	3.11	5.81	3.52	-
Z_{80}@PBI-HFA ($Py_{35}T_{35}N_{30}$)						
Air drying time	-	30	60	90	120	300
P (H_2)	-	17354	5749	3842	4103	4689
P (N_2)	-	6193	1092	839	1081	1106
P (H_2/N_2)	-	2.80	5.26	4.58	3.80	4.24

At the low air exposure time, the concentration could not build high enough at the top surface of casted dope to offer a selective skin. At the larger time intervals, the top layer becomes almost gel with solvent loss and water absorption from atmosphere makes it to delaminate from the bottom layer immediately after solidifying in the water bath. The delamination of two layers could be seen in the Figure 4.10d. For enhancing the compatibility of two layers, we added some amount of NMP (10 -30%) as the solvent in the top layer dope solution. It would help to increase the miscibility of two layers as the bottom layer also contains NMP as solvent. Though the volatile solvents could not be completely replaced by NMP, we increased the NMP concentration up to 30%. This has helped to reduce the delamination to some extent during membrane making, but in dried conditions, these membranes exhibited delamination as could be observed in the cross section image (Figure 4.10d). This could be attributed to the difference in shrinkage of top and bottom layers during the drying of membrane. The NMP as solvent is improving the intermixing of two dope layers but it obstruct the selective skin formation at the top, as it does not evaporate easily from the surface. For longer air exposure, the top layer is probably precipitating partially with moisture absorption from air and thus could not form

the selective skin. Thus, though the composite membranes had comparatively better adhesion of bottom and top layers yet it did not resulted in good membrane selectivity (Table 4.4). With appropriate selection of host polymer, solvent pair, evaporation and gelation conditions, such composite membranes can be obtained in future.

4.5 Conclusion

In case of ZIF-8@PBI-BuI composite membranes, good compatibility and homogeneous filler distribution were obtained by blending of as synthesized nano-sized filler. A good improvement in the gas permeability of ZIF-8 based composite membranes was observed. PBI-BuI showed almost linear increase in the gas permeability with ZIF loading (H_2 permeability improved by 3.5 times at 30% ZIF loading). The good compatibility and subsequent improvement in the gas permeability prevails even after elimination of H-bonding while substituting two nitrogen of PBI-repeat unit by alkyl groups. This indicates that not only the H-bonding, but imidazole content in PBI is largely responsible for obtaining composite membranes with good compatibility. The ZIF-8@DMPBI-BuI composites showed exponential increase in the gas permeability due to unique structural features of individual components, combined together positively. The ZIF-8@DBzPBI-BuI composites also showed improvement in the gas permeability with increasing ZIF-8 loading. Thus, both, properties of MOF as well as polymer used for making composites are important in governing gas permeation properties of resulting composites. By appropriate selection of the polymer and MOF (e.g. DMPBI-BuI and ZIF), excellent combination of high permeability and selectivity can be achieved. The efforts were made to prepare dual layer composite membranes with selective layer containing 80% ZIF-8 (w/w). Unfortunately, good selectivity could not be obtained with these membranes and further optimization of membrane preparation procedure is needed.

Chapter 5

Separation of Olefin-paraffin using ZIF-8@polymer composite membranes

5.1 Introduction

Ethylene (C_2H_4) and propylene (C_3H_6) are the first and second largest feed stock molecules of the petrochemical industry [Pinnau (2001)]. The ethylene is used mainly for the production of polyethylene, ethylene oxide and ethylene dichloride. The propylene is used for the production of polypropylene, acrylonitrile, propylene oxide, cumene, oxo alcohols, acrylic acids, isopropyl alcohol, oligomers and other chemicals. The global demand of ethylene and propylene was 133 million tons and 83 million metric tons respectively in 2013 [Lewandowski (2014)]. The consumption of these gases is increasing with a growth rate of 4-5% per year [Bender (2014)].

The olefins are produced by the hydrocarbon cracking process. The outcome of cracker contains a mixture of olefins and paraffins which are fractionated by low temperature distillation. The first stage fractionates contains mixture of olefin and paraffin with close boiling points like ethylene-ethane and propylene-propane which are further separated by the large splitter column. These processes are highly energy intensive and thus expensive. It increases the operational as well as capital cost. The membrane process could be a promising alternative with low energy cost for separation and small unit costs (lower footprints). At present, most of the commercial gas separation membranes are of polymeric in nature due to their easy fabrication at low cost. Various polymers are investigated for the olefin/paraffin separation [Burns (2003), Rungta (2013)]. Polymeric membranes have low C_2H_4/C_2H_6 selectivity of 2-6 [Rungta (2013)]. On the other hand, they show moderate selectivity of 4-27 for C_3H_6/C_3H_8 [Burns (2003)], but have low C_3H_6 flux. This selectivity usually reduces in the mixed gas permeation and at higher pressures (above 4 bar) due to strong plasticization effect of C_3

hydrocarbons on the membrane [Tanaka (1996)]. Typically, polymeric membrane materials exhibit a trade-off relationship in the separation performance (the improvement in the selectivity by the structural modification of polymer comes at the cost of reduction in the permeability and *vice versa*) [Robeson (1991, 2008)]. Thus, rather than new polymeric material development, there could be other promising techniques of membrane design for this type of separation.

The property of selective sorption of olefins by the transition metal ions was employed for the preparation of membrane materials for olefin/paraffin separation [Pinnau (2001), Ho (1994), Hsiue (1993), Sungpet (1997)]. Unfortunately, these materials are very sensitive to the feed impurities (especially sulfur), which strongly bind to the metal sight [Pinnau (2001), Eldridge (1993)], leading to deterioration of their performance.

Recently, some microporous materials have been discovered to show good kinetic separation characteristics for the olefin/paraffin separation, especially propylene/propane separation [Olson (2002), Li (2009), Lee (2011)]. These materials are difficult to transform into practical membrane and are mechanically very brittle. As discussed in the chapter 1, blending these materials with polymers to fabricate the composite membranes could be very promising approach. Among these materials, ZIF-8 is the most suitable for the fabrication of composite membranes due to its pore aperture (3.4 Å). Moreover, its organic functionality is expected to offer compatibility with the polymer matrix. Composite membranes based on ZIF-8 and PBI (Chapter 3) have shown good enhancement in the gas permeability. Among the used PBIs, DBzPBI-BuI based composite membranes showed the highest enhancement in the gas permeability with moderate selectivity. Thus, they are expected to show good flux for the hydrocarbons. This was the basis to choose ZIF-8@DBzPBI-BuI composite membranes for analyzing their performance towards olefin-paraffin separation. We also planned to fabricate and analyze thin film composite (TFC) membranes with an objective to reduce thickness of the selective layer, in order to further elevate the gas flux.

In the second part of this study, we have employed polyphenylene oxide (PPO) as another matrix material for the preparation of ZIF-8 based composite

membranes. The PPO could be a potential matrix material with adequate separation performance. It is among the very few polymers which show significantly high C_3H_6 permeability to be used for the practical separation [Tanaka (1996)]. The PPO is already commercialized as the membrane material for the practical gas separation applications [Baker (2002)]. This aspect improves the possibility of the scale-up of its ZIF-8 based composite membranes, if the significant improvement in the separation performance could be achieved.

5.2 ZIF-8@DBzPBI-BuI dense composite membranes

5.2.1 Physical properties of ZIF-8@DBzPBI-BuI composite membranes

The physical properties of the ZIF-8@DBzPBI-BuI composite membranes are described in the section 4.3.1 of chapter 4. The WAXD (Figure 5.1a), TGA analysis (Figure 5.1b) and SEM characterization (Figure 5.2) of the membranes used for olefin/paraffin separation study were repeated to check the structural integrity, composition and homogeneity of membranes, respectively. The results were well in agreement with as described in the section 4.3.1 of chapter 4.

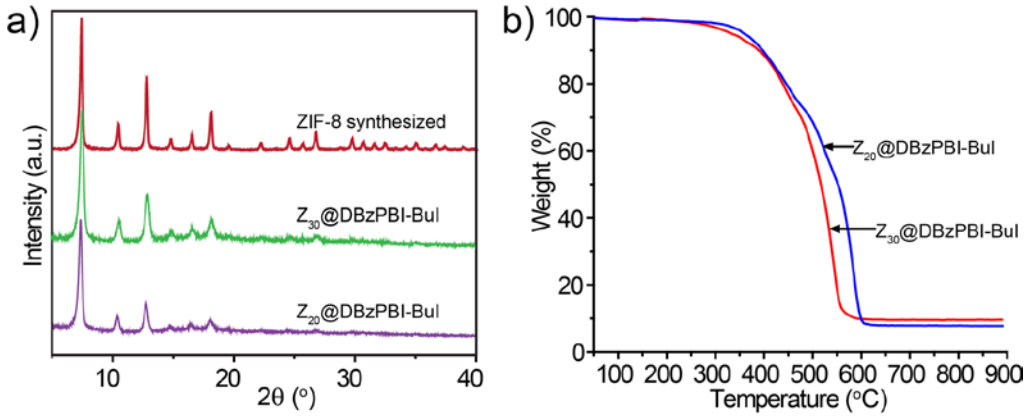

Figure 5.1 (a) XRD and (b) TGA spectra of the DBzPBI-BuI, ZIF-8 and composite membranes.

The WAXD spectra of the composite membranes showed characteristic sharp peaks of ZIF-8 and broad hump for polymer confirming their integrity (Figure 5.1a). The accurate loading of the ZIF-8 in the composite membrane is determined by the char yield of the composites in thermo gravimetric analysis performed in the air (Figure 5.1b). The

ZIF-8 content by this method was found to be 21% and 27.4%, which is close to the calculated one by the gravimetric estimation of ZIF-8 suspension.

The SEM images of the cross section of composite membrane also show similar highly homogeneous distribution of ZIF-8 nanoparticles without any agglomeration (Figure 5.2) as described in section 4.3.1 of chapter 4. There are no voids observed at the polymer-particle interface indicating good compatibility of the two materials.

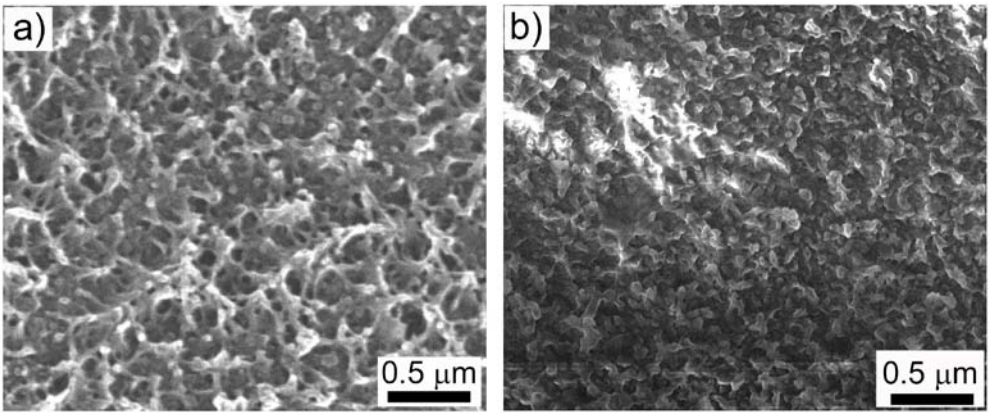

Figure 5.2 SEM images of the composite membranes cross-section;
(a) Z_{20}@DBzPBI-BuI and (b) Z_{30}@DBzPBI-BuI.

5.2.2 Gas permeation properties of ZIF-8@DBzPBI-BuI composite membranes

Pure gas permeability of C_2H_4, C_2H_6, C_3H_6 and C_3H_8 was determined using variable pressure method. As mentioned in the chapter 4, the composite membrane with 30% ZIF-8 loading was brittle. Hence membrane mounting in the permeation cell was done as described in section 2.6b of chapter 2 in order to avoid any rupture of the membrane (the small membrane of 5.6 cm^2 area was masked with the aluminum foil on edges and then was tested for the gas permeation). The permeability analysis was carried out at 3 bar pressure and at 35 °C temperature. The pristine DBzPBI-BuI membranes showed permeability for the C_2H_4 and C_3H_6 of 5 Barrer and 2.4 Barrer, respectively (Table 5.1), which is appreciably high. It shows the ideal selectivity of 3.2 for the pair C_2H_4/C_2H_6 and 12.6 for C_3H_6/C_3H_8. The effect of ZIF-8 content on the gas permeation could be seen in the Figure 5.3b, c. The addition of ZIF-8 greatly improved the permeability of the composite membranes than that of pristine polymer. The ethylene permeability was 25 and 50 Barrer in the membranes with 20 and 30% ZIF-8 content,

respectively. The propylene permeability also shows simultaneous improvement up to 20 Barrer. The C_3H_6/C_3H_8 ideal selectivity also greatly improved in the composite membranes up to 44 (Figure 5.3c, Table 5.1). To our knowledge, this is the highest selectivity than known in the literature for polymeric membranes. Zhang *at al.* has shown elevation in the C_3H_6/C_3H_8 selectivity by addition of ZIF-8 (48%) in 6FDA-DAM from 12.4 to 31 [Zhang (2012)].

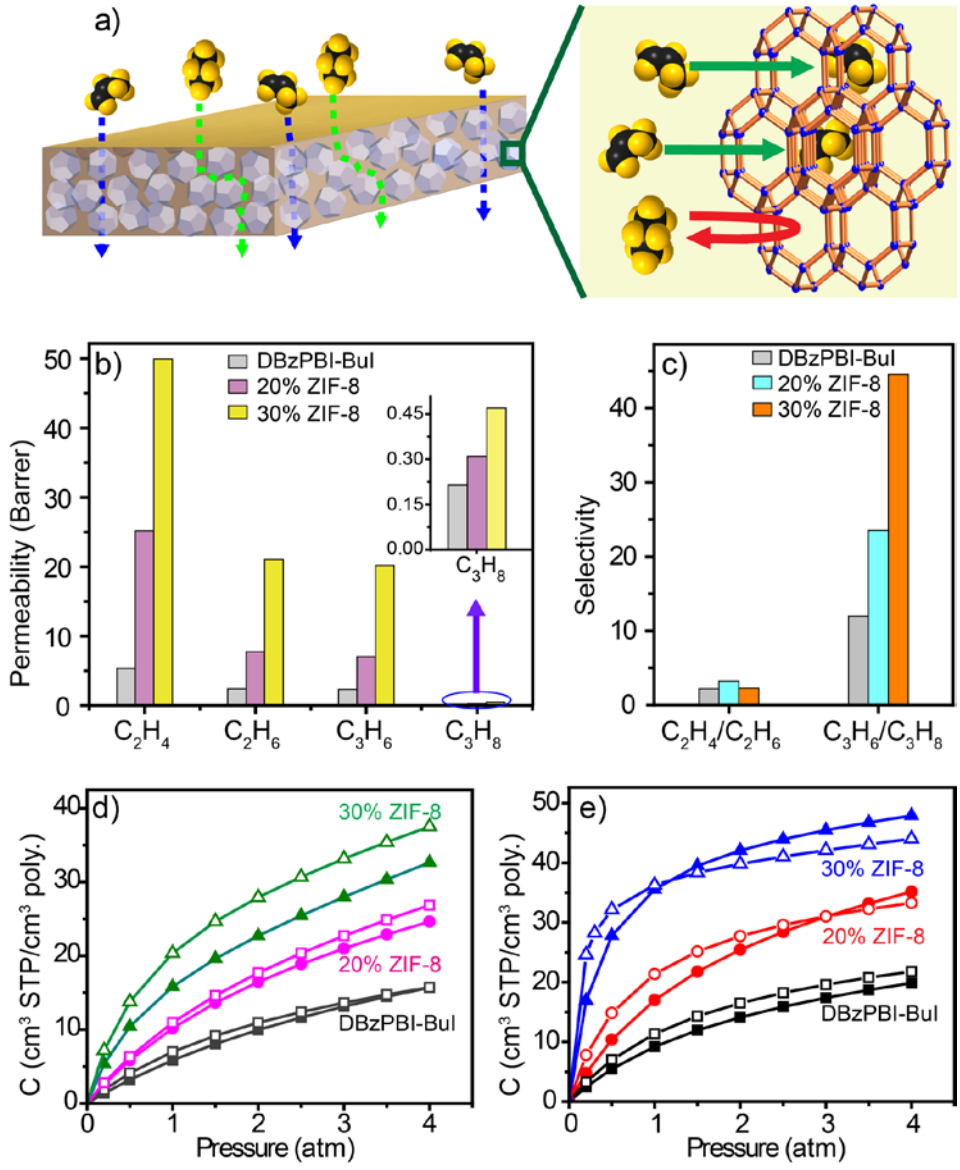

Figure 5.3 (a) Schematic permeation mechanism of the propylene and propane molecules through the composite membrane and ZIF-8 pores, (b) pure gas permeability, (c) ideal selectivity, (d) ethylene-ethane sorption and (e) propylene-propane sorption of the DBzPBI-BuI and composite membranes.

These promising effects of increase in permeability as well as selectivity were achieved by the addition of ZIF-8 into DBzPBI-BuI matrix having desired structural features. Firstly, this polymer has imidazole moiety that would offer compatibility with ZIF-8, avoiding any kind of agglomeration or interface voids. This is further assisted by the adequate permeability and selectivity of the matrix for propylene over propane. The DBzPBI-BuI's separation performance is near to the empirical upper bound given by the Burns et al [Burns (2008)] (Figure 5.4b).

The C_2H_4/C_2H_6 selectivity does not show any significant change with ZIF loading. Though the pore aperture size of the ZIF-8 (3.4 Å) is smaller than the Lennard Jonnes diameter (σ_{LJ}) of C_2H_4 (4.23 Å) and C_2H_6 (4.42 Å), the flexibility of of pore aperture size (due to conformational freedom of imidazole moieties) [Zhang (2012)] allows both the gases to pass through the aperture without much resistance. It is also reported that the diffusivity of only propane (σ_{LJ} = 5.06 Å) and larger molecules reduces sharply reduces in ZIF-8 pores [Zhang (2012)]. Thus, it can separate propylene (σ_{LJ} = 4.68 Å) from the propane but not the ethylene from ethane.

The attractive performance of composite membranes is further ascertained by performing mixed gas permeation using 1:1 composition of C_3H_6/C_3H_8. The mixed gas composition in feed and permeate side of the membranes was analyzed by gas chromatograph as mentioned in the section 2.7.2 of chapter 2. The C_3H_6 permeability of pristine DBzPBI-BuI membrane is decreased to 1.53 Barrer and also the C_3H_6/C_3H_8 selectivity up to 9.5 (Table 5.3). The decrease in the permeation performance while performing experiment with mixed gas could be understood by the competitive sorption of gases in the matrix. The composite membranes also showed similar reduction in the separation performance while using mixed gas as a feed stream (Table 5.3). The selectivity for C_3H_6/C_3H_8 shown by Z_{30}@DBzPBI-BuI membrane was reduced to 35.8, which is still higher than those known in the literature [Zhang (2012), Aksari (2013)]. Such a reduction of gas selectivity while using mixed gas as feed is well reported in the literature [Yang (2012), Zhang (2012)].

The gas sorption analysis in the present membranes was carried out in order to shed a light on their attractive permeation performance. The sorption isotherms of C_2H_4, C_2H_6, C_3H_6 and C_3H_8 for DBzPBI-BuI as well as composite membranes are given in Figure

5.3d, e. All the three membranes showed typical dual mode sorption behavior. The sorption for all gases showed high improvement with the increasing ZIF-8 content in the DBzPBI-BuI. The sorption coefficients for gases were increased by more than two times. The Langmuir type sorption was increasing with the ZIF-8 content in the composite membrane (Figure 5.3d-e). It is also indicated by the sorption parameters given in the Table 5.2. The high internal surface area of ZIF-8 results in the increase in the capacity constant (C_H'). The sorption of gases was increased according to their respective condensability. The membranes do not show selective sorption for either C_2H_4/C_2H_6 or C_3H_6/C_3H_8 (Figure 5.4a). This clearly indicates a role of ZIF-8 in increasing the gas sorption that is nonselective for olefin-paraffin.

Table 5.1 Permeability, solubility and diffusivity of the polymer and the composites.

	DBzPBI-BuI			**Z_{20}@DBzPBI-BuI**			**Z_{30}@DBzPBI-BuI**		
Gas	P	S	D	P	S	D	P	S	D
C_2H_4	5.2	4.4	0.91	25.4	7.0	2.76	49.0	9.3	4.00
C_2H_6	2.3	4.6	0.39	7.9	7.6	0.80	21.8	11.1	1.50
C_3H_6	2.4	5.8	0.32	7.3	10.3	0.54	20.2	15.2	1.01
C_3H_8	0.19	6.5	0.022	0.31	10.6	0.023	0.47	14.0	0.026

*Sorption coefficients calculated for 3 atm pressure

Table 5.2 Henry and Langmuir sorption parameters of the polymer and the composites.

	DBzPBI-BuI			**Z_{20}@DBzPBI-BuI**			**Z_{30}@DBzPBI-BuI**		
Gas	K_D	C'_H	b	K_D	C'_H	B	K_D	C'_H	b
C_2H_4	0.84	24.09	0.26	1.65	28.67	0.42	3.88	20.03	1.47
C_2H_6	0.83	18.72	0.48	2.36	26.42	0.48	3.22	28.83	1.46
C_3H_6	0.88	24.03	0.52	1.84	38.45	0.65	1.3	46.46	2.8
C_3H_8	0.55	26.83	0.67	0.75	35.88	1.35	1.56	38.88	8.34

Table 5.3 Mixed gas permeability and selectivity for propylene over propane (feed mixture composition is 1:1).

	P (C_3H_6)	**α (C_3H_6/C_3H_8)**
DBzPBI-BuI	1.53	9.5
Z_{20}@DBzPBI-BuI	4.28	17.9
Z_{30}@DBzPBI-BuI	14.87	35.8

Upon concluding negligible role of sorption in governing selectivity as above, gas diffusivity coefficients are further matter of consideration. As seen from Figure 5.4a, the diffusion selectivity of the C_2H_4/C_2H_6 remained unchanged while the C_3H_6/C_3H_8 selectivity increased with increasing ZIF-8 content in the membrane. The diffusion coefficient of C_3H_6 increased up to three times, while the diffusion coefficient of C_3H_8 did not show any significant change with 30% ZIF-8 addition (Table 5.1). This proves the role of the molecular sieving effect of ZIF-8 (Figure 5.3a) in improving the selective permeation of propylene over propane. The selective diffusion of C_3H_6 through the aperture of ZIF-8 with concurrent high diffusivity through polymer matrix led the present composite membranes far above the empirical upper bound proposed by the Burns *et al*. [Burns (2003)] (Figure 5.4b).

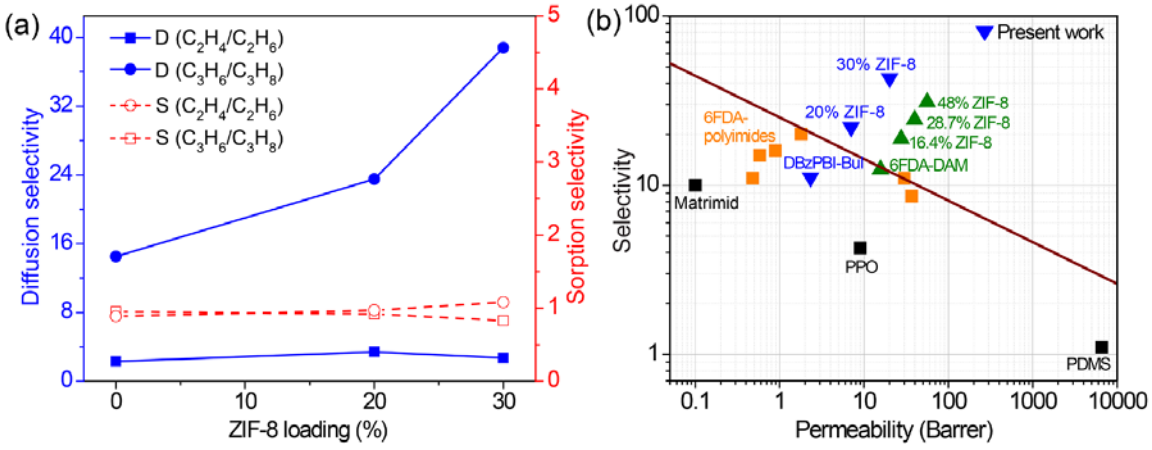

Figure 5.4 (a) Diffusion and sorption selectivity variation with ZIF-8 loading and

(b) placement of composite membranes on the empirical upper bound for propylene/propane separation performance.

5.3 ZIF-8@DBzPBI-BuI thin film composite membranes

5.3.1 Characteristics of ultrafiltration PAN support

The flat sheet PAN based supported ultrafiltration membrane was available in the lab that was made by a phase inversion method with controlled porosity. The water flux of the as prepared membrane was 40 $l.m^{-2}.h^{-1}$ at 1 bar pressure. The dried support membrane was very brittle and did not show any measurable air permeance. The support membrane dried after the solvent exchange procedure (mentioned in the chapter 2, section 2.4.2b) was maintaining the porosity and showed good nitrogen permeance of 33000 GPU at 5 psi pressure.

5.3.2 Cross-section morphology of the TFC membranes

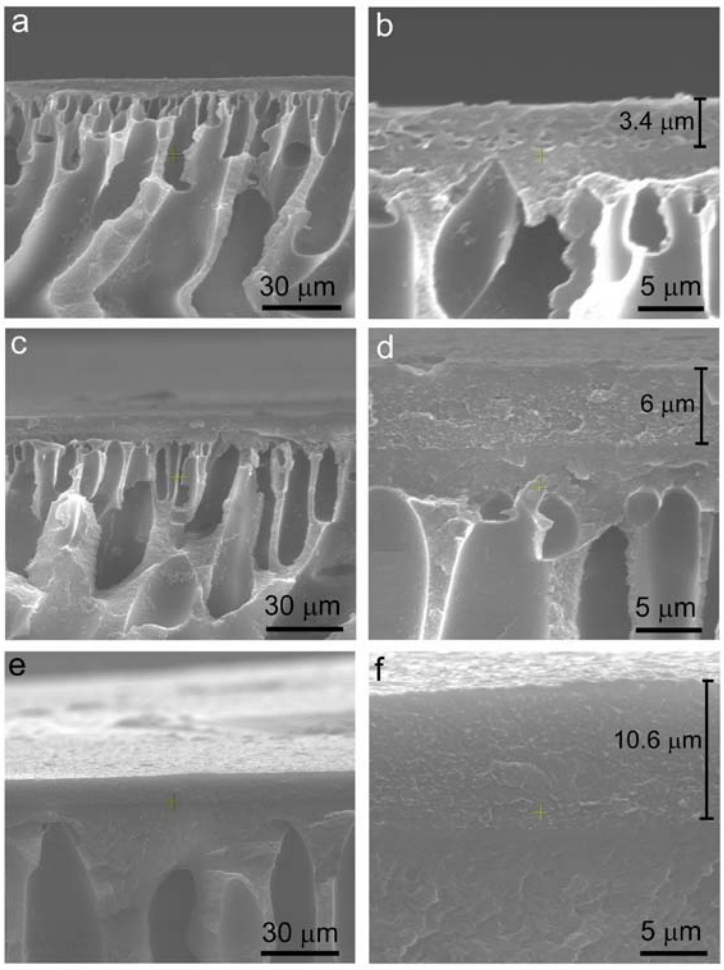

Figure 5.5 SEM images of (a, b) DBzPBI-BuI, (c, d) Z_{20}@DBzPBI-BuI and (e, f) Z_{30}@DBzPBI-BuI TFC membranes.

The SEM cross section of the TFC membranes is shown in Figure 5.5. They showed distinct coated layer on the PAN support (Figure 5.5 b, d, and f). There was no delamination of coating layer observed from the support PAN-membrane. This shows that there is a good adhesion of the two layers. It is necessary for the mechanical stability of the membrane at high pressures.

5.3.3 Gas permeation properties of the TFC membranes

The gas permeation analysis of the TFC membranes was carried out by the variable volume method at room temperature with 40 psi upstream pressure. The gas permeance of C_3H_6 and C_3H_8 was analysed using variable volume method. The permeance and the ideal selectivity data are given in the Figure 5.6. The DBzPBI-BuI based TFC membrane showed propylene permeance of 1 GPU with the C_3H_6/C_3H_8 selectivity of 16.6. This selectivity is slightly higher than the dense membrane selectivity data (Table 5.1), which may be due to the small error of the method of determination of permeance. This high selectivity proves that the DBzPBI-BuI coating was defect free. The Z_{20}@DBzPBI-BuI TFC membrane showed great improvement in the propylene permeance as well as selectivity. The permeance of C_3H_6 was increased by three times to 3.08 GPU. The C_3H_6/C_3H_8 selectivity was also increased by 1.4 times to 23. The further increase of ZIF-8 content up to 30% in the selective layer was improving the C_3H_6 permeance up to 4.9 GPU with excellent C_3H_6/C_3H_8 selectivity of 32.5. The C_3H_6/C_3H_8 selectivity of the ZIF-8 containing composite membranes was lower than the dense membrane data; it may be due to the minor defects in the selective layer. We also tried to further increase the ZIF-8 content in the selective layer, but unfortunately those membranes were not showing any selectivity, possibly due to the defective coating morphology. The improvement in the permeation performance is still significantly high with the ZIF-8 loading up to the 30%. These results demonstrate that the ZIF-8@DBzPBI-BuI composite based TFC membranes could be successfully scaled up with promising separation properties. Thickness of the coating layer need be further reduced by the optimization of membrane preparation parameters.

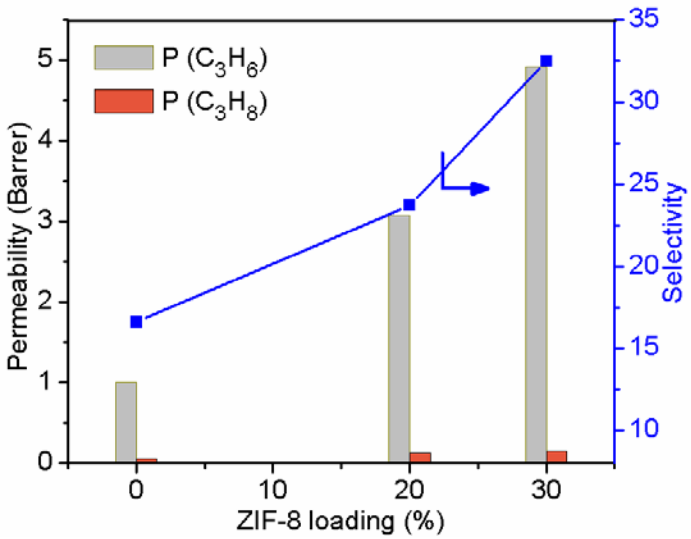

Figure 5.6 Propylene separation performance of TFC membranes with increasing ZIF-8 loading.

5.4 ZIF-8@PPO composite membranes

5.4.1 Synthesis of PPO

The commercially available PPO powder (P803) was not used for our study as it has low molecular weight and thus has lower mechanical properties which are not favorable for the composite membrane preparation. The synthesis of high molecular weight PPO was carried out by modifying the reported procedure [Penczek (1986)] of oxidative coupling in the presence of $CuCl_2$ as catalyst as given in Chapter 2, Section 2.3.3. The obtained purified polymer showed high intrinsic viscosity of 1.53 with good film forming ability.

5.4.2 Composite membrane preparation

The normal casting led to fast evaporation of chloroform which did not yield good transparent composite membranes. It is documented in the literature that the fast solvent evaporation creates thermal gradient in the casted solution which results in the formation of convection cells in the solution [Chung (2007)]. These convection currents bring the nanoparticles (with comparatively lower density) at the surface, destroying the homogeneity of the resulting membrane. Thus, in order to avoid fast evaporation of the solvent, casted solution was covered with an inverted funnel having a small opening at the top. This methodology worked

successfully and the obtained membranes exhibited good transparency (Figure 5.7a). The composite membranes were very brittle and could be prepared only up to 25% loading. The composite membrane with 25% ZIF loading was though fairly transparent, it showed some patches of gel like precipitate (Figure 5.7a).

5.4.3 Physical properties of the membranes

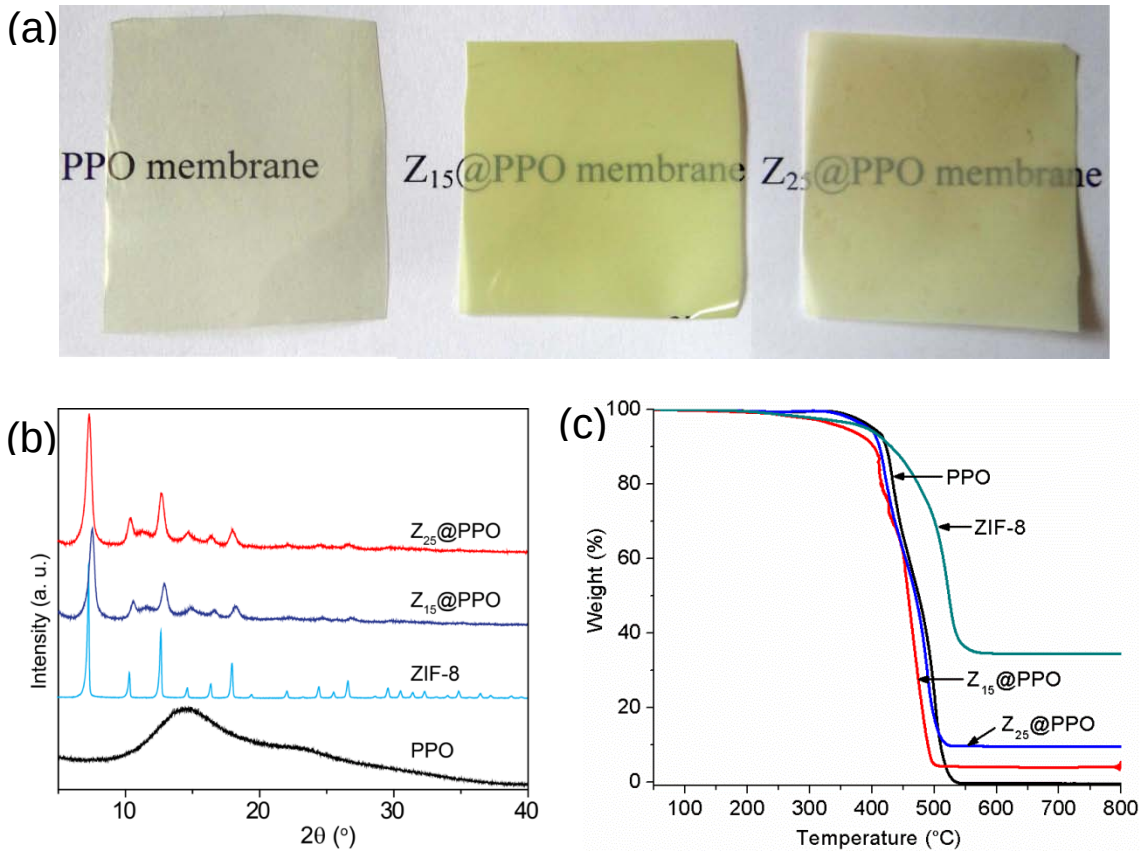

Figure 5.7 (a) Photographs of the membranes, (b) XRD and (c) TGA spectra of spectra of the ZIF-8, PPO and composite membranes.

The WAXD spectra of the PPO membrane showed a broad hump like peak which corresponds to the inter-chain spacing (d_{sp}). The d_{sp} is a qualitative indication of internal free volume of polymer. The d_{sp} calculated by the Bragg's equation for PPO was 6.14 Å, which is in agreement with the reported value [Aguilar (1993)]. A small shoulder like peak was also present corresponding to 3.7 Å indicating bimodal distribution of free volume. The large value of d_{sp} is an indication of high free volume of PPO, which causes easy diffusion of gas

molecules through polymer matrix and thus produces high gas permeability. The XRD spectra of composite membranes showed sharp multiple peaks belonging to ZIF-8, in addition to the characteristic amorphous hollow of matrix polymers (Figure 5.7b). This indicates that the structure of ZIF-8 is intact in the composite membranes.

The thermo-gravimetric analysis (TGA) of the polymer and composite membranes was done in the air. In the TGA the PPO showed thermal stability up to 420 °C (Figure 5.7c). This is in agreement with the literature reports [Aguilar (1993)]. As the ZIF-8 is stable up to 450 °C, the composite membranes start degrading at 420 °C due to the degradation of PPO. From the char yield of TGA analysis the exact ZIF-8 content in the Z_{15}@PPO and Z_{25}@PPO membranes was estimated. It was found 13.4 and 26.8% respectively, near to the initially calculated amount.

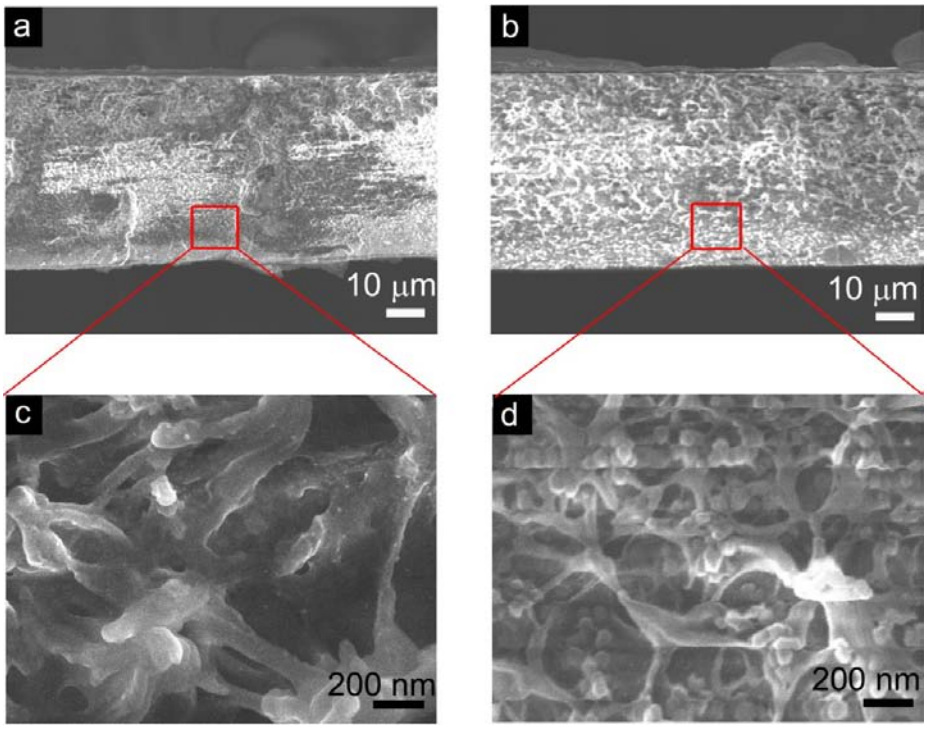

Figure 5.8 SEM images of the composite membrane cross section, (a) with 15% ZIF-8 content and (b) with 25% ZIF-8 content.

SEM images of the cross section of composite membranes (Figure 5.8) did not show any gradient of the particles throughout the thickness. In the composite

membrane with 15% ZIF-8 loading, a nice homogeneous distribution of the nanoparticles throughout the membrane cross sections was observed without any agglomeration in the SEM image (Figure 5.8a and c). On the other hand some agglomeration of ZIF-8 nanoparticles was observed in the SEM image of composite membrane with 25% ZIF-8 loading (Figure 5.8b and d).

The TEM images also showed similar morphology (Figure 5.9). In the composite membrane with 15% ZIF loading, almost homogeneous distribution of ZIF particles was observed with some small particle agglomerates appearing (Figure 5.9a and c). On the other hand the composite membrane with 25% ZIF-8 loading showed large agglomerates of ZIF-8 nanoparticles in the TEM image (Figure 5.9b and d).

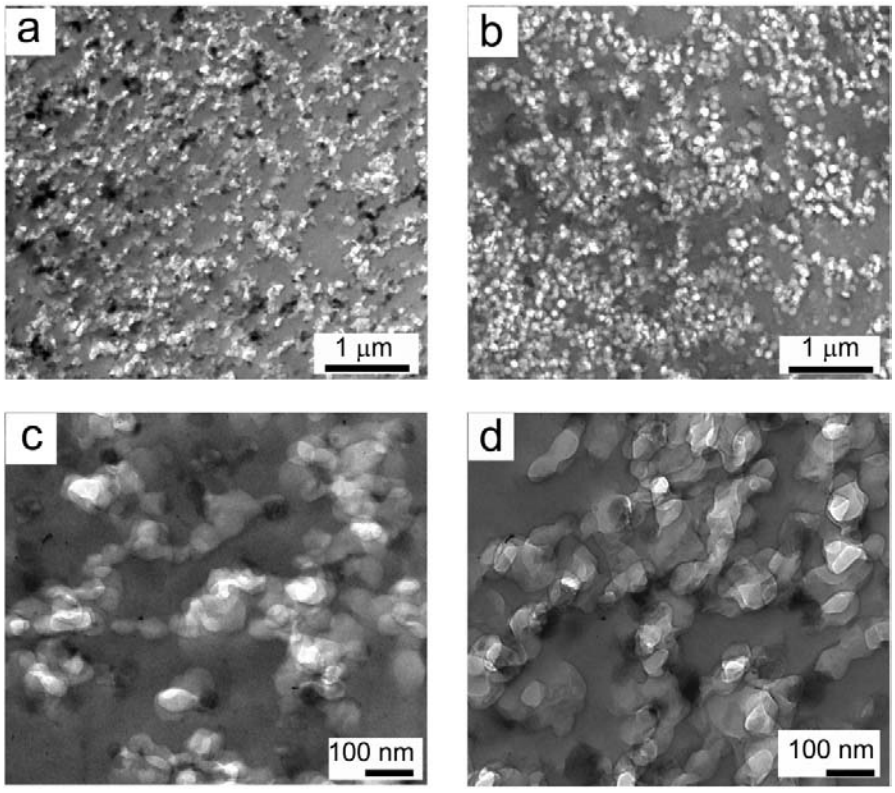

Figure 5.9 TEM images of the composite membranes, (a, c) 15% ZIF-8 containing membrane and (b, d) 25% ZIF-8 containing membrane.

5.4.4 Gas permeation properties

The single gas permeability of the H_2, N_2, CH_4, CO_2 C_3H_6 and C_3H_8 was measured by the variable pressure method. The obtained gas permeability data of

the permanent gases for the pristine polymer membrane were in agreement with the literature reported values [Aguilar (1993)]. The C_3H_6 and C_3H_8 permeability were somewhat higher than the reported data [Tanaka (1996)] but the C_3H_6/C_3H_8 selectivity was matching well. This may be due to difference in the temperature and pressure conditions of gas permeation measurement of reported data. The addition of ZIF-8 significantly improved the gas permeation properties of the resultant composite membranes as shown in the Figure 5.10. The composite membrane with 15% ZIF-8 content showed an increase in the H_2 permeability from 94.8 to 147.5 Barrer with small decrease in its selectivity over N_2 and CH_4. Similarly, the CO_2 permeability also showed increase from 59.8 to 100.42 with small decrease in its selectivity over the N_2 and CH_4. This result was expected as the ZIF-8 could not discriminate between these small molecules and only facilitate their easy diffusion through its pores. On the other hand the C_3H_6 permeability increased from 3.9 to 6.4 with simultaneous improvement in it selectivity over C_3H_8 by 254%. This high improvement in the C_3H_6/C_3H_8 separation performance shows the effectiveness of ZIF-8 as filler in the PPO based composite membrane. The high kinetic selectivity for the C_3H_6 over C_3H_8 is reported in the ZIF-8 crystals [Li (2009)]. Thus as a filler it facilitates the preferentially faster permeation of the C_3H_6 through its pores over C_3H_8 which resulted in the improvement in the selectivity.

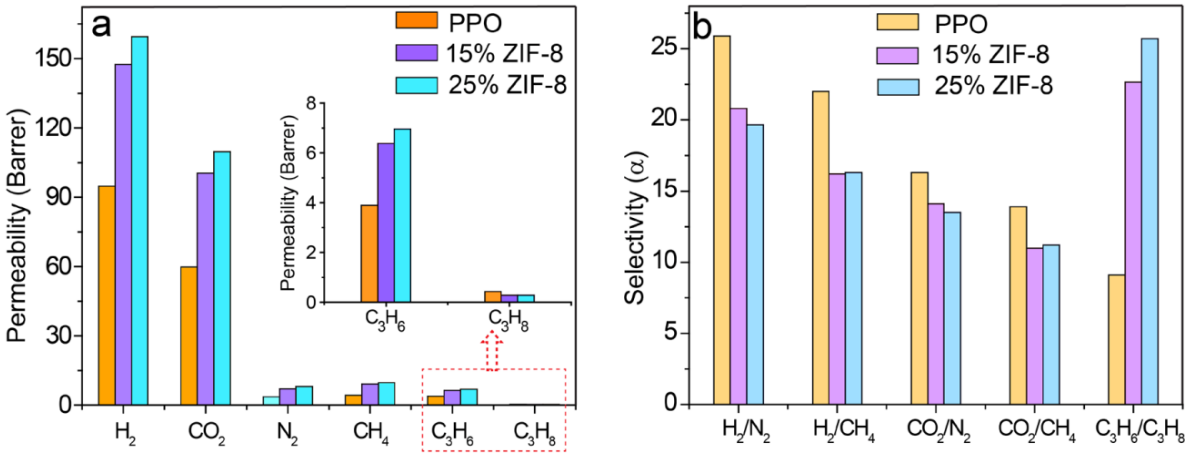

Figure 5.10 (a) Gas permeability and (b) ideal selectivity of the membranes.

The composite membrane with 25% ZIF-8 loading also showed increase in the gas permeability and C_3H_6/C_3H_8 selectivity but the improvement was no greater than the Z_{15}@PPO containing membranes. This was a surprising result but could be explained by understanding the membrane morphology. As discussed above, in 25% ZIF containing composite membrane, the dispersion of ZIF-8 nanoparticles was not highly homogeneous and agglomerates of the nanoparticles were prominent. This poor dispersion of the ZIF nanoparticles is considered as defective morphology [Song (2012)] and not produces high improvement in the permeation properties. The filler agglomeration in the composite happens due to the weak interactions between the filler particles and the surrounding matrix. The polymer-filler adhesion is dependent on the energy of self association of two phases (polymer and filler) and energy of the association with each other. Thus for good adhesion, polymer-filler interactions should be stronger than the polymer inter-chain and filler-filler interactions. The PPO have low inter-chain interaction due to lack of any strong force like H-bonding, ionic interactions or π- π stacking etc. That is why it has high free volume (high d_{sp}) and high gas permeability. Its ether group is crowded by the two adjacent methyl groups and which hinders its effective H-bonding with the imidazole (Im) on the ZIF-8 surface. But ZIF particles can interact with each other by Im-H...Im hydrogen bonding or Im-Zn coordination. Thus the filler-filler interactions are possibly dominating the polymer-filler interactions, not favoring the ideal composite formation. In the solution state the solvent molecules wets the particles and keep them dispersed. When the solvent evaporates and membrane solidifies then these polymer-filler interaction comes to play. At low ZIF-8 loading, ZIF-8 nanoparticles are comparatively more separated at time of membrane formation, thus gets arrested in the dispersed phase. In case of higher ZIF-8 loading particles becomes abundant and comes to proximity during membrane formation, leading to the agglomeration of the particles in the absence of strong polymer-filler interaction.

Even though the higher particle loading is not fruitful, merely 15% ZIF loading is resulting in the good improvement in the C_3H_6/C_3H_8 separation performance of the membrane making it promising for the application. The present

improved permeation performance of the composite membranes is crossing the empirical upper bound (Figure 5.11) defined by Burns *et al.* [Burns (2008)].

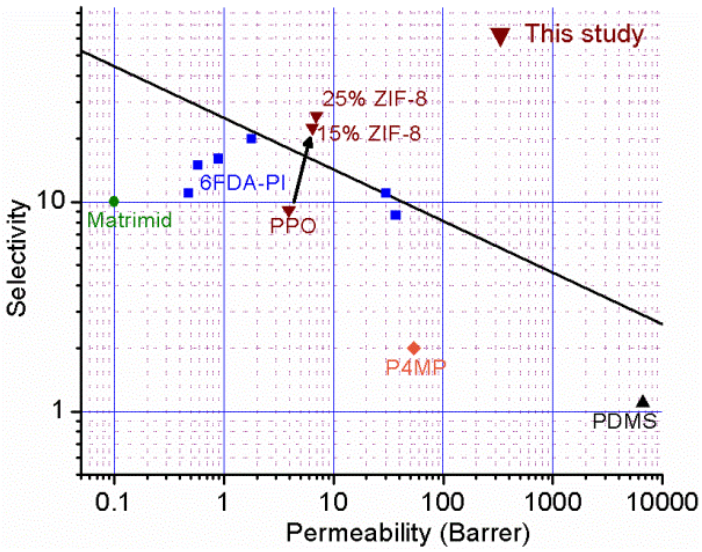

Figure 5.11 Placement of ZIF-8@PPO composite membranes on the empirical upper bound.

5.5 Conclusion

The DBzPBI-BuI works as the ideal matrix material for the ZIF-8 based composite membranes due to its structural analogy with the ZIF-8 which helps it to have a good compatibility with the nanofiller. This results in to the excellent improvement in the propylene separation performance. This high performance composite material was also transformed into thin membrane, supported on the PAN support for the possible scale-up for practical application. Though these membranes's separation performance was lesser than the dense composite membranes yet it is promising for the scale up. On the other hand, the PPO as matrix is showing good improvement in the separation performance only up to 15% ZIF-8 loading. Further increase in the ZIF loading is not resulted in the improvement in the membrane separation performance due to the agglomeration of ZIF-8 nanoparticles. This study shows that the chemical functionality and gas permeation properties of the matrix are very crucial for realizing the full potential of separation performance of filler material.

Chapter 6

Conclusions and future perspective

6.1 Conclusion

This is the first detailed study on investigation of effects of polymer structure on the gas permeation properties of the MOF-based composite membranes. This study would help in optimizing polymer structural architecture for the better compatiblization of polymers with MOFs as the filler particles. The polybenzimidazoles with structural variation were chosen as matrix materials due to their excellent thermochemical and gas permeation properties. The CuBTC and ZIF-8, two representative MOFs are chosen as filler material due to their easy synthesis and promising separation characteristics. MOF nanoparticles used as filler were expected to show better compatibility with chosen polymer matrix due to the high surface area exposed to interact. This was also reflected in the SEM images, as no voids at MOF-polymer interface were observed in any of the membrane. The effect of polymer structural variation on the CuBTC based composite membrane gas separation performance was very surprising as discussed in the chapter 3. All four polymers showed very different change in the gas permeation properties with CuBTC filler addition. The composites of PBI-HFA showed good improvement in the gas permeability with simultaneous increase in CO_2 based selectivities. This improvement of separation performance reflects good interfacial interactions between the polymer and filler. In contrast the PBI-BuI based composite membranes showed loss of selectivity with moderate improvement in permeability. This concludes that the polar groups of the PBI-HFA are better interacting with the MOF surface. The *N*-substituted PBIs (DMPBI-BuI and DBzPBI-BuI) with no inter-chain hydrogen bonding also showed very diverse results. The DMPBI-BuI based composite membranes showed no loss in the selectivity which shows that the vanished inter-chain H-bonding is helping the polymer chains in better adherence with the filler surface. DBzPBI-BuI based composite membranes showed a reduction in the permeability compared to pristine polymer. This is only possible when the filler pores at the surface are blocked to reduce the filler

impermeable. This pore blockage is assumed to be due to the intrusion of bulky t-butyl pendent groups of strongly adsorbed polymer chains into pore apertures. Thus composite membranes of PBI-BuI, DMPBI-BuI and DBzPBI-BuI show gradual change in the gas permeation properties showing increasing MOF-polymer interaction. This is the reverse to their d-spacing order (indication of inter-chain distance).

The effect of polymer structural variation on the composite membrane gas separation performance was also investigated using ZIF-8 as filler in three different polymers (PBI-BuI, DMPBI-BuI and DBzPBI-BuI) as discussed in the chapter 4. The ZIF-8 with structural analogy with PBIs, was expected to show better compatibility. The addition of ZIF-8 in all three PBIs led to high (generally 3-4 times) permeability enhancement. This was accompanied with no significant change in selectivity. This concludes that the structural similarity helps to establish better interaction between the complementary groups leading to ideal interface formation for maximizing filler effect. These composite membranes showed a peculiar phenomenon of reduction in the density of matrix phase. This reduction was very large (~14%) in case of DMPBI-BuI based membranes. This large change in the matrix density led to permeability increase up to ten times than the pristine case. Both CuBTC and ZIF based composite membrane's gas permeation properties concludes the critical importance of the polymer's structural features. The excellent improvement in the gas permeability in ZIF based composite membranes inspired us to make dual layer composite membranes with top layer containing high ZIF loading and bottom support layer with no ZIF content. The dual layer composite membranes are expected to show better mechanical stability than the single layer composite membranes. This effort was partially successful as the composite membranes could be formed without delamination between the selective layer and support layer. Unfortunately complete defect elimination in the selective layer was not achieved with optimization of membrane preparation parameters. The improvement in the phase inversion process and maintenance of high degree of homogeneity is crucial for complete defect elimination.

The DBzPBI-BuI show high permeability than the other PBIs. It is the only PBI which could show the measurable flux for the higher hydrocarbons like propylene and propane. Thus DBzPBI-BuI and its composite membranes with ZIF-8 were studied for

the olefin-paraffin separation as discussed in the chapter 5. The composite membranes showed excellent improvement in the gas permeability up to eight times. This was also accompanied by the C_3H_6/C_3H_8 selectivity improvement by three times. These composite membranes have far superior separation performance than the reported in the literature. This concludes that this imidazole based polymer has ideal compatibility with the ZIF-8 nanoparticles leading to maximizing of filler's effect on composite membrane gas permeation properties. The mixed gas permeation was conducted to further evaluate these membranes for practical significance. The mixed gas separation performance was comparatively lower than the pure gas data but was still superior to the reported literature values. The good solubility properties of the DBzPBI-BuI enabled us to transform these composite membranes into thin film composite membranes which have more practical significance. Though the TFC membranes were not as selective as the dense composite membranes but still they showed selectivity of practical significance which could be further enhanced by the careful optimization of membrane preparation parameters.

Polyphenylene oxide (PPO) is another polymer with suitable flux for the propylene. It is a commercialized polymer with low cost. As the synthesis of substituted PBI (DBzPBI-BuI) is an elaborated procedure, PPO could be more advantageous for composite membrane preparation. Thus the ZIF-8@PPO composite membranes were fabricated and studied for the C_3H_6/C_3H_8 separation properties as discussed in the chapter 5. The ZIF-8@PPO composite membranes showed good improvement in the separation performance at the 15% ZIF loading. Higher ZIF loading was not improving the separation properties further due to the agglomeration of the ZIF-8 particles. This study shows the limitation of PPO as matrix material for the ZIF-8 based composite membrane preparation.

6.2 Future perspective

Our work on the ZIF-8@DBzPBI-BuI membranes for propylene/propane separation is highly promising due to high mixed gas selectivity. These materials could be of great practical significance if composite membranes with ultrathin selective layer ($\leq$ 1μm) free of defects could be formed with sufficient mechanical robustness. Ideally in such composite membranes the polymer should work only as a binding agent and the permeation should occur predominantly through the molecular sieve as shown in the

Figure 6.1. The dual layer composite and TFC membranes prepared in our study are mechanically stable even at high ZIF loading. There is need for further optimization of membrane fabrication parameters to obtain thin selective layer. The dual layer composite hollow fiber is another way to obtain the thin selective MOF@polymer composite layer with better control the process parameters and delamination related problems.

References

Adams R., Carson C., Ward J., Tannenbaum R., Koros W., *Microporous Mesoporous Mater.*, **2010**, 131, 13-20.

Aguado S., Nicolas C.-H., Moizan-Baslé V., Nieto C., Amrouche H., Bats N., Audebrand N., Farrusseng D., *New J. Chem.*, **2011**, 35, 41-44.

Aguilar M., Paul D.R., *J. Polym. Sci. Part B: Polym. Phys.*, **1993**, 31, 1577-1589.

Ameloot R., Vermoortele F., Vanhove W., Roeffaers M.B.J., Sels B.F., De Vos D.E., *Nature Chemistry*, **2011**, 3, 382-387.

Askari M., Chung T.S., *J. Membr. Sci.*, **2013**, 444, 173-183.

Bae T.H., Lee J.S., Qiu W., Koros W.J., Jones C.W., Nair S., *Angew. Chem. Int. Ed.*, **2010**, 49, 9863-9866.

Bae T.H., Long J.R., *Energy Environ. Sci.*, **2013**, 6, 3565-3569.

Baker R.W., *Ind. Eng. Chem. Res.* **2002,** *41*, 1393-1411.

Baker R.W., *Membrane Technology and Applications*, 2nd Ed., Wiley, New York, **2004**.

Banerjee R., Phan A., Wang B., Knobler C., Furukawa H., O'Keeffe M., Yaghi O.M., *Science*, **2008,** 319, 939-943.

Barbari T.A., *J. Polym. Sci. Part B. Polym. Phys.*, **1997**, 35, 1737-1746.

Basu S., Cano-Odena A., Vankelecom I.F.J., *J. Membr. Sci.*, **2010**, 362, 478-487.

Beldon P.J., Fábián L., Stein R.S., Thirumurugan A., Cheetham A.K., Friščić T., *Angew. Chem.*, **2010**, 122, 9834-9837.

Belohlav L.R., *Angew. Makromol. chemie.*, **1974**, 40, 465-483.

Ben T., Lu C., Pei C., Xu S., Qiu S., *Chem. – Eur. J.*, **2012**, 18, 10250-10253.

Bender M., *ChemBioEng Rev.*, **2014**, 4, 136-147.

Bhole Y.S., Karadkar P.B., Kharul U.K., *Eur. Polym. J.*, **2007a**, 43, 1450-1459.

Bickel C.S., Koros W.J., *J. Membr. Sci.*, **2000**, 170, 205-214.

Bondar I.V., Freeman B.D., Pinnau I., *J. Polym. Sci.; Part B: Polym. Phys.*, **2000**, 38, 2051-2062.

Bondi A., *J. Phys. Chem.*, **1964**, 68, 441-451.

Burns R.L., Koros W.J., *J. Membr.* Sci., **2003,** 211, 299-309.

Bushell A.F., Attfield M.P., Mason C.R., Budd P.M., Yampolskii Y., Starannikova L., Rebrov A., Bazzarelli F., Bernardo P., Jansen J.C., Lanč M., Friess K., Shantarovich V., Gustov V., Isaeva V., *J. Membr. Sci.*, **2013**, 427, 48-62.

Bux H., Liang F., Li Y., Cravillon J., Wiebcke M., Caro J., *J. Am. Chem. Soc.*, **2009**, 131, 16000-16001.

Car A., Stropnik C., Peinemann K.V., *Desalination,* **2006**, 200, 424-426.

Chen X.Y., Thang H.V., Rodrigue D., Kaliaguine S., *Ind. Eng. Chem. Res.*, **2012**, 51, 6895-6906.

Chui S.S.Y., Lo S.M.F., Charmant J.P.H., Orpen A.G., Williams I.D., *Science,* **1999,** 283, 1148-1150.

Chung T.S., Jiang L.Y., Li Y., Kulprathipanja S., *Prog. Polym. Sci.*, **2007**, 32, 483-507.

Cohen S.M., *Chem. Rev.*, **2012**, 112, 970-1000.

Coleman M.R., Koros W.J., *J. Membr. Sci.*, **1990**, 50, 285-297.

Costello L.M., Koros W.J., *J. Polym. Sci.; Part B: Polym. Phys.*, **1994**, 32, 701-713.

Cravillon J., Münzer S., Lohmeier S.J., Feldhoff A., Huber K., Wiebcke M., *Chem. Mater.*, **2009**, 21, 1410-1412.

Crawford D., Casaban J., Haydon R., Giri N., McNally T, James S.L., *Chem. Sci.*, **2015**, 6, 1645-1649.

Czaja A.U., Trukhan N., Müller U., *Chem. Soc. Rev.*, **2009**, 38, 1284-1293.

Daynes H.A., *Proc. Roy. Soc.*, **1920**, 97A, 286-307.

de Sales J.A., Patrício P.S.O., Machado J.C., Silva G.G., Windmöller D., *J. Membr. Sci.*, **2008**, 310, 129-140.

Díaz K., López-González M., Castillo L.F.d., Riande E., *J. Membr. Sci.*, **2011**, 383, 206-213.

Dong X., Huang K., Liu S., Ren R., Jin W., Lin Y. S., *J. Mater. Chem.*, **2012**, 22, 19222–19227.

Duval J.M., Kemperman A.J.B., Folkers B., Mulder M.H.V., Descjrandchamps G., Smolders C.A., *J. Appl. Polym. Sci*, **1994**, 54, 409-418.

Eddaoudi M., Sava A.F., Eubank J.F., Adila K., Guillerm V., *Chem. Soc. Rev.*, **2015**, 44, 228-249.

Eldridge R.B., *Ind. Eng. Chem. Res.*, **1993**, 32, 2208-2212.

Fan S., Sun F., Xie J., Guo J., Zhang L., Wang C., Pan Q., Zhu G., *J. Mater. Chem. A*, **2013**, 1, 11438-11442.

Feng C., Khulbe K.C., Matsuura T., Farnood R., Ismail A.F., *Journal of Membrane Science and Research*, **2015**, 1, 49-72.

Furukawa H., Cordova K.E., O'Keeffe M., Yaghi O.M., *Science*, **2013,** 341, 974-986.

Gascon J., Aguado S., Kapteijn F., *Microporous Mesoporous Mater.*, **2008**, 113, 132-138.

Ge L., Zhou W., Rudolph V., Zhu Z., *J. Mater. Chem. A*, **2013**, 1, 6350-6358.

Ghanem B.S., Swaidan R., Litwiller E., Pinnau I., *Adv. Mater.*, **2014**, *26*, 3688-3692.

Ghosal K., Chern R.T., Freeman B.D., *Macromolecules*, **1996**, 29, 4360-4369.

Ghosal K., Chern R.T., *J. Membr. Sci.*, **1992**, 72, 91-97.

Ghosal K., Freeman B.D., *Polym. Adv. Tech.*, **1994**, 5, 673- 697.

Goh P.S., Ismail A.F., Sanip S.M., Ng B.C., Aziz M., *Sep. Purif. Rev.*, **2011,** 81, 243-264.

Graham T., *Phil. Mag.*, **1866**, 32, 401-420.

Graham T., *Proc. R. Soc. Lond.*, **1867-1868**, 16, 422-427.

Guerrero V.V., Yoo Y., McCarthy M.C., Jeong H.K., *J. Mater. Chem.*, **2010**, 20, 3938-3943.

Guiver M.D., Thi H.N.L., Robertson G.P., *US patent*, **2003**, US6605140 B2.

Gülmüs S.A., Yilmaz L., *J. Polym. Sci.; Part B: Polym. Phys.*, **2007**, 45, 3025-3033.

Guo H., Zhu G., Hewitt I.J., Qiu S., *J. Am. Chem. Soc.*, **2009**, 131, 1646-1647.

Hao L., Li P., Yang T., Chung T.S., *J. Membr. Sci.*, 2013, 436, 221-231.

Hara N., Yoshimune M., Negishi H., Haraya K., Hara S., Yamaguchi T., *J. Membr. Sci.,* **2014**, 450, 215-223.

Hellums M.W., Koros W.J., Husk G.R., Paul D.R., *J. Membr. Sci.*, **1989**, 46, 93-112.

Hennis J.M.S., Tripodi M.K., *US Patent*, **1980**, US 4230463.

Ho W.S., Dalrymple D.C., *J. Membr. Sci.*, 1994, 91, 13-25.

Horn N.R., Paul D.R., *Polymer*, **2011**, 52, 5587-5594.

Hsiue G.H., Yang J.S., *J. Membr. Sci.*, **1993**, 82, 117-128.

Hu Y., Dong X., Nan J., Jin W., Ren X., Xu N., Lee Y. M., *Chem. Commun.,* **2011**, 47, 737-739.

Huang A., Bux H., Steinbach F., Caro J., *Angew. Chem.,* **2010**, 49, 4958-4961.

Huang A., Chen Y., Liu Q., Wang N., Jiang J., Caro J., *J. Membr. Sci.*, **2014**, 454, 126-132.

Huang A., Dou W., Caro J., *J. Am. Chem. Soc.*, **2010**, 132, 15562-15564.

Huang A., Wang N., Kong C., Caro J., *Angew. Chem. Int. Ed.*, **2012**, 51, 10551-10555.

Huang L.M., Wang H.T., Chen J.X., Wang Z.B., Sun J.Y., Zhao D.Y., Yan Y.S., *Microporous Mesoporous Mater.*, **2003**, 58, 105-114.

Hunter J.B., *US Patent*, **1956**, US 2773561.

Ismail A. F., David L. I. B., *J. Membr. Sci.*, **2001**, 193, 1-18.

Jeazet H.B.T., Staudt C., Janiak C., *Chem. Commun*., **2012**, 48, 2140-2142.

Jeazet H.B.T., Staudt C., Janiak C., *Dalton Trans.*, **2012**, 41, 14003-14027.

Jiang L.Y., Chung T.S., Cao C., Huang Z., Kulprathipanja S., *J. Membr. Sci.*, 2005, 252, 89-100.

Kanehashi S., Nagai K., *J. Membr. Sci.*, **2005**, 253, 117-138

Karadkar P.B., *M.E. Thesis*, **2006**, Nagpur University, India.

Karger J., Ruthven D.M., *Diffusion in Zeolites and Other Microporous Solids.*; John Wiley & Sons, Inc., **1991**.

Karra J.R., Walton K.S., *J. Phys. Chem. C*, **2010**, 114, 15735-15740.

Kaye S.S., Dailly A., Yaghi O.M., Long J.R., *J. Am. Chem. Soc.*, **2007**, 129, 14176-14177.

Keil F.J., Krishna R., Coppens M.O., *Rev. Chem. Eng.,* **2000**, 16, 71-197.

Keskin S., Liu J., Johnson J.K., Sholl D.S., *Microporous Mesoporous Mater.*, **2009**, 125, 101-106.

Khan N.A., Jhung S.H., *Bull. Korean Chem. Soc.*, **2009**, 30, 2921-2926.

Kharul U.K., Kulkarni S.S., *US Patent*, **2002**, US 6420511.

Kim J., Kim S.H., Yang S.T., Ahn W.S., *Microporous Mesoporous Mater.*, **2012**, 161, 48-55.

Kim T.-H., Koros W.J., Husk G.R., *J. Membr. Sci.*, **1989**, 46, 43-56.

Klimakow M., Klobes P., Thünemann A.F., Rademann K., Emmerling F., *Chem. Mater.*, **2010**, 22, 5216-5221.

Koros W.J., *J. Polym. Sci. Polym. Phys. Ed.*, **1985**, 23, 1611-1628.

Kulprathipanja S., Neuzil R.W., Li N.N., *US patent*, **1988**, US 4740219.

Kumbharkar S.C., Karadkar P.B., Kharul U.K., *J. Membr. Sci.*, **2006**, 286, 161-169.

Kumbharkar S.C., Kharul U.K., *Eur. Polym. J.*, **2009**, 45**,** 3363-3371.

Kwon H.T., Jeong H.K., *J. Am. Chem. Soc.*, **2013**, 135, 10763-10768.

Laínez J.S., Zornoza B., Mayoral A., Murcia A.B., Amorós D.C., Téllez C., Coronas J., *J. Mater. Chem. A*, **2015**, 3, 6549-6556.

Lee C.Y., Bae Y.S., Jeong N.C., Farha O.K., Sarjeant A.A., Stern C.L., Nickias P., Snurr R.Q., Hupp J.T., Nguyen S.T., *J. Am. Chem. Soc.*, **2011**, 133, 5228-5231.

Leo A., Liu S., Diniz da Costa J.C., Shao Z., *Sci. Tech. Adv. Mater.*, **2006**, 7, 819-825.

Lewandivskii S., http://www.ptq.pemex.com/productosyservicios/eventosdescargas/Documents/Foro%20PEMEX%20Petroqu%C3%ADmica/2014/Steve%20Global%20Olefin%20September%202014.pdf

Li H., Song Z., Zhang X., Huang Y., Li S., Mao Y., Ploehn H.J., Bao Y., Yu M., *Science*, **2013**, 342, 95-98.

Li K., Olson D. H., Seidel J., Emge T. J., Gong H., Zeng H., Li J., *J. Am. Chem. Soc.*, **2009**, 131, 10368-10369.

Li Y, Guan H.M., Chung T.S., Kulprathipanja S., *J. Membr. Sci.*, **2006,** 275, 17-28.

Li Y., Chung T.S., Cao C., Kulprathipanja S., *J. Membr. Sci.*, **2005**, 260, 45-55.

Li Y., Yang R.T., *Langmuir*, **2007, 23**, 12937-12944.

Li Y.S., Liang F.Y., Bux H., Feldhoff A., Yang W.S., Caro J., *Angew. Chem.*, **2010**, 49, 548-551.

Liang Z., Marshall M., Chaffee A.L., *Energy Procedia*, **2008**, 1, 1265-1271.

Lin R., Ge L., Hou L., Strounina E., Rudolph V., Zhu Z., *ACS Appl. Mater. Interfaces*, **2014**, 6, 5609-5618.

Lin W.H., Chung T.S., *J. Membr. Sci.*, **2001**, 186, 183-193.

Liu C.[c], McCulloch B., Wilson S.T., Benin A.I., Schott M.E., *US patent*, **2009**, US7637983.

Liu L.[b], Chakma A., Feng X., Lawless D., Can. J. Chem. Eng., **2009**, 87, 456-465.

Liu X., Demir N.K., Wu Z., Li K., *J. Am. Chem. Soc.*, **2015**, 137, 6999-7002.

Liu Y.[a], Ng Z., Khan E.A., Jeong H.-K., Ching C.-b., Lai Z., *Microporous Mesoporous Mater.*, **2009**, 118, 296-301.

Liu Y., Hu E., Khan E.A., Lai Z., *J. Membr. Sci.*, **2010**, 353, 36-40.

Liu Y., Zeng G., Pan Y., Lai Z., *J. Membr. Sci.*, **2011**, 379, 46–51.

Loeb S, Sourirajan S. *Advances in Chemistry Series*, **1962**, 38, 117-132.

Lohokare H., Bhole Y., Taralkar S., Kharul U., *Desalination*, **2011**, 282, 46-53.

Ma J., Ying Y., Yang Q., Ban Y., Huang H., Guo X., Xiao Y., Liu D., Li Y., Yang W., Zhong C., *Chem. Commun.*, **2015**, 51, 4249-4251.

Mahajan R., Koros W.J., *Polym. Eng. & Sci.*, **2002**, 42, 1420-1432.

Majano G., Pérez-Ramírez J., *Adv. Mater.* **2013**, 25, 1052-1057.

Mallada R., Menéndez M., *Inorganic membranes: Synthesis, characterization, and applications*, Elsevier, **2008**, pp. 33-73.

Mao Y., Li shi, Huang H., Cao W., Li J., Sun L., Jin X., Peng X., *Chem. Commun.*, **2013**, 49, 5666-5668.

Masuda T., Isobe E., Higashimura T., *J. Am. Chem. Soc.*, **1983**, 105, 7473-7474.

Matsumoto H., Shimura T., Iwahara H., Higuchi T., Yashiro K., Kaimai A., Kawada T., Mizusaki J., *J. Alloy. Comp.*, **2006**, 408-412, 456-462.

McCarthy M.C., Guerrero V.V., Barnett G.V., Jeong H.-K., *Langmuir*, **2010**, 26, 14636-14641.

McHattie J.S., Koros W.J., Paul D.R., *Polymer*, **1992**, 32, 840-850.

McKeown N.B, Budd P.M., *Macromolecules*, **2010**, 43, 5163-5176.

Merkel T.C., Bondar I.V., Nagai K., Freeman B.D., Pinnau I., *J. Polym. Sci.; Part B: Polym. Phys.*, **2000**, 38, 415-434.

Merkel T.C., Freeman B.D., Spontak R.J., He Z., Pinnau I., Meakin P., Hill A.J., *Chem. Mater.*, **2003**, 15, 109-123.

Mitchell J.K., *Roy. Inst. J.*, **1831**, 2, 101-118.

Moaddeb M., Koros W.J., *J. Membr. Sci.*, **1997**, 125, 143-163.

Moore T.T., Koros W.J., *J. Mol. Struct.*, 2005, 739, 87-98.

Mueller U., Puetter H., Hesse M., Wessel H., *US Patent*, **2012**, US8163949 B2.

Muruganandam N., Koros W.J., Paul D.R., *J. Polym. Sci.; Part B: Polym. Phys.*, **1987**, 25, 1999-2026.

Musto P., Karasz F.E., MacKnight W.J., *Polymer*, **1993**, 34, 2934-2945.

Nagaraju D., Bhagat D. G., Banerjee R., Kharul U.K., *J. Mater. Chem. A*, **2013**, 1, 8828-8835.

Nair R.R., Wu H.A., Jayaram P.N., Grigorieva V., Geim A.K., *Science*, **2012**, 335, 442-444.

Nan J., Dong X., Wang W., Jin W., Xu N., *Langmuir*, **2011**, 27, 4309-4312.

Nik O.G., Chen X.Y., Kaliaguine S., *J. Membr. Sci.*, **2012**, 413-414, 48-61.

Nune S.K., Thallapally P.K., Dohnalkova A., Wang C., Liu J. Exarhos G.J., *Chem. Commun.*, **2010**, 46, 4878-4880.

Olson D.H., *US Patent*, **2002**, US6488741.

Ordoñez M.J.C., Balkus K.J., Ferraris J.P., Musselman I.H., *J. Membr. Sci.*, **2010**, 361, 28-37.

Paglieri S.N., Way J.D., *Sep. Purif. Rev.*, 2002, 31, 1-169.

Pan Y., Liu Y., Zeng G., Zhao L., Lai Z., *Chem. Commun.*, **2011**,47, 2071-2073.

Panella B., Hirscher M., Pütter H., Müller U., *Adv. Funct. Mater.*, **2006**, 16, 520-524.

Park K.S., Ni Z., Côtô A.P., Choi J.Y., Huang R., Uribe-Romo F.J., Chae H.K., O'Keeffe M., Yaghi O.M., *Proc. Natl. Acad. Sci. USA*, **2006**, 103, 10186-10191.

Paul D.R., Kemp D.R., *J. Polym. Sci: Polym. Symp.*, **1973**, 41, 79-93.

Paul D.R., Yampolskii Y.P., *Polymeric Gas Separation Membranes*, CRC Press, Boca Raton, FL, **1994**, pp. 1-15.

Pechar T.W., Kim S., Vaughan B., Marand E., Tsapatsis M., Jeong H.K., Cornelius C.J., *J. Membr. Sci.*, **2006,** 277, 195-202.

Pellitero J.P., Amrouche H., Siperstein F.R., Pirngruber G., Draghi C.N., Chaplais G., Masseron A.S., Bachi D.B., Peralta D., Bats N., *Chem. Eur. J.*, **2010**, 16, 1560-1571.

Penczek I., Bialy J., Zbingniew D., *US Patent*, **1986**, US4607085.

Phan A., Doonan C.J., Uribe-Romo F.J., Knobler C.B., O'Keeffe M., Yaghi O.M., *Acc. Chem. Res.*, **2010**, 43, 58-67.

Pinnau I., Toy L.G., *J. Membr. Sci.*, **2001**, 184, 39-48.

Pixton M.R., Paul D.R., *Macromolecules*, **1995**, 28, 8277-8286.

Prasad R., Notaro F., Thompson D.R., *J. Membr. Sci.*, **1994,** 94, 225-248.

Rangnekar N., Mittal N., Elyassi B., Caro J., Tsapatsis M., *Chem. Soc. Rev.*, **2015**, 44, 7128-7154.

Ranjan R., Tsapatsis M., *Chem. Mater.*, **2009**, 21, 4920-4924.

Robeson L.M., *J. Membr. Sci.*, **1991**, 62, 165-185.

Robeson L.M., *J. Membr. Sci.*, **2008**, 320, 390-400.

Rodenas T., van Dalen M., Pérez E.G., Crespo S.C., Zornoza B., Kapteijn F., Gascon J., *Adv. Funct. Mater.*, **2013,** 24, 249-256.

Rowe B.W., Freeman B.D., Paul D.R., *Polymer*, **2009**, 50, 5565-5575.

Rungta M., Zhang C., Koros W.J., Xu L., *AlChE J.*, **2013**, 59, 3475-3489.

Ryu S.H., Chang Y-W. Polym. Bull. 55 (2005) 385-392.

Sánchez A.C., Imaz I., Sarabia M.C., Maspoch D., *Nature Chemistry*, **2013**, 5, 203-211.

Sea B.K., Kusakabe K., Morooka S., *J. Membr. Sci.* **1997**, 130, 41-52.

Seo Y.K., Hundal G., Jang I.T., Hwang Y.K., Jun C.H., Chang J.S., *Microporous Mesoporous Mater.*, **2009**, 119, 331-337.

Seoane B., Zamaro J.M., Tellez C., Coronas J., *RSC Advances*, **2011**, 1, 917-922.

Shah M.N., Gonzalez M.A., McCarthy M.C., Jeong H.K., *Langmuir*, **2013**, 29, 7896-7902.

Song ., Nataraj S.K., Roussenova M.V., Tan J. C., Hughes D.J., Li W., Bourgoin P., Alam A.A., Cheetham A.K., Al-Muhtaseb S.A., Sivaniah E., Energy Environ. Sci., **2012**, 5, 8359-8369.

Stannett V., *J. Membr.* Sci., **1978**, 3, 97-115.

Stern S.A., Gareis P.J., Sinclair T.F., Mohr P.H., *J. Appl. Polym. Sci.*, **1963**, 7, 2035-2051.

Story B.J., Koros W.J., *J. Appl. Polym. Sci.*, **1991**, 42, 2613-2626.

Sungpet A., Way J.D., Thoen E.M., Dorgan J.R., *J. Membr. Sci.*, **1997**, 136, 111-120.

Tanaka K., Taguchi A., Hao J., Kita H., Okamoto K., *J. Membr. Sci.*, **1996**, 121, 197-207.

Tranchemontagne D.J., Hunt J.R., Yaghi O.M., *Tetrahedron*, **2008**, 64, 8553-8557.

Uemiya S., *Sep. Purif. Rev.*, **1999**, 28, 51-85.

Van Amerongen G.J., *J. Appl. Polym. Sci.*, **1950**, 5, 307-332.

Vankelecom I.F.J., Broeck S.V.D., Mercks E., Geerts H., Grobet P., Yutterhoeven J.B., *J. Phys. Chem.*, **1996**, 100, 3753-3758.

Venna S.R., Carreon M.A., *J. Am. Chem. Soc.*, **2009**, 132, 76-78.

Victor J.G., Torkelson J.M., *Macromolecules*, **1987**, 20, 2241-2250.

Vieth W.R., Howell J.M., Hseih J.H., *J. Membr. Sci.*, **1976**, 1, 177- 220.

Vieth W.R., Tam P.M.., Michaels A.S., *J. Colloid and Interface Sci.*, **1966**, 22, 360-370.

Vogel H., Marvel C.S., *J. Polym. Sci.*, **1961**, 50, 511-539.

Vogel H., Marvel C.S., *J. Polym. Sci.; Part A: Gen. Papers*, **1963,** 1, 1531-1541.

Won J.G., Seo J.S., Kim J.H., Kim H.S., Kang Y.S., Kim S.J., Kim Y.M., Jegal J.G., *Adv. Mater.*, **2005**, 17, 80-84.

Xie Z., Li T., Rosi N.L., Carreon M.A., *J. Mater. Chem. A*, **2014**, 2, 1239-1241.

Yang T., Chung T.S., *J. Mater. Chem. A*, **2013**, 1, 6081-6090.

Yang T., Shi G.M., Chung T.S., *Adv. Energy Mater.*, **2012**, 11, 1358-1367.

Yang T., Xiao Y., Chung T.S., *Energy Environ. Sci.*, 2011, 4, 4171-4180.

Yao J., Wang H., *Chem. Soc. Rev.*, **2014**, 43, 4470-4493.

Yehia H., Pisklak T.J., Ferraris J.P., Balkus K.J., Musselman I.H., *Polymer Preprints*, **2004**, 45, 35-36.

Yong W.F., Li F.Y., Xiao Y.C., Li P., Pramod K.P., Tong Y.W., Chung T.S., *J. Membr. Sci.*, **2012**, 407-408, 47-57.

Yoo Y., Lai Z., Jeong H.-K., *Microporous Mesoporous Mater.*, **2009**, 123, 100-106.

Zhang C., Dai Y., Johnson J.R., Karvan O., Koros W.J., *J. Membr. Sci.*, 2012, **389**, 34-42.

Zhang F., Zou X., Gao X., Fan S., Sun F., Ren H., Zhu G., *Adv. Funct. Mater.*, **2012**, 22, 3583-3590.

Zhang Y., Musselman I.H., Ferraris J.P., Balkus Jr.K.J., *J. Membr. Sci.*, **2008**, 313, 170-181.

Zhou S., Zou X., Sun F., Ren H., Liu J., Zhang F., Zhao N., Zhu G., *Int. J. Hydrogen Energy*, **2013**, 38, 5338-5347.

Zhou S., Zou X., Sun F., Zhang F., Fan S., Zhao H., Schiestel T., Zhu G., *J. Mater. Chem.*, **2012**, 22, 10322-10328.

Zolandz R.R., Fleming G.K., Gas permeation theory and applications, in: Ho W.S.W., Sirkar K.K. (Eds.), *Membrane Handbook*, Van Nostrand Reinhold, New York, **1992**, pp. 25-53, 78-94.

Zornoza B., Tellez C., Coronas J., Gascon J., Kapteijn F., *Microporous Mesoporous Mater.*, **2013**, 166, 67-78.

Synopsis of the Thesis to be submitted to the Academy of Scientific and Innovative Research for Award of the Degree of Doctor of Philosophy in Chemistry	
Name of the Candidate	Mr. Anand Bhaskar
Degree Enrolment No. & Date	Ph. D in Chemical Sciences (10CC11J26062); January 2011
Title of the Thesis	Design and Synthesis of Metal Organic Frameworks (MOFs)-polymer composite membranes for gas separation
Research Supervisor	Dr. Ulhas K. Kharul (AcSIR, CSIR-NCL, Pune)

Introduction

Membrane based gas separation is being increasingly used for variety of industrial gas separations applications due to its advantages such as lower capital costs, operational simplicity, modular nature and space efficiency [Sanders (2013)]. These features make membranes more suitable over the conventional technologies of gas separation (adsorption and cryogenic distillation) for various applications such as H_2 recovery from purge streams, syn-gas ratio adjustment, enhanced oil recovery, biogas up gradation, N_2/O_2 enrichment of air, etc. For widening application of this technology, separation performance of membranes and their stability in the aggressive feed environments need to be improved. The current polymeric membranes face trade-off relationship in performance [Robeson (1991, 2008)] The microporous materials like zeolites, carbon molecular sieves and metal organic frameworks (MOFs) have excellent permeation properties and expected to be less sensitive to the temperature and condensable feed components due to their rigid framework [Goh (2011)]. Unfortunately, these materials are difficult to process into thin membranes for practical separations. These mocroporous particles are added to the polymer matrix to improve their gas separation performance. Most of the efforts are not able to produce significant improvement in the membrane performance due to either improper distribution of filler in the matrix or non-ideal interface formation between the filler and matrix [Chung (2007)].

Statement of the problem

The non-ideal interface may be a void formation due to the lack of compatibility between the filler and matrix or barrier formation by polymer chain adsorption at filler pore apertures. This void formation or barrier formation is dependent on the interaction between matrix and

filler, function of their chemical nature. Thus the careful choice of filler and polymer is essential, comprising suitable permeation properties and chemical functionality.

Aims and objectives

The aim of this work was to investigate MOF@polymer composite membranes with an anticipation of improvement in permeation performance and to evaluate their applicability for the separation of industry relevant problem of olefin-paraffin separation. The aim of the work was addressed by the following objectives of the work:

(i) Evaluation of the effect of polymer structural variation on the gas permeation properties of the composite membranes based on CuBTC and ZIF-8.
(ii) Transform the composite membrane materials into the thin selective membrane for practical application.
(iii) Evaluate capability of the chosen ZIF-8 based composite membranes for olefin-paraffin separation.

Methodology used

The MOF nanoparticles were used for composite membrane preparation to achieve better interaction with matrix polymer. The as synthesized MOF nanoparticles were mixed into polymer solution without drying (to avoid particle agglomeration) to prepare highly homogeneous composite membranes.

Sample results

Scheme 1: *Effect of polymer structural features on gas permeation properties CuBTC@PBI composite membranes*

CuBTC was added to the four PBI polymers (PBI-HFA, PBI-BuI, DMPBI-BuI and DBzPBI-BuI) and gas permeability of the composite membranes was evaluated to reveal the effect of polymer structure. The CuBTC based composite membranes with PBI-HFA showed the best improvement in the gas separation performance. The 30% CuBTC addition led to CO_2 permeability enhancement from 4.4 Barrer to 8.1 Barrer with simultaneous increase in CO_2/N_2 selectivity from 20.9 to 32.4. The addition of CuBTC in the DBzPBI-BuI surprisingly led to permeability reduction. The CO_2 permeability decreased from 25.8 Barrer to 14.7 Barrer with no significant change in the selectivity.

Scheme 2: *Effect of polymer structural features on gas permeation properties ZIF-8@PBI composite membranes*

The ZIF-8 was added to the three structurally different PBIs (PBI-BuI, DMPBI-BuI and DBzPBI-BuI) to evaluate the effect of polymer structure on the resultant composite membrane gas separation. PBI-BuI showed almost linear increase in the gas permeability with ZIF loading (3.5 times increase in H_2 permeability at 30% ZIF loading). The good compatibility and subsequent improvement in the gas permeability prevails even after elimination of H-bonding while substituting two nitrogen of PBI-repeat unit by alkyl groups. The ZIF-8@DMPBI-BuI composite membranes showed unusually high increase in the gas permeability at 30% ZIF loading with drastic reduction in selectivity. The H_2 permeability increased from 12.8 to 127.5 with H_2/CH_4 selectivity reduced from 157.4 to 37.

Scheme 3: *Separation of Olefin-paraffin using ZIF-8@polymer composite membranes*

The DBzPBI-BuI and PPO based composite membranes of ZIF-8 are evaluated for the olefin/paraffin separation properties. The DBzPBI-BuI showed C_3H_6 permeability enhancement from 2.3 Barrer to 20.2 Barrer with 30% ZIF content. The C_3H_6/C_3H_8 selectivity also increased from 12.6 to 44. ZIF-8@DBzPBI-BuI composite membranes also prepared as thin film composite morphology showed high C_3H_6/C_3H_8 selectivity up to 32. On the other hand PPO composite membranes showed C_3H_6 permeability enhancement from 3.9 Barrer to 6.4 Barrer with 15% ZIF-8 content. The C_3H_6/C_3H_8 selectivity also increased from 9.1 to 22.6. The further increase in ZIF loading (25%) did not resulted in further significant increase either permeability or selectivity.

References

[1] D. F. Sanders, *et al*., *Polymer*, **54** (2013) 4729–4761.

[2] L. M. Robeson, *J. Membr. Sci.*, **62** (1991) 165-185.

[3] L. M. Robeson, *J. Membr. Sci.*, **320** (2008) 390–400.

[4] C. Zhou, *et al*., *J. Membr. Sci.*, **225** (2003) 125–134.

[5] P. S. Goh, *et al*., *Sep. Purif. Technol.*, **81** (2011) 243–264.

[6] T. S. Chung, *et al*., *Prog. Polym. Sci.*, **32** (2007) 483–507.

List of publications:-

1) **A. Bhaskar**, R. Banerjee, U.K. Kharul,* ZIF-8@PBI-BuI composite membranes: elegant effects of PBI structural variations on gas permeation performance, Journal of material chemistry, 2, 12962-12967 (2014).
2) B. P. Biswal, **A. Bhaskar**, R. Banerjee, U.K. Kharul,* Selective interfacial synthesis of metal–organic frameworks on a polybenzimidazole hollow fiber membrane for gas separation, Nanoscale, 7, 7291–7298 (2015).
3) **A. Bhaskar**, K. Pandare, R. Banerjee, U.K. Kharul,* Highly selective ZIF@PBI composite membranes for olefin/paraffin separation, *To be submitted*.
4) **A. Bhaskar**, R. Banerjee, U. Kharul,* CuBTC@PBI composite membranes: Effect of PBI-molecular structure on gas permeation, *To be submitted*.

Patents:-

1) Patent (IN 3078/DEL/2014)- U.K. Kharul, R. Banerjee, **A. Bhaskar**, ZIF Based Composite Membranes for Olefin-Paraffin Separation.
2) Patent (IN 3324/DEL/2014)- U.K. Kharul, R. Banerjee, B.P. Biswal, **A. Bhaskar**, Growth of MOFs on Polybenzimidazole Hollow Fiber Membranes via Interfacial Synthesis Approach.

Presentations in conferences:-

1) **A. Bhaskar**, R. Banerjee and U.K. Kharul,* Polybenzimidazole–Metal Organic Framework Composites as Membrane Material for Gas Separation; Presented at international conference ‘MACRO’ held at IISC Bangluru; 15-18 May 2013.
2) **A. Bhaskar**, R. Banerjee and U.K. Kharul,* Metal Organic Framework (MOF)-PBI Composite membranes: Effect of polymer structure variation on the gas permeation properties; held at IACS Kolkata; 23-26 January 2015.
3) **A. Bhaskar**, R. Banerjee and U.K. Kharul,* ZIF-8@PBI composite membranes for olefin-paraffin separation: Preparation and permeation analysis; Presented at International Membrane Conference; held at Kochi; 20-22 August 2015.